11.4 9.pm

Computer Simulation Of Micelle Self-Assembly

Thomas Dalby, BSc (Hons)

A thesis submitted in partial fulfilment of the requirements of Sheffield Hallam University for the degree of Doctor of Philosophy

March 2000

In collaboration with Albright & Wilson Ltd., Birmingham

Abstract

Results are presented from a three dimensional lattice model of amphiphile-solvent and amphiphile-amphiphile-solvent systems studied using Monte Carlo simulations. This model builds upon previous models [1–11] allowing for a longer amphiphilic head group and the inclusion of a second, different amphiphile.

Detailed simulations are run using both a single amphiphile and double amphiphile model to study the self-assembly of micelles. Analysis of the results from these simulations shows that the models exhibit a critical micelle concentration together with cluster size distributions consistent with experiment and theory. Simulations of the single amphiphile model also give information on the free energy of micelle formation with the entropic and enthalpic contributions determined. It is found that the competition between the decreasing internal energy per monomer and entropy per monomer is the source of micellar behaviour. This result is then confirmed independently by calculating the partition function of an amphiphilic cluster using an extension to the Rosenbluth scheme [12–14].

Further results are also presented from simulations studying the effect of changing the head length, the hydrophilicity and the chain stiffness of the modelled amphiphiles. Similar results for the internal energy and entropy are found concerning changes to the amphiphilic head group, however changes in amphiphilic chain stiffness highlight the importance of the structure of the micelle core.

Contents

List of Figures

List of Tables

Acknowledgements

I would like to thank my supervisors Professor Chris Care, Dr Doug Cleaver and Dr John Haigh for their support and help during my PhD. I would also like to acknowledge the technical and financial support of Albright & Wilson especially Ed Messenger and Kevan Hatchman whose help with the Chemistry has been extremely useful.

Finally I would like to thank my family and friends for their constant support and encouragement.

Chapter 1

Introduction

The word amphiphile, or surfactant, describes a molecule consisting of two very different parts. One end of the molecule is polar, or ionic, and is water soluble while the other is non-polar and is soluble in oils, but only sparingly soluble in water. These characteristics mean that amphiphiles will absorb strongly at water/oil interfaces and, as a result, they are used for a variety of applications, including: emulsification, lubrication, catalysis, tertiary oil recovery and especially in cleaning products such as soaps and detergents. It is therefore of interest to surfactant manufacturers such as Albright & Wilson, who sponsor this PhD, that these systems are studied in more detail than can be achieved experimentally.

This thesis presents results obtained using a surfactant model originally developed by Care [1] and later extended by Brindle [7] and Desplat [10]. The aims of the PhD are to undertake simulations in the micellar region, obtaining information

on the free energy of micellisation and how the competition of its constituent parts the enthalpy and entropy of micellar packing contribute towards micellar growth.

1.1 Overview of Thesis

Chapter 2 includes a literature review describing the materials which show micellar behaviour, surfactants. The driving forces behind micellisation are discussed as well as their structural properties. A brief description of liquid crystal and mixture behaviour is included. Chapter 2 also includes the theoretical and mathematical models that have been developed to enable the mathematical treatment of micelles. This material is presented so as to lay the foundations for the analysis shown later.

Chapter 3 describes the mathematical model simulated in this thesis and the simulation methods used to accomplish this. Limited results regarding surfactant mixtures are also presented.

Chapter 4 contains results from simulations showing micellar behaviour and analysis through which the entropy associated with packing the chains into micelles can be extracted.

In chapter 5 a novel technique to enumerate the packing entropy directly is developed and used to confirm the results in chapter 4.

Chapter 6 moves slightly away from chapters 4 and 5 by examining the effect that changing amphiphilic head length, hydrophilicty and chain stiffness have on the

Chapter 2

Review of Amphiphile Properties

2.1 Amphiphilic Materials

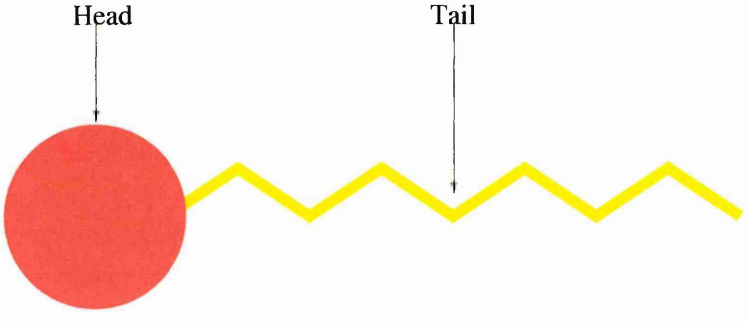

Figure 2.1: Surfactant schematic

An amphiphile consists of a polar, or ionic, hydrophilic head and one or more non-polar hydrophobic tails (CH_2). The tail section usually consists of a hydrocarbon or fluorocarbon chain while the polar or ionic head can be a variety of chemical structures, having a minimum polarity just larger than that of a single CH_2OH

group. These different chemical structures can give the head an overall charge which will alter the properties of the amphiphile. This charge is therefore used to categorise the amphiphile into one of the following groups (with the head group shown):

- Non-ionic (neutral)

  e.g. Fatty Alcohols Ethers $\rightarrow (CH_2CH_2O)_nH$

- Anionic ($-ve$ charge)

  e.g. Alkyl Ether Sulphate $\rightarrow (CH_2CH_2O)_3OSO_3^-Na^+$

- Cationic ($+ve$ charge)

  e.g. Dodecyl Ammonium Chlorides $\rightarrow C_{21}H_{25}NH_3^+Cl^-$

Amphiphiles are widely used for detergency, where oil/water interfaces exist, and are present in all cell-based biological systems where they are important in such structures as the membranes of cell walls. It is the competition between the hydrophobic and hydrophilic parts of the molecule which give the amphiphiles the ability to form and alter the properties of these interfaces. Hydrophobic substances, such as the tail of an amphiphile are readily soluble in many non-polar solvents but only sparingly soluble in water. This is the opposite of hydrophilic substances, such as the head of an amphiphile, which are readily soluble in water. This can be explained by examining the water molecules which will on average have strong local ordering with strong attractive forces between them. This arrangement becomes

distorted if a substance is dissolved in the water, resulting in an energy barrier to its solvation. Ionic or polar substances, *e.g.* the head of an amphiphile, form strong bonds to the water molecules which compensate for this disruption. Non-polar groups, however, offer no compensation and their solution in water is strongly resisted. Amphiphiles at an oil/water interface therefore arrange themselves so that the tail part is situated in the oil, where it is soluble, while the heads remain solubilised in the water. The oil is now 'bonded' to the tail and can therefore be solubilised in the water. This solubility can be finely tuned by using either temperature, mixtures of different amphiphiles, or by altering the head composition/tail length to give surfactant properties which may be advantageous to certain applications.

It is clear that the hydrophobic/hydrophilic interactions are the main driving forces [17, 18] behind amphiphilic behaviour. Other driving forces, however, are present and these become more prominent as the surfactant solution becomes more concentrated. These include the effects of head group repulsion and alkyl chain stiffness. The effect on surfactant behaviour due to the latter of these is the subject of Chapter 6 of this thesis.

In an aqueous solvent at a certain concentration, and as a consequence of the unfavourable interactions between the tail and the solvent, the surfactants spontaneously aggregate into globular constructions known as micelles, shown as region $L1$ on figure (2.2) with a simple schematic shown in figure (2.3). A basic description of a micelle is one of a pure liquid hydrocarbon core surrounded by the head groups which are in contact with the solvent due to their hydrophilicity. This is, however,

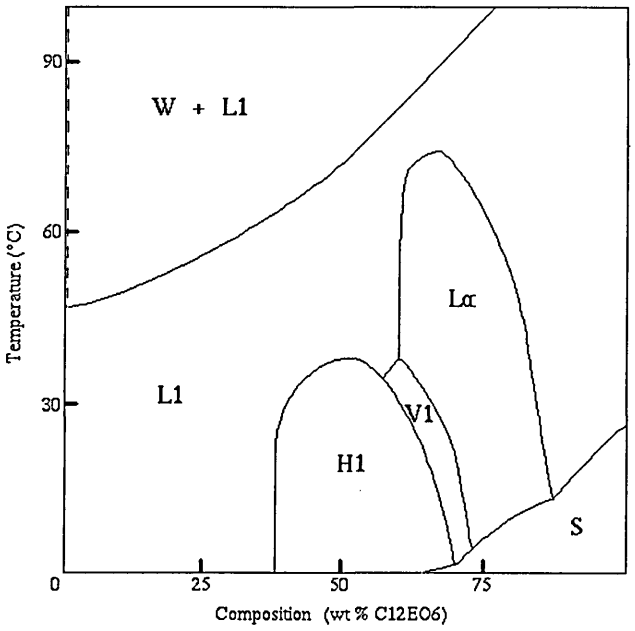

Figure 2.2: Typical non-ionic phase diagram

a rather simplistic explanation of a subtle thermodynamic balance; much work has been completed in the literature, both experimentally and theoretically, to clarify the description [19–36]. Micelles are transient species which are constantly breaking up and reforming in thermodynamic equilibrium with each other with the lifetime of a single micelle being in the order of micro seconds.

The concentration at which micelles begin to form in abundance is known as the critical micelle concentration (*cmc*) [37]. Below this point there is still a small but non-zero possibility of a micelle existing along with monomers and smaller clusters (dimers, trimers) [38]. At the *cmc* the micelles simply change their aggregation number forming bigger more stable aggregates [39]. Therefore the position of the *cmc* cannot be determined on the appearance of micelles but by monitoring physical properties of a surfactant solution see figure (2.4). The formation of micelles is also

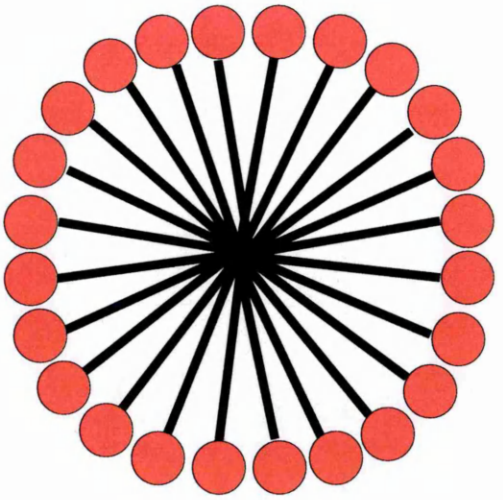

Figure 2.3: Micelle schematic

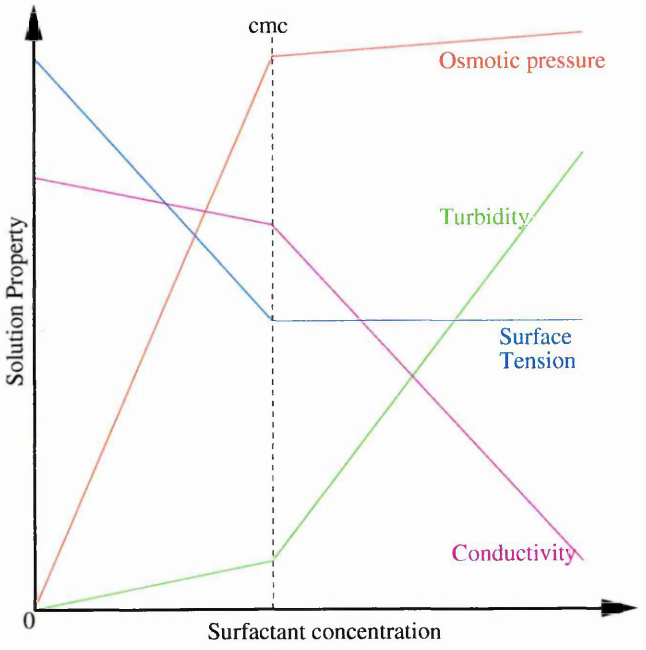

Figure 2.4: Physical properties of dilute aqueous surfactant solutions, from [15]

governed by the Kraftt point [40] which is the temperature at which the surfactant becomes sufficiently soluble to form micelles. Below this temperature the surfactant is almost insoluble and will phase separate.

Examining figure (2.2) shows that if the total surfactant concentration is increased from that which forms micelles at room temperature three distinct lyotropic liquid crystal phases are formed, which are hexagonal $H1$, cubic $V1$ and lamellar L_α, a description of each follows [40–43].

2.1.1 The Micellar "Phase"

As previously stated, when the amphiphiles that compose a surfactant are dissolved in water they will form micelles if their concentration is higher than the *cmc* and the temperature is above the Kraft point. Aggregation occurs because the free-energy (chemical potential) change that is associated with the removal of a monomer from solution into an aggregate is negative. This itself is due to the energy penalty associated with a tail molecule being in contact with the solvent, the hydrophobic effect [17]. As aggregation reduces the contact of the hydrophobic tail with the water the position of the *cmc* varies with the nature of the amphiphile, for example an increase in tail length will decrease the *cmc*. Ionic surfactants have a larger value for the *cmc* due to the head group repulsion and fluorocarbon tails have a lower *cmc* than their hydrocarbon cousins.

Most surfactants produce micelles of approximately spherical shape near the

cmc and can have aggregation numbers of the order of 40-200 depending on the tail length. The conformation of the amphiphiles in micelles differs from that of the isotropic liquid and it also varies from one micellar geometry to another. These different conformations alter the physical properties of the micelles and it is therefore important to understand this better. Dill and Flory [20] have shown that the molecular organisation of the cores of micelles resembles neither the all-trans crystalline state or the randomly structured liquid state or even the liquid-crystalline state. It may be likened to the interphase between crystalline and amorphous regions in a semi-crystalline polymer. It is also apparent that the configurational freedom of the chains is greatest at the surface of the micelle.

The most widely held opinion is that there is minimal water penetration into the hydrocarbon core. However, this does not mean that the fraction of hydrocarbon contact with water is small, as more than half of the surface of the hydrocarbon core is unprotected by the head groups [19]. This is observed in the simulations presented here and is consistent with experiments which measure the bulk properties of hydrophobic cores [23]. Tail-solvent contact is one of the balancing factors controlling micelle shape, the others being head-head repulsion and molecular stiffness. It may also be noted that an important constraint on the micelle is that its radius cannot be longer than the length of an all-trans tail chain although the entropy of the all-trans conformation means that this state is less favourable for long chains. Information on micelle size and shape can be obtained from a variety of techniques such as light scattering, neutron scattering, viscosity measurements and osmotic pressures [43, 44].

2.1.2 Lyotropic Liquid Crystal Phases

Increasing the surfactant concentration a little further produces the lyotropic liquid crystal phases: hexagonal $\rightarrow$ cubic $\rightarrow$ lamellar.

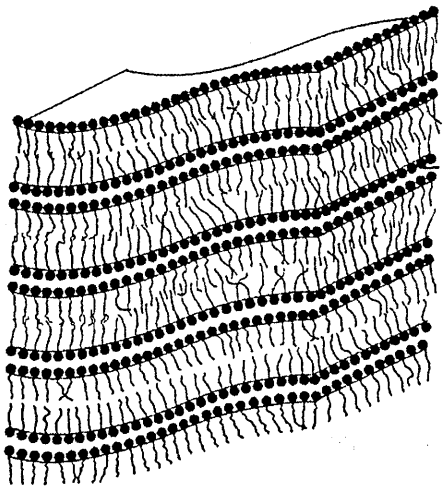

Figure 2.5: Lamellar L_α liquid crystal phase

The lamellar phase, also known as neat phase, consists of surfactant molecules which are arranged in bilayers separated by water layers. The bilayers are assembled with the amphiphiles layered head to head (or tail to tail) and the bulk lamellar phase may be envisioned as the stacking of these bilayers in the z direction (see figure (2.5)). This gives the phase one dimensional long range order. The lamellar bilayers extend over large distances which are usually in the order of microns or even more. The water layer thickness can vary from $\sim 8\mathring{A}$ to $> 100\mathring{A}$, depending on the water content, while the surfactant layer thickness is generally about $10 - 30\%$ less than the length of two all-trans surfactant chains. For a given sample the thickness of each water layer is usually the same for each layer to within $\pm 0.5\mathring{A}$.

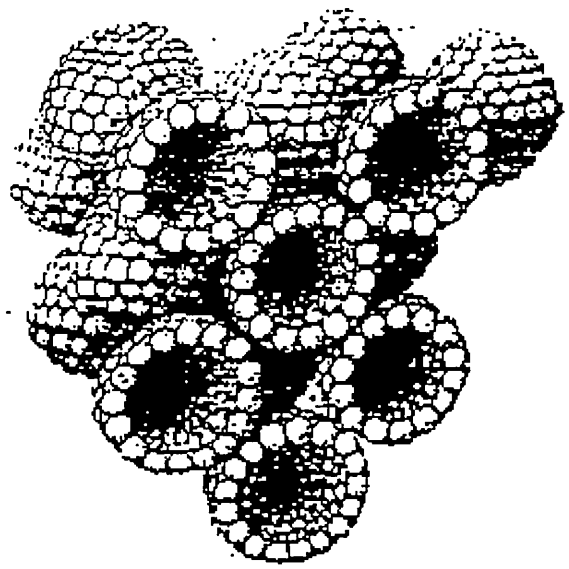

Figure 2.6: Bicontinuous cubic $V1$ liquid crystal phase

The presence of too much solvent destroys the lamellar phase and leads to the formation of the cubic phases. There are at least two types of cubic phase structure, and these can occur in the normal or reversed form. One proposed structure for these phases involves normal (or reversed micelles) packed in a cubic array. This phase occurs at compositions between the micellar and hexagonal phases. The second type of structure has short surfactant or water micellar rods joined to form a continuous network and is called the bicontinuous cubic phase, $V1$ (see figure (2.6)). This phase occurs at compositions between hexagonal and lamellar phases. Both of these phases possess three dimensional long range order.

A too high level of hydration destroys the bicontinuous cubic phase and leads to the formation of the hexagonal phases or its cousin the rectangular phase. The hexagonal class of phases consists of two well established phase structures, the normal hexagonal phase, otherwise known as the middle soap phase and the reversed

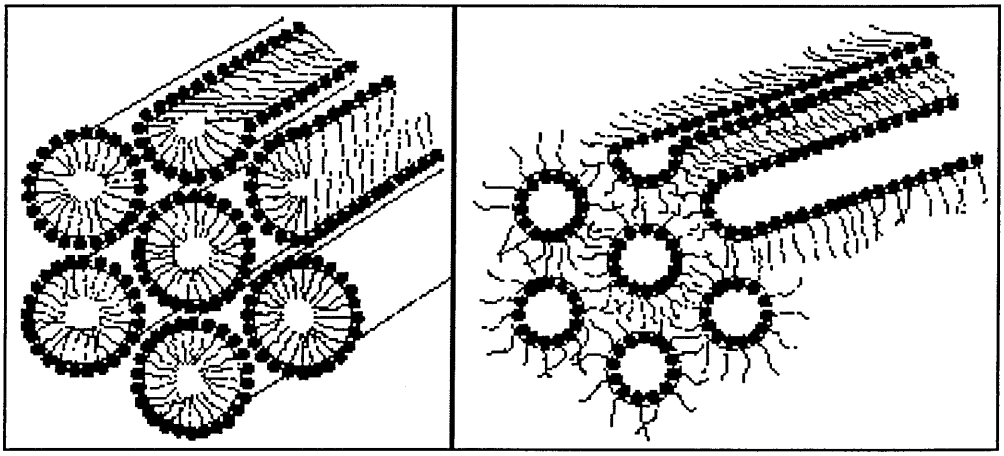

Figure 2.7: Hexagonal $H1$ liquid crystal phases

hexagonal phase (see figure (2.7)). The normal hexagonal phase consists of rod shaped micelles of indefinite length packed in an hexagonal array and separated by a continuous water region. In the reversed hexagonal phase it is the water which forms rods and these rods are then surrounded by a continuous region of hydrocarbon chains. A plane passing through this structure (perpendicular to the direction of the rods) reveals two dimensional order. For the normal hexagonal phase, the cylinder diameter is usually $\sim 10 - 30\%$ less than the thickness of the all trans surfactant chains, as for the bilayer thickness of lamellar phase. The distance between adjacent cylinders is dependent on water content, but can vary over the range $8 - 40\mathring{A}$. With reversed hexagonal phase, the water cylinder diameter is usually in the range $10 - 20\mathring{A}$, while the surfactant layer separating the cylinders is ~ 1.5 times the thickness of a fully extended chain.

Identifying the Liquid Crystal Phases

Probably the easiest way to observe the phase of a surfactant solution is to look at a sample in a test tube. The turbidity and the rheology of the solution changes for each phase allowing for an initial "guess" as to the phase present. For the lamellar phase, the solution appears opaque and runny or mucus-like, the cubic phase is a clear and thick gel, and the hexagonal phase is an opaque gel which exhibits shear thinning.

This direct observation, however, does not provide definite information as to the phase structure so further investigation is needed. Polarised light is often used if the texture is easily recognisable. A lamellar phase examined under the microscope shows a streaky or mosaic texture, whereas the hexagonal phase shows a fan-like texture. Both of these phases show a texture as they are optically birefringent, however the cubic phase is isotropic and therefore further investigation is needed.

Phase structure is most reliably determined using powder X-ray studies. Liquids, crystals and liquid crystals can be distinguished since liquids display a diffuse short spacing at large diffraction angles, crystals display many lines at both long and short spacing that span a wide range of diffraction angles, and liquid crystals display a few sharp lines that are often associated primarily with the long spacing of the structure. For X-ray studies all that has to be remembered is: the lamellar phase has one dimensional order, the repeat distance being the mean separation between the bilayers; the hexagonal phase has two dimensional order within a cross sectional

plane perpendicular to the direction of the rods; and the cubic phases possess three dimensional long range order.

2.1.3 Surfactant Mixtures

Most of the surfactants that are used for practical applications consist of a mixture of surfactants. Pure surfactants are expensive and have very little advantage over the less expensive mixtures [45]. In many applications a mixture of dissimilar surfactants can have superior properties to those of the pure surfactant components involved [46]. It may also be noted that even some commercially pure surfactants have a degree of chain length dispersity [47].

Individual surfactants vary in the way that they form aggregates and mixtures of surfactants form aggregates that differ from these. An example of this is the variation of the critical micelle concentration since a mixture of surfactants may not form micelles at the same concentration as the pure surfactant. Another phenomenon that a mixture can exhibit is that the surfactant composition of a micelle may differ greatly from that of the surfactant monomers with which it is in equilibrium. This is of practical importance as a certain monomer or micelle composition maybe needed. An example of this is the absorption of surfactant on solids. This depends on the monomer concentration while the solubilisation of these solids in turn depends on the micelle composition. For example a binary solution of A and B surfactants may form micelles which contain a 50/50 mix of surfactants with the monomers that are in equilibrium having a ratio of 90/10 [45]. Since either of these may be

crucial to the practical application, predicting this behaviour is important. In a typical surfactant mixture, the concentration of the monomers is so dilute that no significant interactions between the monomers will occur. The monomer micelle equilibrium is, therefore, dictated by the tendency of the surfactant components to form micelles and the interactions involved in this process. Predicting the monomer-micelle equilibria requires, therefore, the modelling of the thermodynamics of mixed micelle formation.

For an ideal mixture of two similarly structured surfactants of like charge the total monomer concentration lies between the *cmc*s of the individual surfactants at or above the mixture *cmc* [47]. For a mixture of an ionic and a non-ionic surfactant the *cmc* is substantially less than that shown by the ideal mixture and this is termed negative deviation from ideality [47]. This behaviour arises because the mixed micelle formation is enhanced. A mixture of a hydrocarbon base and a fluorocarbon base shows a *cmc* higher than that of the ideal solution, positive deviation [47]. This is due to the phobicity between the dissimilar hydrophobic groups in the mixed micelle. These properties have remarkable effects on the solubilisation. A micelle composed of 50/50 ideal mixture of two surfactants would have a solubilisation capacity which is an average of the two pure surfactants. A mixture which shows a negative deviation will have less solubilisation and a system having a positive deviation will have a greater solubilisation due to the shifting *cmc*s altering the micelle formation.

A non-ionic/non-ionic mixture will show a negative deviation from ideality if the

two groups are of different sizes. This is due to the packing of the chains in a micelle as same length chains will pack the most efficiently. Different chain lengths will cause the micelles to be less compactly structured than in the pure case and solubilisation will become less favourable. This is also the case for cationic/non-ionic and for short chain anionic/non-ionic mixtures. For larger chains of anionic/non-ionic mixtures the attraction between the two head groups will dominate and the micelles will tend to be more compact and therefore the solubilisation will increase.

2.2 Thermodynamics of Amphiphile Self-Assembly in Dilute Solutions

An equilibrated solution of amphiphiles in water (above the *cmc*), is a system of aggregates (micelles) of different shapes and sizes, coexisting with a nearly constant concentration of monomers. The preferred aggregation geometry and equilibrium size distribution are determined by the molecular characteristics of the amphiphiles, as well as the total concentration (including inter-aggregate forces at high concentration) and other thermodynamic variables. A thermodynamic description of these solutions is of great interest and these theoretical treatments can easily be tested against experimental quantities such as free energies, *cmc* values, heats of formation and micelle size and shape. They can also be compared to computer simulations which will be explained later.

Four different approaches have been used in the thermodynamic description of

surfactant aggregation. These are the phase separation model, the mass action model, the small system model and the multiple equilibrium model [23].

2.2.1 Phase Separation Model

At a certain concentration, the *cmc*, a number of solution properties change. It is possible to consider this as a "phase transition" from a one phase region to a two phase region allowing us to treat a micellar system as a two phase system with the *cmc* being the transition into this region. This is called the phase separation assumption. Although a micellar system is, by standard criteria, a one phase region this approximation can be useful for the conceptual understanding of micellar systems, whereas it cannot describe the properties of the micellar aggregates.

By regarding the micelles as a separate phase the chemical potential of the amphiphiles in aqueous solution (monomers), μ_1, is:

$$\mu_1 = \mu_1^0 + kT \ln (f_1 X_1)$$

where μ_1^0 is the chemical potential of a monomer at infinite dilution, f_1 is the concentration or activity coefficient and X_1 is the monomer mole fraction. At a certain critical concentration (the *cmc*), X_1^{crit}, the chemical potential will become equal to that of the micellar phase.

$$\mu_1(X_1^{crit}) = \hat{\mu}_{mic}^0$$

where $\hat{\mu}_{mic}^0$ is the chemical potential of a micelle at infinite dilution. This is where the phase separation occurs and the concentration of monomers will now remain

constant. This is however not correct as the monomer concentration does not stay quite constant above the *cmc* and this leads to some important changes in micelle size and shape.

2.2.2 Mass Action Model

In the mass action model, the micelles can be described by an aggregate M_n with a single aggregation number n. In solution, the single process occurring is the transformation:

$$nM_1 \rightleftharpoons M_n$$

With the equilibrium constant:

$$K = \frac{(f_n X_n/n)}{(f_1 X_1)^n}$$

where f_n is the appropriate activity coefficient for a molecule in a cluster of size n and X_n is the concentration (activity) of molecules in aggregates of size n. For large values of n ($n \geq 50$) this model has consequences that are similar to the phase separation model with the concentration of monomers remaining constant after the *cmc*.

2.2.3 Small System Model

The previous two models are sufficiently accurate when used to account for the concentration dependence of molecular properties. However, as soon as changes in

micelle size and shape are of interest, refinements in the models are needed.

The phase separation model can be extended such that the micelle is regarded as a small system surrounded by a bath which defines the environmental variables. Micelles of different size are then taken to be in a dynamic equilibrium with each other. The relevant environmental variables are T, the temperature, p, the pressure, and μ_1, the chemical potential of the monomers in aqueous solution. These variables determine various properties such as the micelle size distribution.

2.2.4 Multiple Equilibrium Model

Extending upon the mass action model it is possible to introduce aggregates of different size which are in equilibrium with each other. These multiple equilibria can be written in two ways, either as a step wise growth, equation (2.1), or as each aggregate being formed directly from the monomers, equation (2.2).

$$M_1 + M_{n-1} \rightleftharpoons M_n \qquad n = 2, 3... \tag{2.1}$$

$$nM_1 \rightleftharpoons M_n \qquad n = 2, 3... \tag{2.2}$$

If equation (2.1) is the process that actually occurs then the equilibrium constant of the system may be written with a constant K_n determining the aggregation process:

$$K_n = \frac{(f_n X_n)/n}{(f_1 X_1 f_{n-1} X_{n-1})/(n-1)} \tag{2.3}$$

where X_n is the concentration (activity) of molecules in aggregates of size n ($n = 1$,

μ_1^0 and X_1 correspond to monomers) and f_n is the activity coefficient for a chain belonging to a cluster of size n.

An alternative formulation can be obtained by writing the chemical potential of the aggregate M_n as:

$$\hat{\mu}_n = \hat{\mu}_n^0 + kT \ln\left(\frac{f_n X_n}{n}\right) \tag{2.4}$$

where $\hat{\mu}_n$ is the chemical potential of an aggregate of size n and $\hat{\mu}_n^0$ is the chemical potential of an aggregate of size n at infinite dilution. Expressing equation (2.4) in terms of monomers in clusters of size n gives:

$$\mu_n = \mu_n^0 + \frac{kT}{n} \ln\left(\frac{f_n X_n}{n}\right) \tag{2.5}$$

where μ_n is the chemical potential of a monomer in an aggregate of size n and μ_n^0 is the chemical potential per monomer in an aggregate of size n at infinite dilution. In order to satisfy equilibrium thermodynamics, the chemical potential of identical molecules in different aggregates must be equal.

$$\mu_1 = \mu_1^0 + kT \ln(f_1 X_1) = \mu_n^0 + \frac{kT}{n} \ln\left(\frac{f_n X_n}{n}\right) \tag{2.6}$$

which can be rearranged in terms of X_n to give:

$$X_n = n \frac{(f_1 X_1)^n}{f_n} \exp\left(-\frac{n(\mu_n^0 - \mu_1^0)}{kT}\right) \tag{2.7}$$

which determines the size distribution in the micellar solution. The total concentration X_a of surfactant molecules:

$$X_a = \sum_{n=1}^{\infty} X_n = \sum_{n=1}^{\infty} n \frac{(f_1 X_1)^n}{f_n} \exp\left(-\frac{n(\mu_n^0 - \mu_1^0)}{kT}\right)$$

Equations (2.3) & (2.6) are related through:

$$-kT\sum_{i=2}^{n}\ln K_i = n\left(\mu_n^0 - \mu_1^0\right)$$

2.3 Review of Surfactant Models and Molecular Simulation Techniques

There are two main reasons for wanting to simulate molecular species. One of these is to obtain information which is not accessible by experimentation. These types of simulation will need realistic models of the system under study. The other reason is to test a concept or a theory. This type only requires the model to be simple with as much detail as possible taken out allowing the theory to be tested directly. The interest in this thesis is with the later and as a result the following review studies simulations of simplified models using Molecular Dynamic, Mean Field and Monte Carlo techniques.

2.3.1 Molecular Dynamic Simulations

Molecular dynamic (MD) simulations are based upon the numerical solution to Newton's equation of motion, tying the system averages to the time evolution of the models constituent parts. MD has been used to study many different aspects of amphiphilic behaviour and is especially useful for studying surfactant dynamics such as shape transitions, molecular interactions and relaxation processes. Unfortunately

MD suffers when the system being studied contains parts which have long relaxation times and as a result work with these systems are better simulated using the Monte Carlo scheme, shown later [48, 49].

Smit *et al.* [50, 51] presented an off lattice model of oil and water with two types of particle, oil like and water like. These two particles were then used to model three types of molecules namely oil, water and surfactant. The oil molecule consists of a single oil particle, the water molecule consists of a single water particle while the surfactant molecule consists of n_o oil particles joined to n_w water particles by a strong harmonic force. All of the particles interacted using the Lennard-Jones potential with the interactions adjusted so that the oil and water did not mix. Constant temperature and volume MD simulations of the model were used to study the effect of chain length on interfacial tension. The simulations showed monolayers of surfactants forming at the oil/water interfaces with micelles spontaneously forming in the water phase. Amphiphile depletion layers were also found next to the interfaces which Smit thought may be due to hydration forces repelling surfactants. Density profiles showed that at the interfaces the surfactants had the correct orientation. Smit also studied the structure of the formed micelles showing good comparisons with experiments [50].

Karaboni *et al.* [52, 53] also used MD to study the conformations of model hydrocarbon chains and surfactants in dense nonpolar spheres, model water, oil droplets and model micelles. He found that the intra- and intermolecular potentials did not significantly alter the stucture showing that the chains structure was similar in all

environments except for monomers. Using a solvent field potential he was able to get good agreement with neutron scattering and NMR experiments with the simulated order parameters agreeing although the bond relaxations were too fast.

2.3.2 Spin Based Lattice Models

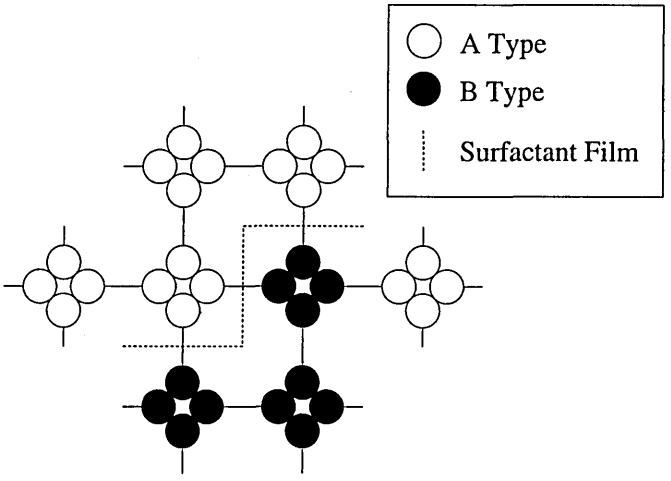

Figure 2.8: Widom model schematic

Wheeler and Widom [54] were interested in studying interfaces between coexisting phases in a mixture of oil, water and amphiphile. To do this they designed a model in which each component of the mixture (water AA, oil BB and amphiphile AB) were represented as the bonds of a regular lattice, such as a simple cubic. Each end of a molecule was associated with a site on the lattice, with the co-ordination number of the lattice c being the number of molecule ends at each site. An interaction energy of $+\infty$ was applied between a pair of molecules occupying the same bond of the lattice and also if an A end of one molecule associates with a B end. This means that the bonds are forced to be singly occupied and the lattice sites can

only be of all type A or B. For initial simulations all other interactions were given an energy of zero allowing As to associate with other As and Bs with Bs. Figure (2.8) shows a typical configuration achieved using this model.

This model is equivalent to the spin $\frac{1}{2}$ Ising model where each site is either spin $+1$ or spin -1. As there is no variation in the potential energy of the system there is no temperature dependance. Temperature can be included but the model is no longer equivalent to a spin $\frac{1}{2}$ Ising and the model becomes more complicated. Using the direct relation to the spin $\frac{1}{2}$ Ising model the energy of the system may be written as:

$$E = J(N_{\uparrow\downarrow} - N_{\uparrow\uparrow} - N_{\downarrow\downarrow}) - H(N_{\uparrow} - N_{\downarrow}) \tag{2.8}$$

where J is a constant spin-spin coupling parameter and H is the product of the magnetic field strength. $\uparrow$ can be associated with every A end of a molecule with $\downarrow$ associated with B ends.

This model was studied using the mean-field approximation and at low concentrations of amphiphile (AB) the system shows the phase separation of oil (BB) and water (AA). Higher concentrations of amphiphile induces the solubility of AA and BB, and a plait point (critical point) is reached when the solution is in equilibrium as a single phase. At very high concentrations of amphiphile the model shows an anti-ferromagnetic like ordering which can be compared to a liquid crystal phase.

For further work the model by Widom was adapted [55] to study the effect of micro-emulsions. The surfactant film shown on figure (2.8) was given a positive curvature energy which tended to keep the film flat creating large oil-coherent and

water-coherent regions. This gave the modelled micro-emulsion its characteristic large osmotic compressibility (only near the critical point) allowing it to be in equilibrium with near pure water and oil regions simultaneously.

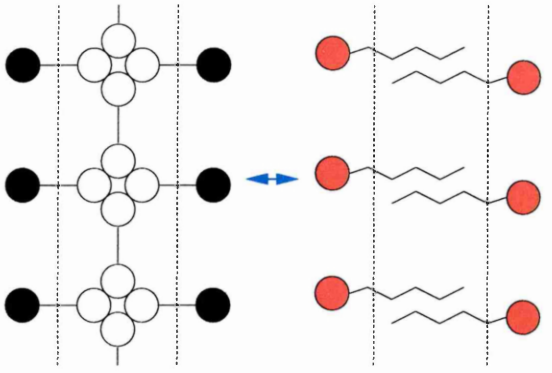

Figure 2.9: The widom model in a bilayer configuration

This adapted model is still equivalent to the two phase spin $\frac{1}{2}$ Ising model meaning that there still can only be two phases in equilibrium and the inter-facial tension can be low. Extra energy was therefore assigned to two AB molecules meeting at one lattice site (representing a bend in the film), see figure (2.8). This adapted model readily displays lamellar structures, however the bending energy also gives extra energy to a bilayer so they are discouraged, figure (2.9).

Many other workers including Dawson *et al.* [56, 57] and Hansen *et al.* [58] have used and adapted Widom's model studying, among other things, three phase coexistence using both Monte Carlo simulations and Mean Field theory. However, all of these models are unable to account for different amphiphile conformations. As the main purpose of this thesis is to study the formation and structure of micelles, models based on chains are better suited.

2.3.3 Self-Assembling Chain based Lattice Models

Much work has been completed in the literature regarding chain based lattice models, with some of the most significant work by Larson *et al.* [59–64] . Larson *et al.* used a Flory-type lattice model to study a mixture of amphiphile, oil and water. He was able to obtain self assembled equilibrium amphiphilic phases with one, two and three dimensional order. The Larson model represents amphiphilic molecules as chains confined to a cubic lattice with nearest and diagonally nearest neighbours. Diagonal nearest neighbours were used as it was discovered that they gave a better approximation of the rotational symmetry of continuous space. Oil and water molecules occupied single lattice sites while the amphiphilic chain could be made up of several head and tail segments which were taken to be the same as water and oil respectively. An energy was associated with the interaction of neighbouring segments and this energy was taken to be independent of the orientation of the segments also the energy was the same for nearest neighbour and diagonal-nearest neighbour interactions. The three energy parameters were: hydrophobic-hydrophilic E_{LH}; hydrophobic-hydrophobic E_{LL}; and hydrophilic-hydrophilic E_{HH}. The model was simulated using Monte Carlo with the initial starting lattice configuration created randomly at an infinite temperature. This lattice was then cooled until ordered patterns formed. Three different types of perturbation were allowed, interchange of a pair of single oil or water sites, amphiphilic chain twisting and amphiphilic chain reptation with one of these perturbations selected randomly. Runs were repeated at different lattice sizes and cooling rates to check if the patterns formed were equilib-

rium bulk states.

Initial runs using this model [61] on a two-dimensional lattice studied the effect of head group hydrophilicty and the solubilisation of oil. Free energies were compared to quasichemical theory showing large deviations although the difference in phase behaviour was not as bad. Further work [62] studied the self-assembly of microstructures and the difference between using three- dimensional lattices. Ordered solution structures were found including micelles and periodic lamellar and cylindrical structures. This was studied in more detail showing that lamellar and hexagonal patterns are readily attainable even on relatively small simulation boxes. These patterns are also shown to break down into cylinders and then into spheroids as the amphiphilic concentration is lowered [63].

Further work using the Larson model has been completed by Mackie *et al.* [65,66] who developed a new technique to study amphiphiles using constant pressure (NPT) simulations. This new scheme used Configuration Bias Monte Carlo [67] to enhance efficiency and involved the removal or addition of whole lattice layers. To accomplish this the probability of removing a layer with n monomers and redistributing these n monomers over the rest of the lattice was made equal to the probability of adding a new layer containing n monomers. For removal, a layer is selected and chains crossing the layer marked and either end of the marked chain selected with equal probability. Chain segments are then removed one by one from the selected end until a single uncut chain fragment remains. If both ends are on the layer then the chain is completely removed and regrown elsewhere on the lattice. This is repeated

for all chains which cross the layer. The layer is then removed and all the chains are regrown with the requirement that the first segment must cross the cut plane, to keep the probability balance. For addition a plane is selected and all chains cutting the plane are marked, have one end selected and have its segments removed as for removal. However it is not possible this time for chains to be completely removed so to satisfy the probability balance a randomly selected number of chains are removed from the lattice and regrown with one end located on the new layer. All regrown chains have their first segment in the new layer.

This new scheme was used to studied the phase behaviour of several short amphiphiles with varying tail and head lengths comparing the simulation results with quasichemical theory [68]. In order to make the formation of planar interfaces preferable Mackie used lattices with one dimension 8x longer then the other two. Even with biased sampling Mackie found it difficult to obtain reliable estimates of quantities such as the location of first order phase transitions. However quantitative agreement was found between quasichemical theory and the simulations except when one of the phases self-assembles or in the vicinity of a critical point.

Recent work by Mackie and co workers [38] has used a self-consistent mean field theory (SCMF) to study the structures of micelles, the position of the *cmc* and the micellar cluster size distribution, comparing results to Larson's lattice model. The SCMF was originally developed to treat the packing of chain molecules in amphiphilic aggregates with the basic idea to look at a central chain with all its intermolecular interactions exactly taken into account while the intermolecular interac-

tions are considered with a mean-field approximation. The probability distribution function (pdf) is determined for the chain conformations by minimising the aggregates free energy, subject to the constraint of lattice single occupancy. The SCMF is similar to the self- consistent theory (SCF) developed by Leermakers & Scheutjens [39] and further studied by Wijmans *et al.* [69] which also used a mean field approximation to examine the aggregation structure of micelles. Mackie's SCMF theory is similar to Leermakers' differing only in the co-ordination number used and the type of mean-field theory. Mackie observed that the structure of micelles found was in excellent agreement with Monte Carlo simulations. SCMF also accurately predicted the *cmc*, although the cluster size distribution is too sharp and at too low values. Comparisons of Leermakers' SCF with Monte Carlo simulations of non-linear surfactant chains showed that the SCF gave a lower position of the *cmc* and a larger aggregation number with a sharper interface between the head and tail segments. It was proposed that the mean field approximation was responsible for the too low *cmc* while the neglect of micellar shape fluctuations in the actual theory is blamed for the larger aggregation number and sharp head to tail interface.

One problem with the Larson model is that there is only one relevant energy parameter. Once the temperature has been fixed the Hydophilic- Lipophilic balance (HLB) of the amphiphiles can only be adjusted by altering head and tail lengths. The model developed by Care [1] and improved by Brindle [7] and Desplat [10] enables the HLB to also be adjusted by not only increasing the ampihiphilic chain length but also by adjusting a head- solvent interaction parameter. Care *et al.* considered a lattice model of an amphiphile-solvent mixture similar to the one proposed by Larson *et*

al.. The amphiphiles are represented as flexible chains of length s with one segment of the chain representing the hydrophilic head and the remaining $(s-1)$ segments representing the hydrophobic tail. All of the sites on the lattice were occupied by either amphiphilic chains or water segments. This model only considers nearest neighbour interactions giving the potential energy of the system as:

$$U = n_{HH}E_{HH} + n_{TS}E_{TS} + n_{HS}E_{HS} + \sum_i E_c^i \tag{2.9}$$

where n_{HH}, n_{TS}, n_{HS} are the total number of head-head, tail-solvent and head-solvent interactions. E_{HH}, E_{TS}, E_{HS} are the associated interaction energies and E_c^i is the energy associated with conformation of the ith amphiphilic chain.

To give this model amphiphilic behaviour the interaction energies were assigned as follows:

$E_{HS} < 0 \rightarrow$ Hydrophilic behaviour

$E_{TS} > 0 \rightarrow$ Hydrophobic behaviour

$E_{HH} > 0 \rightarrow$ Head-head repulsion

with the relative strengths of each type found by running extensive simulations.

This model has been simulated in 2 and 3 dimensions with the self assembly of amphiphilic chains allowed. The simulations run using this model show a well defined *cmc* at low concentrations [8, 10] with increasing amphiphile concentration leading to the formation of liquid crystal type bilayer phases including lamellar structures

and vesicles [11]. This is the model which has been adapted for the work presented in this thesis. A more detailed description of the model can be found in Chapter 3.

2.3.4 Monte Carlo Simulations

Monte Carlo (MC) [70–74] simulations use random numbers to sample the phase space of a system by moving between individual system states. This sampling results in the construction of thermal averages which enable detailed analysis to be undertaken. Unfortunately, simple MC sampling is very inefficient as no distinction is made between one state of a system with a very low probability and another with a very high probability. To improve this efficiency it becomes necessary to use importance sampling.

Importance sampling assigns each state of a given system a probability of existing, ρ, and also defines a probability for moving between each state π. For example, the probability of a system being in state n will be ρ_n and the transition probability of moving from state n to state m will be π_{nm}. By considering the movement from each state in a system to another (it is possible to stay in the same state), a matrix can be constructed defining all of the transition probabilities. A simple example is a 3-state system which gives us the matrix shown below:

$$\underline{\pi} = \begin{pmatrix} \pi_{1\to1} & \pi_{1\to2} & \pi_{1\to3} \\ \pi_{2\to1} & \pi_{2\to2} & \pi_{2\to3} \\ \pi_{3\to1} & \pi_{3\to2} & \pi_{3\to3} \end{pmatrix} \quad \text{with} \quad \sum_{n=1}^{3} \pi_{mn} = 1 \tag{2.10}$$

where m represents states 1,2 or 3.

Starting with the initial probabilities of each state existing it is possible to calculate the probability of the system being in any state on the next time step. This is done using the transition matrix combined with a probability vector which combines all of the state probabilities with the final or limiting distribution of probabilities, $\underline{\rho}$, given by:

$$\underline{\rho} = \lim_{t\to\infty} \underline{\rho}^{(1)} \underline{\pi}^{t} \tag{2.11}$$

making $\underline{\rho}$ independent of the initial probabilities of the system.

From equation (2.11) it is clear that the limiting distribution, $\underline{\rho}$, must satisfy the following eigenvalue equations:

$$\underline{\rho}.\underline{\pi} = \underline{\rho} \tag{2.12}$$

$$\sum_{m} \rho_m \pi_{mn} = \rho_n \tag{2.13}$$

By making an appropriate choice of $\underline{\pi}$ it is possible to construct a chain of successive states so that every state can be eventually reached from another state, this is called a "Markov chain".

In the canonical ensemble (as used in this thesis) the probability of each state

occurring can be written as:

$$\rho_n = \frac{\exp(-\beta E_n)}{Z} \tag{2.14}$$

If the partition function Z was known, it would be possible to calculate the probability vector $\underline{\rho}$ explicitly, but as this is impossible for large systems a transition matrix $\underline{\underline{\pi}}$ is needed which will give the correct limiting distribution of probabilities $\underline{\rho}$. The correct transition matrix has to satisfy equation (2.12) and one way to satisfy this equation is to impose the condition of "microscopic reversibility":

$$\rho_m \pi_{mn} = \rho_n \pi_{nm} \tag{2.15}$$

If $\pi_{mn} = \pi_{nm}$ then $\rho_m = \rho_n$ which is correct for the micro-canonical ensemble. This can then be adapted for the canonical ensemble by altering π to allow for the differing probabilities of each state.

Metropolis Monte Carlo

Metropolis *et al.* [75] developed a scheme which creates a transition probability matrix satisfying equations (2.12) & (2.13). If the states m and n are distinct then the Metropolis solution is:

$$\pi_{mn} = \alpha_{mn} \qquad \rho_n \geq \rho_m \qquad m \neq n \tag{2.16}$$

$$\pi_{mn} = \alpha_{mn}(\rho_n/\rho_m) \qquad \rho_n < \rho_m \qquad m \neq n \tag{2.17}$$

$$\pi_{mm} = 1 - \sum_{n \neq m} \pi_{mn} \tag{2.18}$$

where α is a symmetrical stochastic matrix thus satisfying microscopic reversibility, $\alpha_{mn} = \alpha_{nm}$, and is called the underlying matrix of the Markov chain. The symmetric properties of α can be used to show that for the three cases $\rho_m = \rho_n$, $\rho_n > \rho_m$ and $\rho_n < \rho_m$, the transition matrix described in equations (2.16), (2.17) and (2.18) satisfies equation (2.15). For example when $\rho_n > \rho_m$ then $\pi_{mn} = \alpha_{mn}$ and when $\rho_m < \rho_n$ then $\pi_{nm} = \alpha_{nm}\left(\frac{\rho_m}{\rho_n}\right)$ giving:

$$\rho_m \alpha_{mn} = \rho_n \alpha_{nm}\left(\frac{\rho_m}{\rho_n}\right) \quad \rightarrow \quad \rho_m = \rho_m \tag{2.19}$$

The Metropolis scheme is used extensively for all of the simulations undertaken in this thesis were the change in internal energy of a system determines its probability. Expressing the above equations in terms of internal energy gives:

$$\pi_{mn} = 1 \qquad E_n \leq E_m \tag{2.20}$$

$$\pi_{mn} = \exp[-\beta(E_n - E_m)] \qquad E_n > E_m \tag{2.21}$$

This is implemented practically in the following manner:

Simulations that utilise this scheme have to be run for a sufficiently long time so as to achieve a good representation of the limiting distribution of probabilities. This enables the most important states of the system to be sampled preferentially and hence increase the efficiency of the simulation.

Preferential sampling

In some cases it may be necessary to alter the probabilities for selecting a site or molecule adding a bias which would select a site or molecule in an interesting

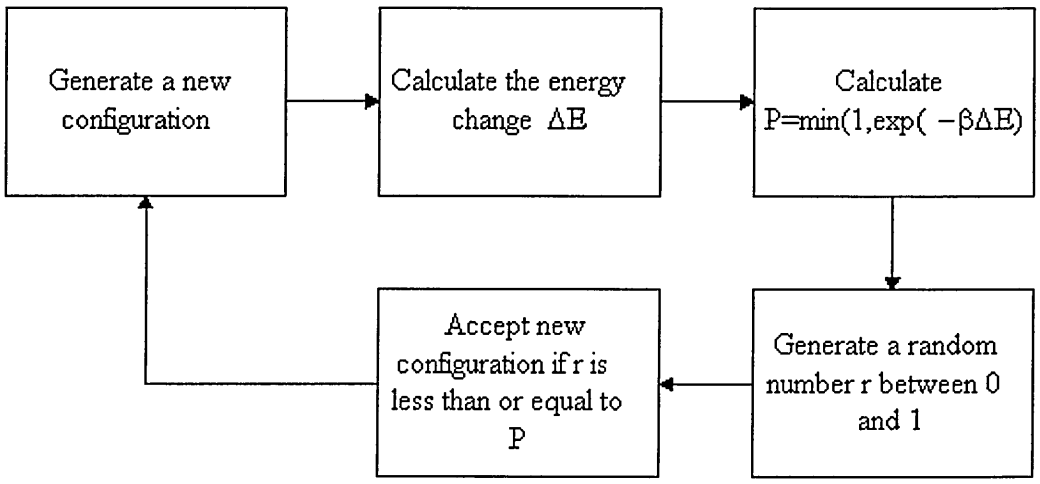

Figure 2.10: The practical implementation of the Metropolis algorithm

part of a system more often that usual, allowing for more effiecient simulations. Owicki & Scheraga [76] developed a technique which allowed solvent molecules in a solute/solvent solution to be preferentially selected.

Owicki & Scheraga were interested in sampling of solvent configurations near to solutes in dilute solutions. Using normal Metropolis techniques most of the sampling time would be spent in the bulk solvent and not near the solute were the interest was. To shift this so that more "interesting" molecules were sampled more frequently two free parameters, $\hat{R}$ and $\hat{\rho}$ were used as follows.

To start with all of the solvent molecules in the system are labelled either *in* or *out* depending on whether they are within a distance $\hat{R}$ of the solute. A solvent molecule is then selected randomly to be moved and if it has an *in* label the move is completed as per normal. If it has an *out* label a random number is generated and only if this number is less than $\hat{\rho}$ is the molecule again moved as normal (i.e. the

molecule was moved with the probability $\hat{\rho}$). Otherwise a new molecule is selected and the cycle started again until a molecule is moved. Once a molecule has been moved the acceptance is determined using the following product:

$$\frac{\pi_j}{\pi_i}\frac{\rho_{ji}}{\rho_{ij}}$$

where π_j/π_i is the ratio of the probabilities of state j existing to state i existing and ρ_{ji}/ρ_{ij} is the ratio between the probability that the given molecule would be moved in state j and the probability that the given molecule would be moved in state i. The later can be evaluated by summing the probabilities over all the selection paths the molecule has taken. By adjusting $\hat{\rho}$ it is possible to select 50% of molecules which are labelled *in* whereas ordinarily only 10-20% of sampling would have involved these molecules.

Chapter 3

Model

3.1 Three Dimensional Lattice Models

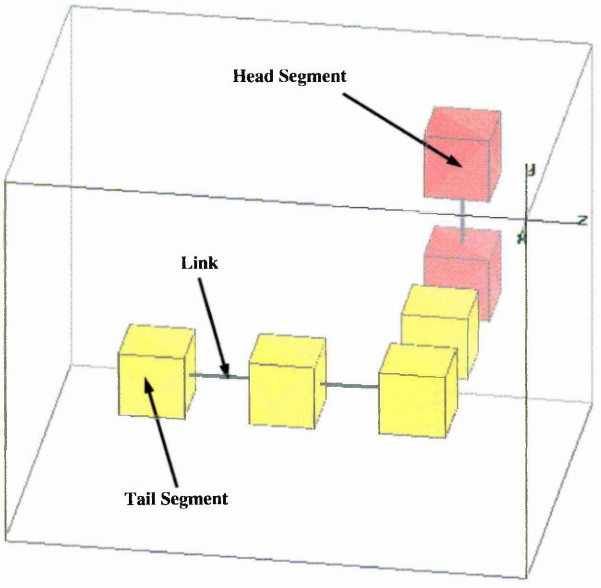

Figure 3.1: Three dimensional lattice representation of an amphiphile

Two models are used in this thesis both of them expanding upon previous work

completed by Care [1], Brindle [7] and Desplat [10]. The first model extends the previous models by allowing for head lengths greater than one (see figure (3.1)). The second model extends this further by incorporating a second amphiphile type onto the lattice allowing mixtures to be studied. The following two sections describe these new models in detail.

3.2 A Three Dimensional Lattice Model for an Amphiphile-solvent Mixture

A three dimensional lattice model of an amphiphile-solvent mixture is considered with the solvent represented as vacant sites on the lattice and amphiphiles as chains on the lattice. N_A is defined as the number of amphiphilic molecules on the lattice and N_S as the number of solvent molecules giving a total of M lattice sites. Each amphiphilic molecule has a total chain length of s segments of which h segments form the head part and $s-h$ the tail part. It is also noted that:

$hN_A = N_H =$ Number of head segments on the lattice.

$(s-h)N_A = N_T =$ Number tail segments on the lattice.

Considering only nearest-neighbour interactions on the lattice it is possible to write down all of the interactions that could occur. These are shown below:

$n_{HH} =$ Number of head to head interactions.

n_{TT} = Number of tail to tail interactions.

n_{HT} = Number of head to tail interactions.

n_{HS} = Number of head to solvent interactions.

n_{TS} = Number of tail to solvent interactions.

n_{SS} = Number of solvent to solvent interaction.

It is also possible to write down the number of head, tail and solvent segments on the lattice in terms of these interactions and the lattice co-ordination number c:

$$cN_H = 2n_{HH} + n_{HT} + n_{HS} \tag{3.1}$$

$$cN_T = 2n_{TT} + n_{HT} + n_{TS} \tag{3.2}$$

$$cN_S = 2n_{SS} + n_{TS} + n_{HS} \tag{3.3}$$

Finally head-tail, tail-tail and head-head interactions can be split into inter-molecular^E and intra-molecular^I parts:

$$n_{HT} = n_{HT}^E + n_{HT}^I \tag{3.4}$$

$$n_{HH} = n_{HH}^E + n_{HH}^I \tag{3.5}$$

$$n_{TT} = n_{TT}^E + n_{TT}^I \tag{3.6}$$

$$n_{HT}^I = N_A \tag{3.7}$$

$$n_{TT}^I = N_A(s - h - 1) \tag{3.8}$$

$$n_{HH}^I = N_A(h - 1) \tag{3.9}$$

Using equations (3.1) to (3.9) the number of independent nearest-neighbour interactions can be reduced to three. These could be any of the above but are chosen to be n_{HH}, n_{TS} and n_{HS}. Table (3.1) shows all of the interactions expressed in terms of these three interactions and the lattice parameters N_A, M, c, h and s.

i	**Type**	**Number of Interactions,** n_i
1	$(HH)^I$	$N_A(h-1)$
2	$(HH)^E$	$n_{HH} - N_A(h-1)$
3	$(TT)^I$	$N_A(s-h-1)$
4	$(TT)^E$	$N_A\,(cs/2 - ch - s + h + 1) + n_{HH} + n_{HS}/2 - n_{TS}/2$
5	SS	$Mc/2 - N_A cs/2 - n_{TS}/2 - n_{HS}/2$
6	HS	n_{HS}
7	TS	n_{TS}
8	$(HT)^I$	N_A
9	$(HT)^E$	$N_A(ch-1) - 2n_{HH} - n_{HS}$
	Total	Mc/2

Table 3.1: Interactions for single amphiphilic systems expressed in terms of the lattice parameters and independent interactions. The total number of bonds sums to $Mc/2$ as it should.

The three independent interactions defined previously can be used to write down the internal energy of the lattice. This internal energy can be expressed as a sum of the three independent interactions with an energy associated with each. A term is also added to the sum to account for the amphiphile chain conformation:

$$U = n_{HH}E_{HH} + n_{TS}E_{TS} + n_{HS}E_{HS} + \sum_i E_c^i \tag{3.10}$$

where E is the energy associated with the respective interaction and E_c^i is the energy associated with the conformation of the ith amphiphile chain.

To simplify this equation, the head-head interactions n_{HH} are chosen to be ignored as the number of head-head interactions is small compared to head-solvent and

tail-solvent interactions for a typical simulation in the micellar region (the subject of this thesis):

$$U = n_{TS}E_{TS} + n_{HS}E_{HS} + \sum_i E_c^i \tag{3.11}$$

The chain conformation depends upon the lattice used for the placement of the amphiphilic molecules. For the work presented here, a simple cubic lattice is used and, as a result, the conformation can be expressed simply as the sum of the number of right angle bonds in each of the amphiphile chains multiplied by the energy associated with a right angle bond:

$$U = n_{TS}E_{TS} + n_{HS}E_{HS} + E_\perp \sum_i n_\perp^i \tag{3.12}$$

where $n_\perp^i$ is the number of right angle bonds in the ith amphiphile chain and $E_\perp$ is the energy associated with a right angle bond.

Equation (3.12) can now be normalised with respect to the tail-solvent energy E_{TS}. Finally, dividing equation (3.12) by kT makes the final equation for the internal energy of the lattice dimension-less:

$$U/kT = \beta \left(n_{TS} + \gamma n_{HS} + \epsilon \sum_i n_\perp^i \right) \tag{3.13}$$

where $\beta = E_{TS}/kT$, $\gamma = E_{HS}/E_{TS}$, $\epsilon = E_\perp/E_{TS}$

This equation is used for nearly all of the simulations presented in this thesis.

3.3 A Three Dimensional Lattice Model for an Amphiphile-amphiphile-solvent Mixture

The model derived in the previous section can be extended such that it can represent a mixture of amphiphiles, resulting in a new expression for the internal energy of the lattice. As before the amphiphiles are present on a three dimensional lattice with a total of M sites. However now there are two types of amphiphile which can be defined as amphiphile A and amphiphile B. This means that the lattice is now composed of N_A A type amphiphilic molecules, N_B B type amphiphilic molecules and N_S solvent molecules. In addition, there are now two different chain head and tail lengths. The lattice parameters now become:

s_A = Chain length of A type amphiphile.

s_B = Chain length of B type amphiphile.

h_A = The number of head segments on an A type amphiphile chain.

h_B = The number of head segments on a B type amphiphile chain.

$(s_A - h_A)$ = The number of tail segments on an A type amphiphile chain.

$(s_B - h_B)$ = The number of tail segments on an B type amphiphile chain.

N_H^A = The total number of A type head segments on the lattice = $h_A N_A$

N_H^B = The total number of B type head segments on the lattice = $h_B N_B$

N_H = The total number of head segments on the lattice = $N_H^A + N_H^B = h_A N_A + h_B N_B$

N_T^A = The total number of A type tail segments on the lattice = $N_A(s_A - h_A)$

N_T^B = The total number of B type tail segments on the lattice = $N_B(s_B - h_B)$

N_T = The total number of tail segments on the lattice = $N_T^A + N_T^B = N_A(s_A - h_A) + N_B(s_B - h_B)$

Again, only considering nearest neighbour contributions, the various interactions present on the lattice can be expressed in the form:

$$n_{yz}^{\mu\nu} \tag{3.14}$$

where $\mu, \nu = A$ or B, $y, z = H, T$ or S, for example:

n_{HH}^{AA} = Number of A type head to A type head.

n_{TT}^{AB} = Number of A type tail to B type tail.

Head-tail, tail-tail and head-head interactions can be split into inter-molecular^E and intra-molecular^I, shown below.

$$n_{yz}^{\mu\nu} = n_{yz}^{\mu\nu E} + n_{yz}^{\mu\nu I} \tag{3.15}$$

where $\mu, \nu = A$ or B, $y, z = H$ or T

By only considering nearest-neighbour interactions it can be shown, for a lattice with co-ordination number c, that the following apply:

$$cN_H^A = 2n_{HH}^{AA} + n_{HT}^{AA} + n_{HS}^{AA} + n_{HH}^{AB} + n_{HT}^{AB} \tag{3.16}$$

$$cN_H^B = 2n_{HH}^{BB} + n_{HT}^{BB} + n_{HS}^{BB} + n_{HH}^{AB} + n_{HT}^{BA} \tag{3.17}$$

$$cN_T^A = 2n_{TT}^{AA} + n_{HT}^{AA} + n_{TS}^{AA} + n_{TT}^{AB} + n_{HT}^{BA} \tag{3.18}$$

$$cN_T^B = 2n_{TT}^{BB} + n_{HT}^{BB} + n_{TS}^{BB} + n_{TT}^{AB} + n_{HT}^{AB} \tag{3.19}$$

$$cN_S = 2n_{SS} + n_{TS}^{AA} + n_{TS}^{BB} + n_{HS}^{AA} + n_{HS}^{BB} \tag{3.20}$$

It can also be shown that:-

$$n_{HT}^{AI} = N_A \tag{3.21}$$

$$n_{HT}^{BI} = N_B \tag{3.22}$$

$$n_{TT}^{AI} = N_A(s_A - h_A - 1) \tag{3.23}$$

$$n_{TT}^{BI} = N_B(s_B - h_B - 1) \tag{3.24}$$

$$n_{HH}^{AI} = N_A(h_A - 1) \tag{3.25}$$

$$n_{HH}^{BI} = N_B(h_B - 1) \tag{3.26}$$

Equations (3.15) to (3.26) reduce the number of independent nearest-neighbour interaction variables to ten. These are chosen to be n_{HH}^{AA}, n_{TS}^{AA}, n_{HS}^{AA}, n_{HH}^{BB}, n_{TS}^{BB}, n_{HS}^{BB}, n_{HH}^{AB}, n_{TT}^{AB}, n_{HT}^{AB} and n_{HT}^{BA}. The total number of independent interactions can then be expressed in terms of these ten interactions and $N_A, N_B, M, c, h_A, h_B, s_A$ and s_B, as is shown in Table (3.2):

From the definitions, the internal energy of the system can be written as:

$$U = \sum_y \sum_z \sum_\mu \sum_\nu n_{yz}^{\mu\nu} E_{yz}^{\mu\nu} + \sum_i E_c^{Ai} + \sum_i E_c^{Bi} \tag{3.27}$$

i	Type	Number of Interactions, n_i
1	$(HH)^{AI}$	$N_A(h_A-1)$
2	$(HH)^{BI}$	$N_B(h_B-1)$
3	$(HH)^{AE}$	$n_{HH}^{AA}-N_A(h_A-1)$
4	$(HH)^{BE}$	$n_{HH}^{BB}-N_B(h_B-1)$
5	$(HH)^{AB}$	n_{HH}^{AB}
6	$(TT)^{AI}$	$N_A(s_A-h_A-1)$
7	$(TT)^{AI}$	$N_B(s_B-h_B-1)$
8	$(TT)^{AE}$	$N_A\left(cs_A/2-ch_A-s_A+h_A+1\right)+n_{HH}^{AA}+n_{HS}^{AA}/2-n_{TS}^{AA}/2$ $+n_{HH}^{AB}/2+n_{HT}^{AB}/2-n_{HT}^{BA}/2-n_{TT}^{AB}/2$
9	$(TT)^{BE}$	$N_B\left(cs_B/2-ch_B-s_B+h_B+1\right)+n_{HH}^{BB}+n_{HS}^{BB}/2-n_{TS}^{BB}/2$ $+n_{HH}^{AB}/2+n_{HT}^{BA}/2-n_{HT}^{AB}/2-n_{TT}^{AB}/2$
10	$(TT)^{AB}$	n_{TT}^{AB}
11	SS	$Mc/2-N_Acs_A/2-N_Bcs_B/2-n_{TS}^{AA}/2-n_{TS}^{BB}/2-n_{HS}^{AA}/2-n_{HS}^{BB}/2$
12	$(HS)^{AA}$	n_{HS}^{AA}
13	$(HS)^{BB}$	n_{HS}^{BB}
14	$(TS)^{AA}$	n_{TS}^{AA}
15	$(TS)^{BB}$	n_{TS}^{BB}
16	$(HT)^{AI}$	N_A
17	$(HT)^{BI}$	N_B
18	$(HT)^{AE}$	$N_A(ch_A-1)-2n_{HH}^{AA}-n_{HS}^{AA}-n_{HH}^{AB}-n_{HT}^{AB}$
19	$(HT)^{BE}$	$N_B(ch_B-1)-2n_{HH}^{BB}-n_{HS}^{BB}-n_{HH}^{AB}-n_{HT}^{BA}$
20	$(HT)^{AB}$	n_{HT}^{AB}
21	$(HT)^{BA}$	n_{HT}^{BA}
	Total	Mc/2

Table 3.2: Interactions for a mixture of amphiphiles expressed in terms of the lattice parameters and independent interactions

where $E_{xy}^{\mu\nu}$ is the energy associated with the respective interaction and E_c^i is the energy associated with the conformation of the ith amphiphile chain. The summations are over all possible combinations of A and B.

In the work presented at the end of this chapter, this equation is simplified to the following form:

$$U = \left(n_{TS}^A E_{TS}^A + n_{HS}^A E_{HS}^A + E_\perp^A \sum_i n_\perp^A\right) + \left(n_{TS}^B E_{TS}^B + n_{HS}^B E_{HS}^B + E_\perp^B \sum_i n_\perp^B\right) \tag{3.28}$$

where $n_\perp$ is the number of right angle bonds in an amphiphile chain and $E_\perp$ is the associated energy.

In order to achieve this form, the following four assumptions are made:

1. Again the head-head interactions are ignored (as for the single amphiphile model.)

2. All of the tail-tail interactions are ignored, as no repulsion or attraction between species is required for this preliminary work.

3. The head-tail interactions are ignored, as it is presumed that all of the heads will be on the surface of the aggregates and all of the tails in the core.

4. As well as these 3 simplifications, the chain conformation term is assumed to be of the form adopted in the single amphiphile model, giving equation (3.28)

Rearranging equation (3.28), dividing by kT and normalising gives the final equation for the internal energy of the lattice:

$$U/kT = \beta\left(n_{TS}^{A} + \gamma^{A} n_{HS}^{A} + \epsilon^{A}\sum_{i} n_{\perp}^{A}\right) + \phi\beta\left(n_{TS}^{B} + \gamma^{B} n_{HS}^{B} + \epsilon^{B}\sum_{i} n_{\perp}^{B}\right) \quad (3.29)$$

where $\gamma^{A} = E_{HS}^{A}/E_{TS}^{A}$,$\epsilon^{A} = E_{\perp}^{A}/E_{TS}^{A}$, $\gamma^{B} = E_{HS}^{B}/E_{TS}^{B}$,$\epsilon^{B} = E_{\perp}^{B}/E_{TS}^{B}$, $\beta = E_{TS}^{A}/kT$ and $\phi = E_{TS}^{B}/E_{TS}^{A}$

3.4 Analysis of the model

Both of the models described above can be studied by running simulations using the Metropolis Monte Carlo technique, described in section 2.3.4, and constructing averages of certain amphiphile properties. All of the work presented in this thesis is concerned with micelles and their properties and in order to determine these properties three quantities are measured: cluster size; cluster shape; and cluster interactions.

1. The size of a cluster is measured from the simulations giving the cluster size distribution which is expressed as the volume fraction of monomers X_n in clusters containing n monomers. From this calculation the monomer concentration as a function of total surfactant concentration can be obtained, which, when, plotted shows the position of the critical micelle concentration, the *cmc*. For the mixture simulations, an extra calculation is made showing the composition of the clusters. This can be used to show the different *cmc*s that the two dis-

tinct amphiphiles display, and to ascertain whether the clusters grow as mixed or separate aggregates.

2. The shape of a cluster is also measured using the principle moments of inertia (PMI) which is expressed as an average per cluster size.

3. The interactions in each cluster are measured, giving the average number of tail-solvent $\bar{t}^n$, head-solvent $\bar{h}^n$ and right angle bonds $\bar{r}^n$ in each size of cluster n. These results are subsequently used to calculate the enthalpic and entropic contributions to micelle formation.

All of the above measurements are made at uniform intervals defined at the start of the simulation. After each measurement, the results are stored and then averaged at the end of the simulation. As well as these measurements, snapshots of the lattice can be viewed using a graphics program written by the author of this Thesis. In order to make use of this program, it is necessary to store the positions of the amphiphiles on the lattice periodically. These lattice snapshots can be seen throughout this thesis.

3.4.1 Cluster analysis

To calculate the cluster size distribution etc., a cluster counting algorithm is used. The original algorithm used was similar to an ant walking around a labyrinth [71], which scans the lattice from the origin until an amphiphilic chain segment is found. The 'ant' is now placed at this starting point from which it walks around the cluster,

incrementing a counter every time it finds a new cluster segment (for the mixture simulations there is a different counter for each type of amphiphile). On its travels the 'ant' records any head-solvent, tail-solvent interactions (for the enthalpic contribution calculations), stores the lattice position of every individual segment (PMI calculations) and will note each different amphiphile present in the cluster (so that the right angle bonds can be enumerated). When the ant has finished, the number of segments present can be used to calculate the cluster size which is then used for the cluster size distribution.

Although this technique works well and is easy to implement, it is not efficient and was therefore modified to improve the performance of the code. In the simulation code each separate amphiphile has its co-ordinates stored in a large array. This array is used in conjunction with a three-dimensional lattice array which stores which amphiphile is present at a specific lattice site. In order to avoid scanning many empty sites, the amphiphile array is scanned instead, guaranteeing an occupied site. Starting at position 1 in the amphiphile array, each of the surface sites belonging to amphiphile number 1 are checked to see if they contain a nearest neighbour. If one has, the amphiphile present is recorded; adding one to the cluster size and stopping the same amphiphile being counted twice. After the surface of the first amphiphile has been examined, any new amphiphiles discovered are subsequently investigated. Once there are no more new amphiphiles, the cluster is recorded and the scan continues on the amphiphile array until it finds a virgin amphiphile. During the surface examination, the same data are collected as for the ant algorithm. This algorithm produces a 25% speed up over the old code.

3.4.2 Principal Moments of Inertia (PMI)

As this thesis is mainly interested in micelle formation, it is important to look at the shape of the clusters formed in the simulations. As the clusters are investigated, the position on the lattice of each amphiphile segment is stored so that an inertia tensor can be calculated. This is used to calculate the principal moments of inertia. Using the positions of each amphiphile segment, the centre of mass for the cluster can be determined ($\underline{c} = (\overline{x}, \overline{y}, \overline{z})$) and the deviation of each cluster segment from the centre calculated, as the tensor is calculated with respect to a set of axis with the origin at the centre of mass. The following inertia tensor matrix is formed.

$$I = \sum_x \sum_y \sum_z \begin{pmatrix} Y^2 + Z^2 & -XY & -ZX \\ -XY & Z^2 + X^2 & -YZ \\ -ZX & -YZ & X^2 + Y^2 \end{pmatrix} \tag{3.30}$$

where $X = x - \overline{x}$, $Y = y - \overline{y}$ and $Z = z - \overline{z}$

The corresponding eigenvalues, λ, calculated from this matrix are called the principal moments of inertia and can be used to characterise the shape of the cluster. For the work completed in this thesis, the eigenvalues are normalised and then ordered. Table (3.3) can be used as an approximate guide to cluster shape as the work in this thesis is carried out on a three dimensional cubic lattice, making it impossible to obtain perfect spherical or rods shaped micelles.

The principal moments of inertia data are averaged for each cluster size, showing how the eigenvalues change with increasing n.

λ Large	λ Medium	λ Small	Shape
$\frac{1}{3}$	$\frac{1}{3}$	$\frac{1}{3}$	Sphere
$\frac{1}{2}$	$\frac{1}{2}$	0	Rod
$\frac{1}{2}$	$\frac{1}{4}$	$\frac{1}{4}$	Disk

Table 3.3: Principle moments of inertia - approximate cluster shape guide

3.5 Simulation schemes

All of the results in this thesis are taken from simulations run in the canonical (NVT) ensemble, with periodic boundary conditions and using the reptation algorithm to move the chains.

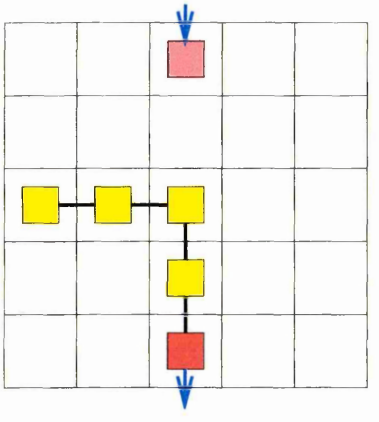

Figure 3.2: Schematic showing periodic boundary conditions

Periodic boundary conditions remove the effect of surfaces on the system under study, meaning that all of the results collected represent the bulk properties. Figure (3.2) is a schematic of this scheme showing that if the amphiphilic chain moves out of one side of the lattice it will re-enter at the other opposite side. The periodic boundary conditions also apply when the interactions are considered as a chain at the edge of the lattice will examine lattice segments at the opposite edge.

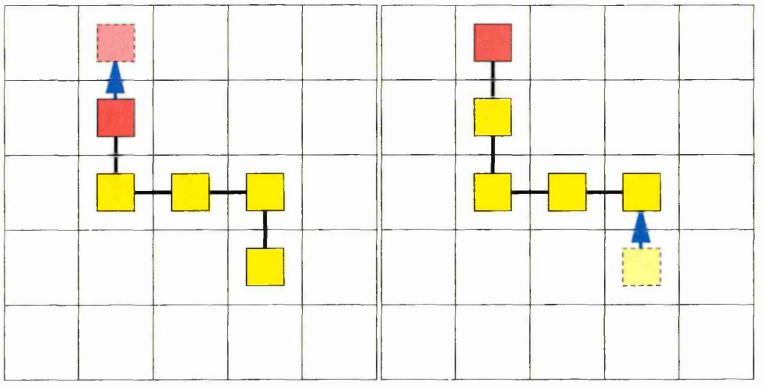

Figure 3.3: The reptation algorithm

To satisfy the condition of 'microscopic reversibility' (see chapter 2) the reptation algorithm is used to move the amphiphilic chains on the lattice. Reptation moves the chains in a snake like fashion which therefore allows any movement of the chain to be reversed. Figure (3.3) shows this movement.

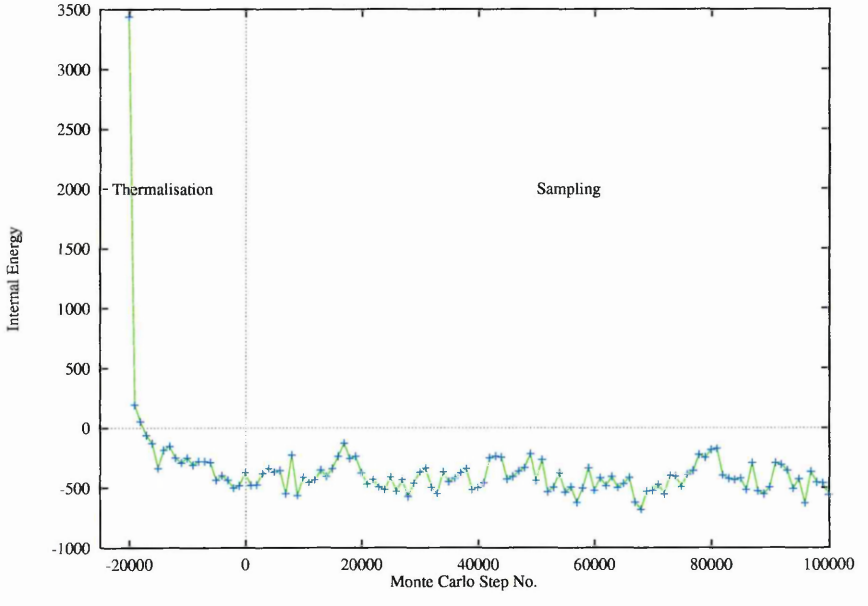

Figure 3.4: Graph showing a system reaching equilibrium

Each attempted reptation is counted as one Monte Carlo move with each Monte

Carlo step being one Monte Carlo move per amphiphile. For example if the number of amphiphiles is 512, 1 Monte Carlo step equals 512 Monte Carlo moves. At the beginning of each simulation, the system is allowed a few thousand steps to reach an equilibrium so that when the system is sampled reliable averages are obtained, figure (3.4). It should, however, be noted that although these simulations give repeatable equilibrilised results, the simulations are statistically inefficient with up to 90% of attempted reptations rejected and, therefore, have a high correlation between successive system states. This means that for reliable statistics to be extracted, the simulations had to be run for something in excess of 1×10^6 MC steps (which, for a system with 4096 molecules, represents over 4 billion attempted reptations). Techniques such as whole cluster moves [50] were implemented in an attempt to improve this statistical inefficiency but had little impact. A surfactant injection technique was also investigated to remove the need for such a long thermalisation step. However, as the lattice became more dense and micelles began to form, any newly added surfactant molecules took too long to reach equilibrium and therefore the simulations became un-feasible.

3.6 Preliminary work with mixtures

Earlier in this chapter the model originally proposed by Care [1] was adapted to allow for the study of a mixture of two distinct amphiphilic chains in solution. This modified model allows the two amphiphiles to have different tail lengths, head lengths, hydrophilic strengths (γ) and chain rigidities (ϵ). It also includes parameters

to make the amphiphiles repel/attract each other but these are not used during this study. In this section, work is presented that has been undertaken with the mixture model for two separate cases:

1. A solubilisation simulation: the behaviour of a mixture of a weakly hydrophilic amphiphile (similar to an alcohol), which will phase separate in solution, and an amphiphile, which exhibits micellar behaviour (similar to a non-ionic surfactant).

2. A mixed micelle simulation: the behaviour of a mixture of two similar non-ionic surfactants, which differ only in head length, over a range of concentrations.

3.7 Solubilisation Simulations

For this work, the pure systems of both the alcohol and the non-ionic surfactant were simulated separately and then as a 50%-50% mixture (percentage by number of chains). As stated before, the alcohol was represented as a weakly hydrophilic amphiphile, having a tail length of 12 with only 1 head segment, while the non-ionic surfactant had a tail length of 10 with a head length of 5. Both molecules were given the same ϵ and γ ($\epsilon = 1.0$, $\gamma = -2$) with ϕ, see equation (3.29), set to unity so that both molecules were simulated with equivalent tail-solvent energies with $\beta^{-}1 = 2.0$. This elevated temperature compared to those used in previous simulations was needed due to the longer chain lengths. Each individual system was cooled from a random starting position, to allow self-assembly, from $\beta^{-1} = 3.0$

to $\beta^{-1} = 2.0$. The systems were allowed 5×10^5 steps per temperature step (2^4 to achieve equilibrium) and the temperature was lowered by $\delta\beta^{-1} = 0.1$ each step. At first, each amphiphile was simulated in its pure state using 1024 molecules and then 512 molecules of each type were combined in a 50%-50% mixture. The results shown were obtained from the $\beta^{-1} = 2.0$ run at a total surfactant concentration of 6% (number of A type times chain length of A + number of B type times chain length of B all divided by total number of lattice sites).

3.7.1 Solubilisation Results

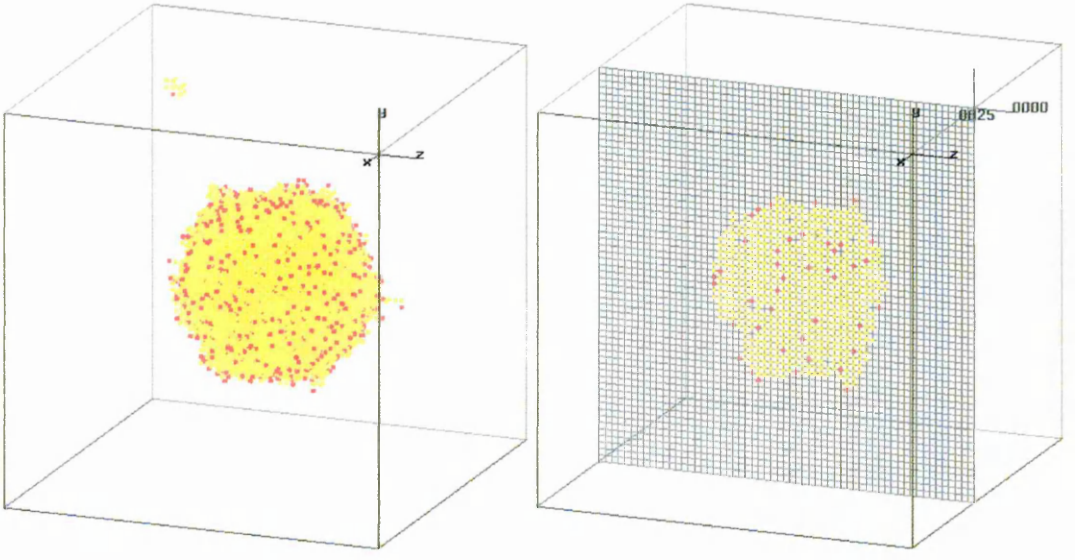

Figure 3.5: Lattice box showing the pure alcohol system with a slice showing core of aggregate (yellow→tail, red→head).

Figure (3.5) shows a lattice snapshot taken from the pure alcohol system and at the concentrations and temperature studied it phase separated forming one large aggregate. Figure (3.6) shows a lattice from the pure non-ionic system and the

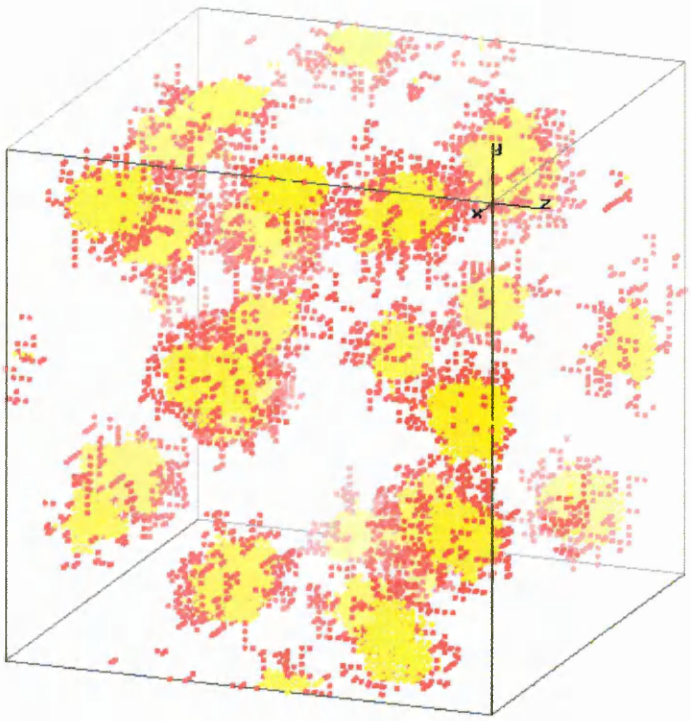

Figure 3.6: Lattice box showing pure non-ionic system (yellow→tail, red→head).

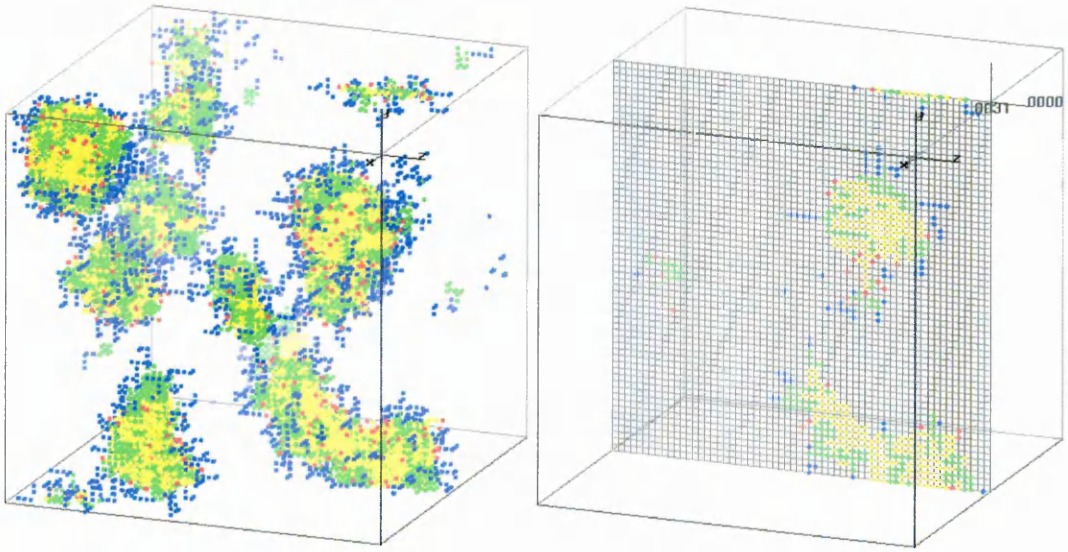

Figure 3.7: Lattice box showing the solubilisation of the alcohol (red & yellow) by the non-ionic surfactant (blue & green) (yellow & green→tail, red & blue→head).

amphiphiles formed well defined micelles with pure tail cores. Figure (3.7) shows a lattice snapshot from the 50%-50% mixture of non-ionic surfactant to alcohol with a slice taken through one of the aggregates revealing its core. When the two molecules were mixed the non-ionic surfactant solubilised the alcohol, forming large mixed aggregates with the alcohol head segments predominantly removed from the core, shown by the slice on figure (3.7).

These preliminary simulations show that the mixture model gives results which are in qualitative agreement with experiments [47,77]. Now it is of interest to study this model in more detail.

3.8 Mixed Micelle Simulations

A further study using the mixture model was undertaken to examine the behaviour of two similar amphiphilic chains in a mixture. The two amphiphiles chosen for these simulation were H_4T_4 (A type) and H_2T_4 (B type). From previous simulations [6] it has been shown that amphiphiles A and B both form spherical micelles with the B micelles being the larger and the *cmc* of the A type being lower than that of the B type. From the literature [45, 78] it is expected that this mixture will form mixed micelles with a *cmc* and mean aggregation number which lies between the respective amphiphiles in their pure states. Using the same simulation technique used for the pure systems [6] the following mixtures were examined (again note that the percentage shown is the number of type and not volume fraction).

- 25% A type, 75% B type: 128 A chains, 384 B chains
- 50% A type, 50% B type: 2048 A chains, 2048 B chains
- 75% A type, 25% B type: 384 A chains, 128 B chains

The 25%A-75%B and 75%A-25%B mixtures were restricted to a total of 512 chains in order to save CPU time; the same cooling and sampling procedure was still applied.

3.8.1 Mixed Micelle Results

Figure (3.8) shows a typical lattice snapshot of a 50% A-50% B mixture at 5% surfactant volume. It can clearly be seen from this that micelles are present and that they are constructed from two different species of amphiphile (red and yellow A type, green and blue B type). To substantiate this observation, the mixed cluster size distribution is calculated for the same system and is shown on figure (3.9). Figure (3.9) clearly shows the formation of mixed micelles, with little or no pure micelles present. This figure also shows that the mixed micelles constitute, on average, 50% A to 50% B (distribution follows diagonal of axis) which is consistent with the literature [45, 78]. Examining the 75% A to 25% B mixture, figure (3.10), and the 25% A to 75% B mixture, figure (3.11), shows that the micellar distribution shifts towards the dominant species which is again as expected.

It is now useful to investigate the effect that these mixtures have on the position of the *cmc*. Figure (3.12) shows the monomer concentration curves for each of

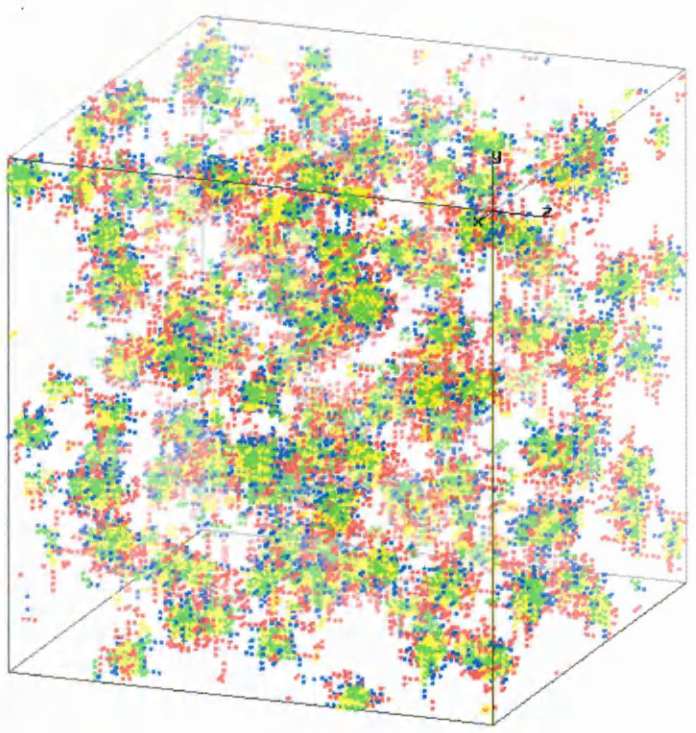

Figure 3.8: Lattice box showing mixed micelles at $X_A = 5\%$, 50%A-50%B mixture.

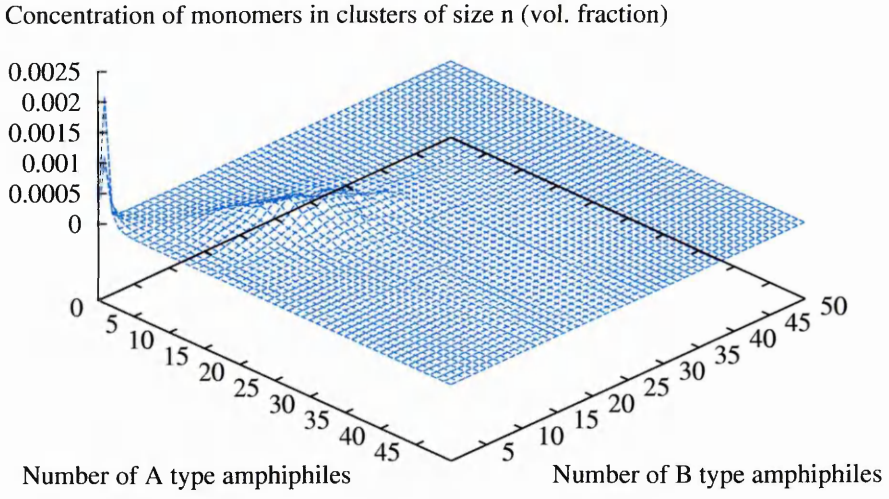

Figure 3.9: Mixed cluster size distribution at $X_A = 5\%$, 50%A-50%B mixture

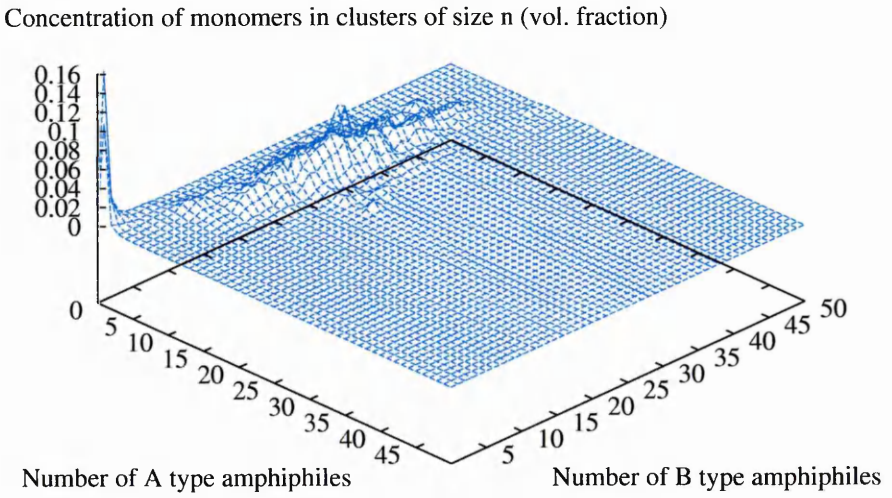

Figure 3.10: Mixed cluster size distribution at $X_A = 5\%$, 25%A-75%B mixture

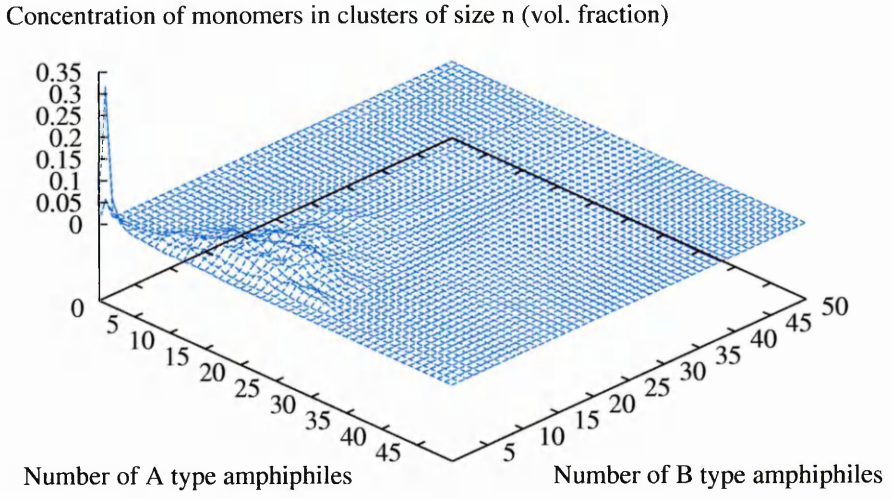

Figure 3.11: Mixed cluster size distribution at $X_A = 5\%$, 75%A-25%B mixture

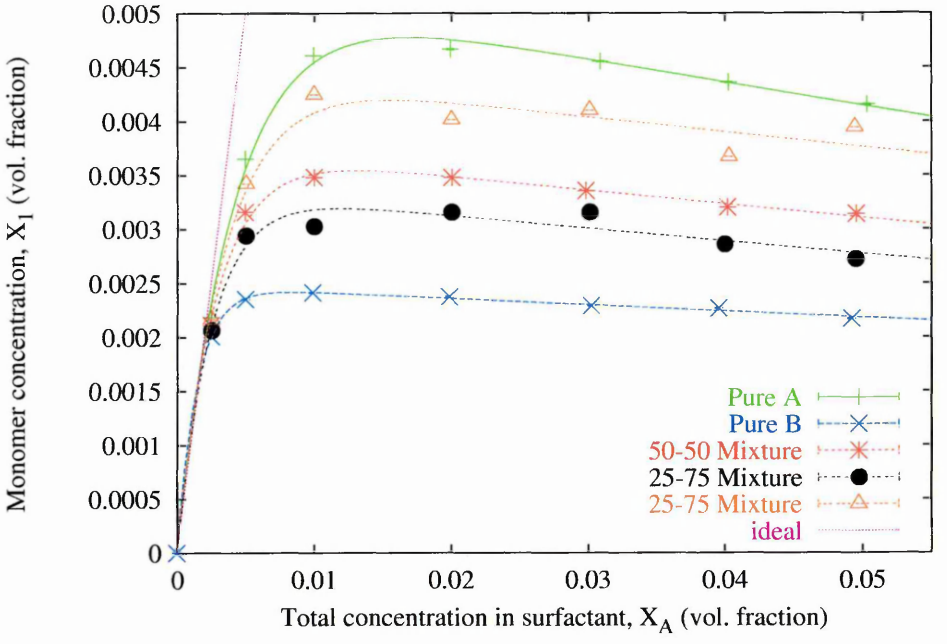

Figure 3.12: Variation of the monomer concentration due to mixture composition

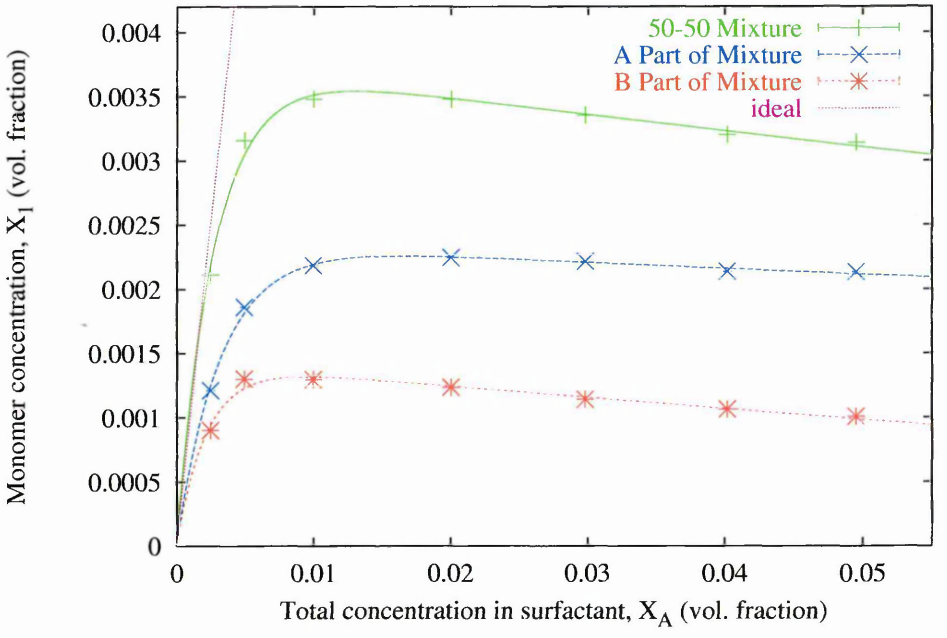

Figure 3.13: The monomer concentration of a 50% A-50% B mixture and its constituent parts

the amphiphilic systems studied. From these curves it is possible to estimate the position of the *cmc* by fitting the monomer curves to the following functional form (the functional form recommended by the curve fitting package CurveExpert [79]):

$$X_1 = (a(1 - \exp(-bx)) + cx) \tag{3.31}$$

and setting X_{cmc} =value of X_A for which X_1 is a maximum.

It is also possible, from the simulations, to calculate the change in the *cmc* of the two amphiphilic types in the mixture by calculating the individual monomer concentrations. Figure (3.13) shows the monomer curves for a mixture of 50% A-50% B and its constituent parts, A & B. Using equation (3.31) it is possible to show this variation of the *cmc* for all of the systems analysed, figure (3.14).

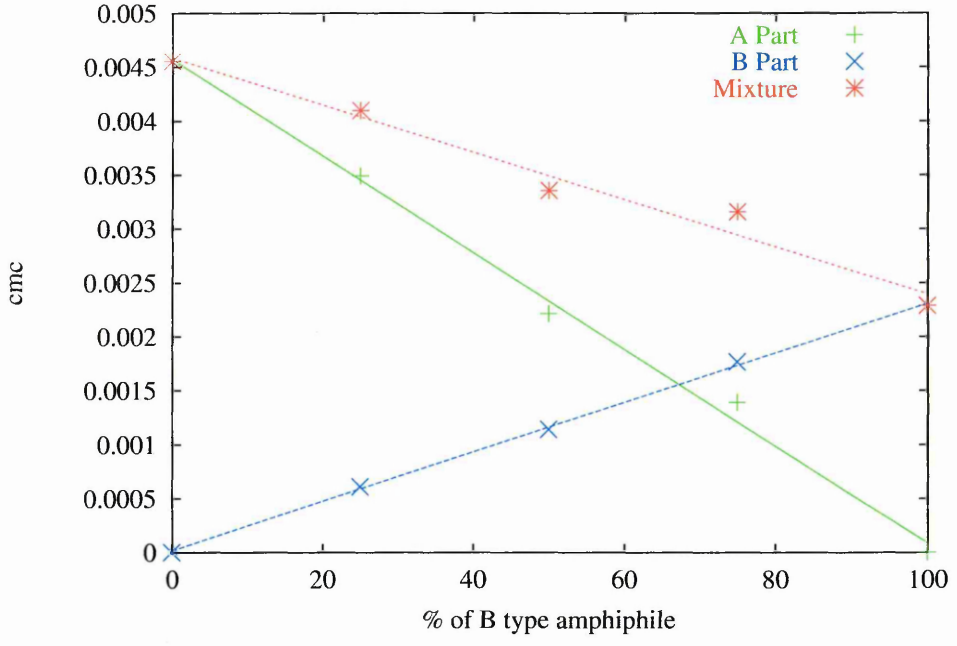

Figure 3.14: How the position of the *cmc* alters for each type of amphiphile due to mixture constitution

3.9 Conclusions

In this chapter the lattice model has been extended to represent an amphiphile mixture and undertaken two preliminary studies. The first study (run as a qualitative test of the model) showed the solubilisation of a weakly hydrophilic amphiphile. The second study, into mixed micelles, demonstrated that, for the selected amphiphiles, the results showed ideal behaviour consistent with [45, 47, 78, 80]. These results demonstrate that the amphiphilic model used throughout this thesis can be adapted to study the self assembly of surfactant mixtures. In the remainder of the thesis simulations are undertaken using models containing only one amphiphilic species.

Chapter 4

Entropic and enthalpic contributions to micelle formation

One of the central problems in micellisation is to establish the mechanism which arrests the growth of micellar clusters and inhibits the formation of infinite clusters. The repulsion between amphiphilic head groups is usually thought to be the limiting factor and this may be an ionic effect [24] (although this cannot be the case for the results presented here as no ionic effects are included). A number of workers have proposed that the entropy associated with amphiphilic chain packing may be important in arresting cluster growth [69, 81, 82]. In this chapter it is shown that the loss of entropic freedom of the head group is equivalent to this repulsion and is therefore important in the arresting of cluster growth. In order to show this, the entropy of chain packing associated with the micellar cluster is extracted, unambiguously, from Monte Carlo simulations of the three-dimensional lattice model

of a binary mixture of amphiphile and solvent described in Chapter 3.

Before this is done, however, it is important to note that the term "packing entropy" refers to the packing entropy associated with the full amphiphilic molecule, not just that of the tail segments which make up the micellar cores. It is also important to distinguish between a) the packing entropy associated with placing the amphiphilic chains in a cluster, b) the cluster translational entropy and c) the entropic contribution to the hydrophobic effect arising from the re-arrangement of bulk water molecules as they interact with tail segments. a) and b) are explicitly present in the model used here and c) is effectively included in the hydrophobic tail-solvent parameter.

4.1 Calculation of the excess entropy of packing

Extracting the entropy of packing from simulations requires the use of several simulation observables, these being the average volume fraction of monomers X_n in clusters containing n monomers and the average cluster properties $\bar{t}^n$, $\bar{h}^n$ and $\bar{r}^n$ in each size of cluster n (see Chapter 3). X_n can be used to obtain the excess chemical potential which can be further used to calculate a value for the excess entropy of packing. The interest in excess quantities arises because it is the differences between the properties of a monomer in solution and those of a monomer packed within a cluster which control the phase behaviour of the system.

4.1.1 The Excess Chemical Potential

It is possible to directly relate X_n to the excess chemical potential at infinite dilution using the result (2.7) from the multi equilibrium model described in Chapter 2. Calculating the excess chemical potential at infinite dilution is necessary in order for other arguments presented later in this chapter to be correct. From Chapter (2):

$$X_n = n\frac{(f_1 X_1)^n}{f_n}\exp\left(-\frac{n\left(\mu_n^0 - \mu_1^0\right)}{kT}\right) \tag{4.1}$$

where f_1 is the activity coefficient for a monomer, f_n is the activity coefficient for a chain belonging to cluster of size n, $(\mu_1^0 - \mu_n^0)$ is the excess chemical potential per monomer at infinite dilution of chains belonging to clusters of size n and X_1 is the monomer concentration.

This equation can be simplified by assuming that the activity coefficients have the following property at low concentration [10]:

$$\lim_{X_A \to 0} f_1\left(X_A\right) = \lim_{X_A \to 0} f_n\left(X_A\right) = 1 \quad \forall n \quad \text{and} \quad \ln(f_n) \simeq aX_A$$

where X_A is the total concentration of amphiphiles.

Using this result in equation (4.1) gives:

$$\ln X_1 - \frac{1}{n}\ln\left(\frac{X_n}{n}\right) = h\left(n, X_A\right) = \underbrace{\frac{\left(\mu_n^0 - \mu_1^0\right)}{kT}}_{intercept} + \underbrace{\left(-a + \frac{a}{n}\right)}_{gradient} X_A \tag{4.2}$$

The set of functions $h(n, X_A)$ defined by equation (4.2) are measurable from simulations undertaken at different concentrations, X_A and yield a set of lines, the y-axis intercepts of which give the infinite dilution excess chemical potential as a function of n whilst the gradients give an estimate of the activity parameter a.

4.1.2 The Cluster Partition Function

It is now possible to make further progress with the analysis by expressing X_n in terms of $\bar{N}_n$, the equilibrium number of clusters of size n:

$$X_n = \frac{n\bar{N}_n s}{M} \tag{4.3}$$

where s is the monomer length in lattice sites and M is the total number of lattice sites.

$\bar{N}_n$ itself can be expressed in terms of a cluster partition function, Q_n [83].

$$\bar{N}_n = \lambda^n Q_n \tag{4.4}$$

with

$$\lambda^n = \exp\left(\frac{n\mu_n}{kT}\right)$$

and

$$Q_n(V,T) = \sum_{<i>} \exp\left(\frac{U_i^n}{kT}\right)$$

where μ_n is the chemical potential of a monomer in an aggregate of size n and Q_n is the cluster partition function for a *single* physical cluster of size n on a lattice with a total of M sites and at temperature T. The summation $< i >$ is over all possible connected physical clusters and U_i^n is the energy of each such cluster as given by equation (3.13). It should be noted that the summation in Q_n includes all M placings of each distinct cluster on the lattice (*ie* the translational entropy). It must also be noted that equation (4.4) is only correct at sufficiently low concentrations at which the clusters do not interact (the system is ideal). It is assumed, for the purpose of

the analysis, that this is an acceptable approximation up to concentrations of the order of 3 vol%. This approximation is necessary because, for large cluster sizes, data can only be collected above the *cmc*; at lower concentrations insufficient data are available for results to be statistically significant. Using equations (4.3) & (4.4) gives:

$$\frac{X_n M}{ns} = \exp\left(\frac{n\mu_n}{kT}\right) Q_n$$

Hence, the free energy per monomer in a cluster of size n, μ_n is given by:

$$\mu_n = -\frac{kT}{n}\ln\left(Q_n\right) + \frac{kT}{n}\ln\left(\frac{X_n}{m}\right) + \frac{kT}{n}\ln\left(\frac{M}{s}\right) \tag{4.5}$$

However, in the dilute solution approximation $\mu_n = \mu_n^0 + \frac{kT}{n}\ln\left(\frac{X_n}{n}\right)$ (equation 2.5). Hence:

$$\mu_n^0 = \frac{kT}{n}\left[\ln\left(\frac{M}{s}\right) - \ln\left(Q_n\right)\right] \tag{4.6}$$

It is further assumed that:

$$-\ln\left(Q_n\right) = \frac{\bar{U}^n}{kT} - \frac{S_{tot}^n}{k}$$

where the average enthalpy per cluster of size n is defined as:

$$\bar{U}^n = \sum_{<i>} p_i^n U_i^n \tag{4.7}$$

and the average entropy per cluster of size n is:

$$\frac{S_{tot}^n}{k} = -\sum_{<i>} p_i^n \ln(p_i^n) \tag{4.8}$$

with

$$p_i^n = \frac{\exp\left(-U_i^n/kT\right)}{Q_n} \tag{4.9}$$

where S^n_{tot} includes both packing and translational entropy. Hence a direct relationship is obtained between the chemical potential of a monomer in a cluster of size n and the cluster entropy:

$$\frac{n}{kT}\mu^0_n = \ln\left(\frac{M}{s}\right) + \frac{\bar{U}^n}{kT} - \frac{S^n_{tot}}{k}$$

In order to omit translational entropy, as it is only the packing entropy that is required, the above equations are considered for clusters existing at only one lattice site (*ie* omitting the summation over the M lattice sites). If p^{cn}_i is the probability of a cluster of size, n, existing at one lattice site then:

$$p^n_i = \frac{p^{cn}_i}{M}$$

where

$$p^{cn}_i = \frac{\exp\left(-U^n_i/kT\right)}{Q^c_n}$$

and $Q^c_n = \frac{Q_n}{M}$ is a cluster partition function which omits the summation over all lattice sites. Giving:

$$\bar{U}^n = \sum_{<i>} p^n_i U^n_i = M \sum_{\{i\}} \frac{p^{cn}_i U^n_i}{M} = \sum_{\{i\}} p^{cn}_i U^n_i = \bar{U}^{cn}$$

and:

$$\frac{S^n_{tot}}{k} = -\sum_{<i>} p^n_i \ln(p^n_i) = -\sum_{\{i\}} M\left[\frac{p^{cn}_i}{M}\right]\ln\left[\frac{p^{cn}_i}{M}\right] = -\frac{S^{cn}}{k} + \ln(M)$$

where the summations $\{i\}$ are over all distinguishable clusters at <u>one</u> lattice site.

This leads to the following equation:

$$\frac{n}{kT}\mu^0_n = \ln\left(\frac{M}{s}\right) + \frac{\bar{U}^{cn}}{kT} - \frac{S^{cn}}{k} - \ln(M) = -\ln(s) + \frac{\bar{U}^{cn}}{kT} - \frac{S^{cn}}{k} \qquad (4.10)$$

where $\bar{U}^{cn}$ and S^{cn} are cluster quantities which OMIT translational entropy. The excess chemical potential may be written:

$$\frac{(\mu_n^0 - \mu_1^0)}{kT} = \frac{1}{kT}\left(\frac{\bar{U}^{cn}}{n} - \bar{U}^{c1}\right) - \frac{1}{k}\left(\frac{S^{cn}}{n} - S^{c1}\right) - \ln(s)\left(\frac{1}{n} - 1\right) \tag{4.11}$$

where the *enthalpic contribution* is identified as:

$$\frac{1}{kT}\left(\frac{\bar{U}^{cn}}{n} - \bar{U}^{c1}\right) = \beta\left(\left(\frac{\bar{t}^n}{n} - \bar{t}^1\right) + \gamma\left(\frac{\bar{h}^n}{n} - \bar{h}^1\right) + \epsilon\left(\frac{\bar{r}^n}{n} - \bar{r}^1\right)\right) \tag{4.12}$$

and the *entropic contribution* is:

$$\frac{1}{k}\left(\frac{S^{cn}}{n} - S^{c1}\right) = -\frac{1}{n}\sum_{\{i\}} p_i^{cn}\ln(p_i^{cn}) + \sum_{\{i\}} p_i^{c1}\ln(p_i^{c1}) \tag{4.13}$$

with $\frac{(\mu_n^0 - \mu_1^0)}{kT}$, $\bar{t}^n$, $\bar{h}^n$, $\bar{r}^n$ measured from the simulations.

4.2 Simulation details

Two types of amphiphile were studied in this chapter, H_2T_4 and H_4T_4, and extensive Metropolis Monte Carlo simulations were undertaken in the NVT ensemble at 8 different concentrations from 0.125 vol% up to 5.0 vol%. Details of lattice parameters used are shown on table (4.1).

This range of concentrations provided data on the transition through the *cmc* and also enough X_n data to calculate the excess chemical potential with some degree of accuracy. As for previous simulations [10], each system was cooled from a random starting configuration, consisting of only 512 amphiphiles, at a temperature $\beta^{-1} =$ 1.5 to $\beta^{-1} = 1.18$ in steps of $\delta\beta^{-1} = 0.02$ with 1.2×10^4 Monte Carlo steps at

X_A	Lattice Size (2H4T)	Lattice Size (4H4T)	Chains
0.125%	270×270×135	298×298×148	2048
0.25%	214×214×107	236×236×118	2048
0.5%	170×170×170	188×188×186	4096
1%	136×134×134	148×148×148	4096
2%	108×108×106	118×118×118	4096
3%	94×94×92	104×104×102	4096
4%	86×86×84	94×94×92	4096
5%	80×78×78	88×86×86	4096

Table 4.1: Final Micelle Simulation Parameters. In all these simulations $\beta^{-1} = 1.18$, $\gamma = -2.0$ and $\epsilon = 1.0$

each temperature. The final configuration from the $\beta^{-1} = 1.18$ run was replicated to provide a thermalised starting point for larger simulations from which cluster averages were taken. These larger simulations were run for 2×10^6 Monte Carlo steps (2×10^4 for equilibration) with cluster properties measured every 10^3 steps. In all simulations, the value of the head-solvent parameter, γ, was set to be -2 and the value of the bond bending parameter, ϵ, set to be 1. These parameters and the reduced temperature of $\beta^{-1} = 1.18$ were chosen because previous simulations of the model have shown that they give the clearest micellar behaviour [10]; at lower temperatures, the time to reach equilibrium became too large. In Chapter 6 the effect of changing γ, ϵ and head length is explored.

4.3 Results

From the lattice snapshots shown on figure (4.1) it is evident that, on average, the model produces well defined spherical clusters coexisting with monomers. This pictorial representation is backed up by the statistics gathered during the simulations.

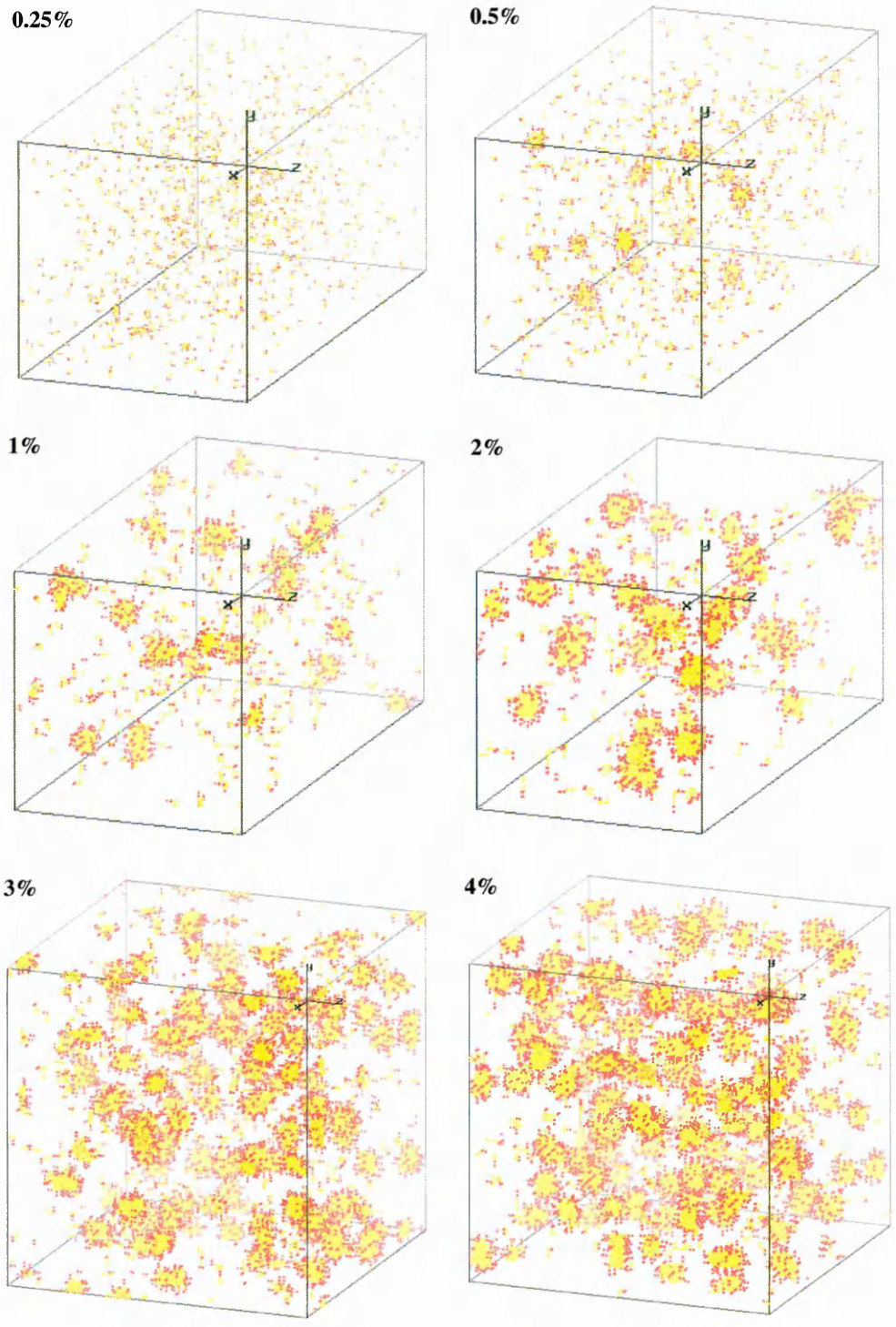

Figure 4.1: Lattice snapshots of the H_2T_4 system showing the transition through the *cmc* and the formation of micelles (yellow→tail, red→head).

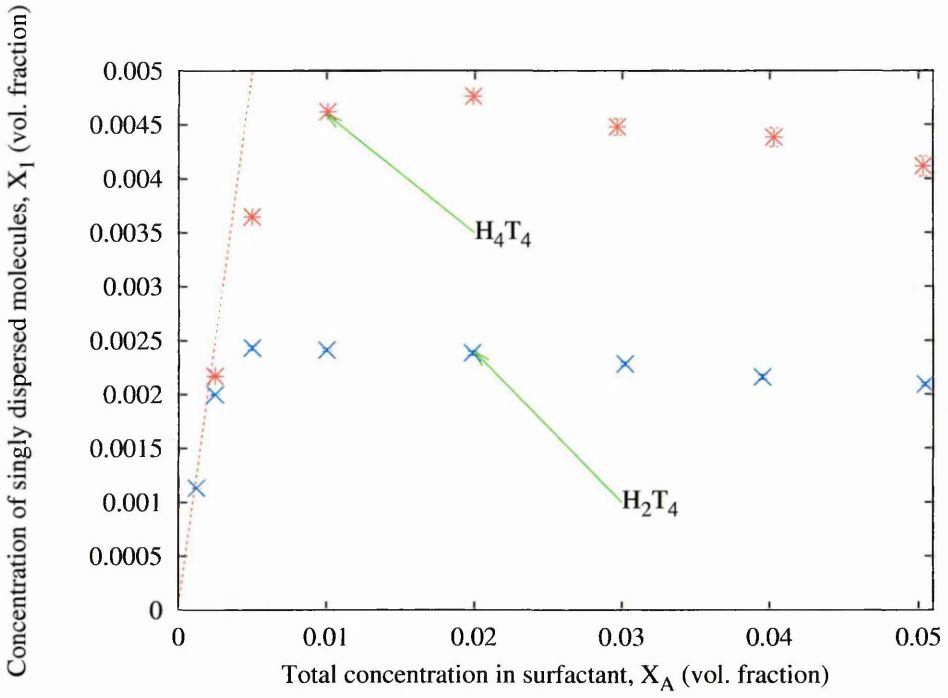

Figure 4.2: Concentration of monomers, X_1, as a function of total amphiphile concentration, X_A, for the two amphiphilic species, H_2T_4 and H_4T_4. Dotted line; $X_1 = X_A$.

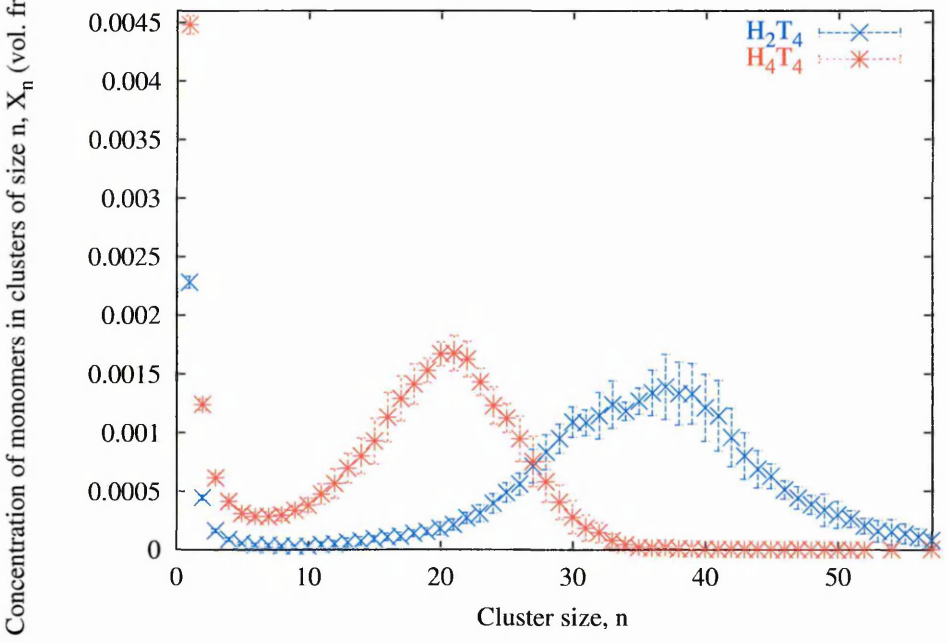

Figure 4.3: Concentration of monomers in clusters of size n, X_n, as a function of n at amphiphile concentration of 3 vol%.

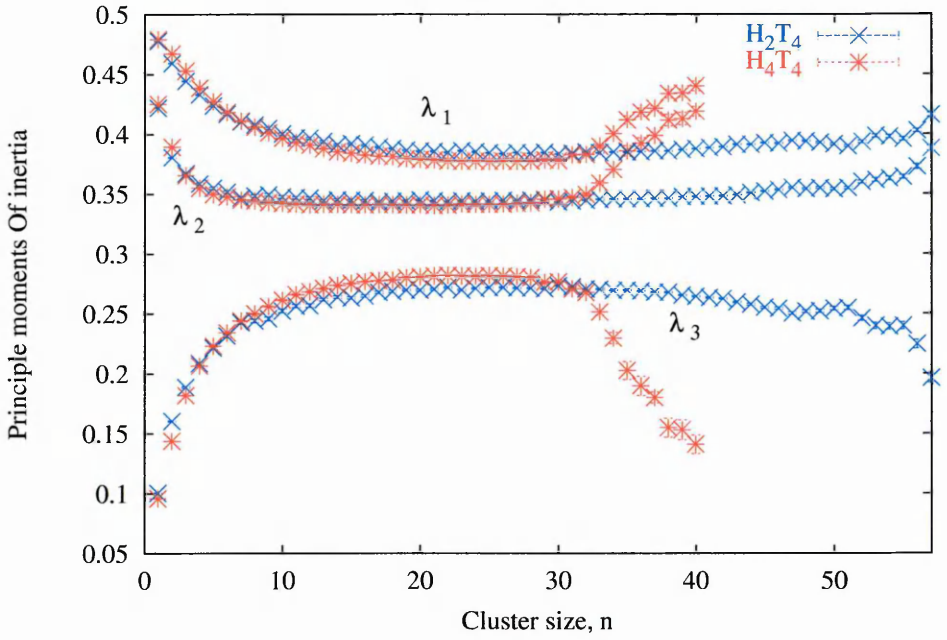

Figure 4.4: Average of the three principal moments of inertia for clusters of size n.

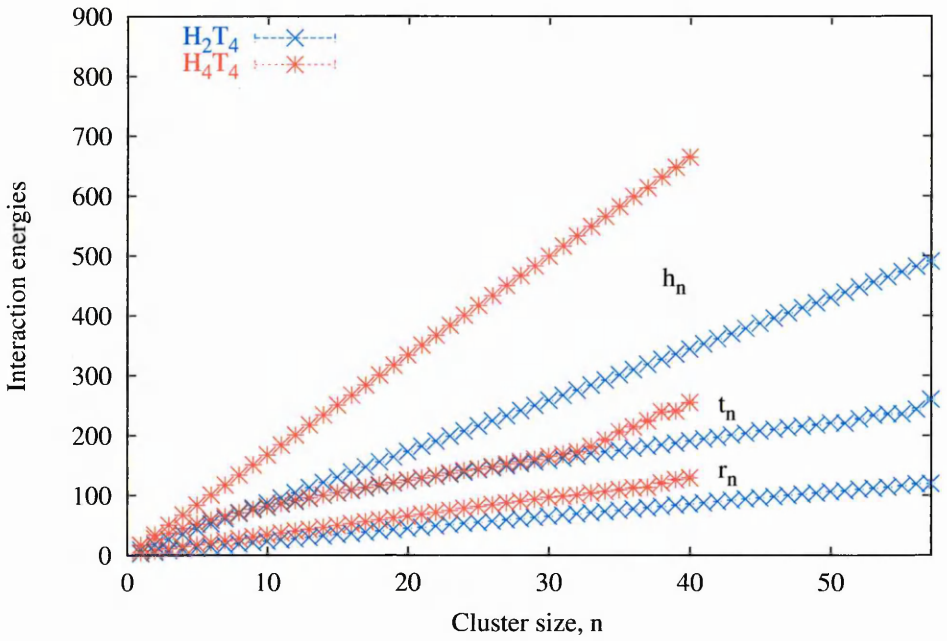

Figure 4.5: Average total number of tail-solvent, head-solvent and right-angle bonds in clusters of n monomers.

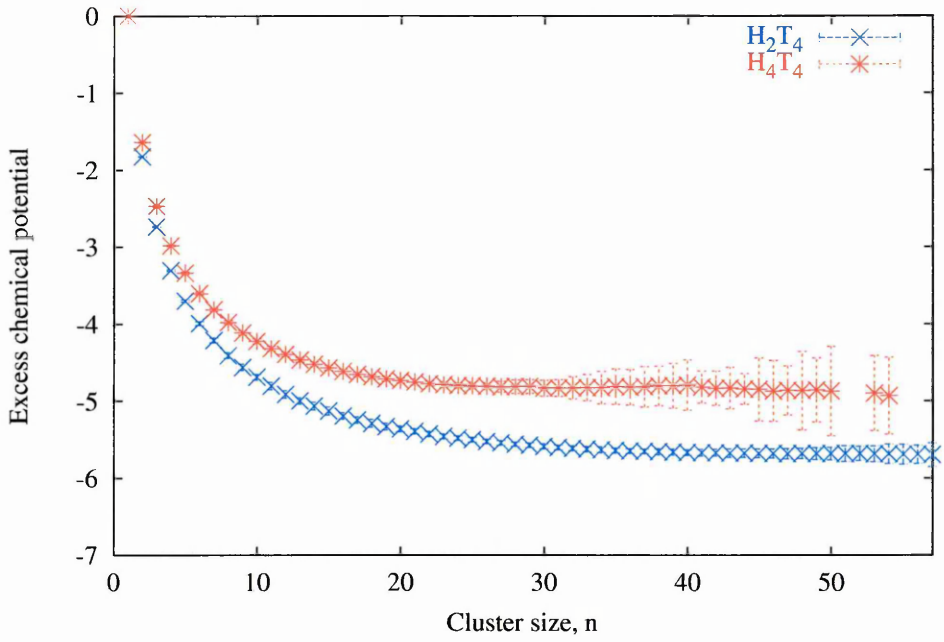

Figure 4.6: Excess chemical potential per monomer, $(\mu_n^0 - \mu_1^0)/kT$

chains is not inhibited significantly by the requirement that the heads remain in contact with the solvent as the clusters grow. It must be remembered that one of the right angle bonds may be associated with the head segments which are free within the solvent. For both species, the number of tail-solvent interactions show two regions as a function of n. For H_2T_4 below $n \simeq 50$ and for H_4T_4 below $n \simeq 30$, $\bar{t}_n$ behaves approximately as $n^{\frac{2}{3}}$ which is consistent with the growth of compact, approximately spherical, clusters. Above this point for both species $\bar{t}^n$ becomes linear which is consistent with the growth of cylindrical micelles, although as stated before the statistics become poor for these large clusters.

The data for X_n for all 8 concentrations of X_A were used to calculate the excess chemical potentials at infinite dilution shown on figure (4.6) and the data for $\bar{t}^n$, $\bar{h}^n$ and $\bar{r}^n$ were used to yield the $\left(\bar{U}^n/n - \bar{U}^1\right)/kT$ values shown on figure (4.7).

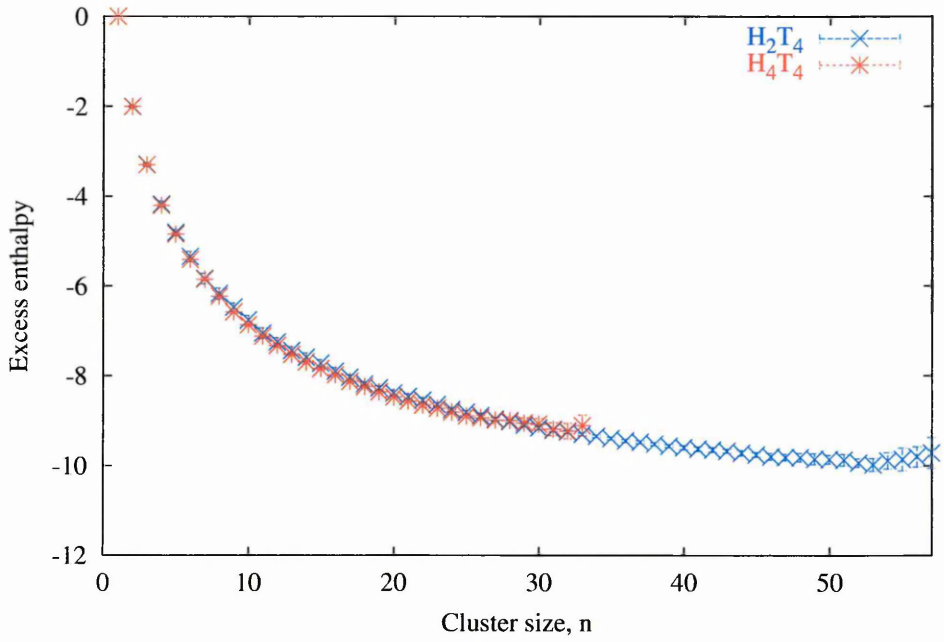

Figure 4.7: Excess enthalpy per monomer, $(U_n/n - U_1)/kT$

Combining these two sets of results using equation(4.11) gives the excess entropy per monomer data shown in figure (4.8). It can be seen from the graph that this quantity initially grows for the smallest cluster sizes and then monotonically decreases as the clusters grow. The initial growth arises because of the rapid increase in the number of distinguishable clusters as the number of monomers in a cluster increases. The subsequent reduction in entropy per monomer, as the clusters grow, must be related to the loss of freedom associated with packing the monomers in such a way as to maintain the head-solvent interactions whilst minimising the tail-solvent interactions.

It can be seen from figures (4.6,4.7 & 4.8) for the two amphiphilic species that it is the different n-dependence of the packing entropy which controls the position of the *cmc*, and the maximum in the cluster size distribution, since both species

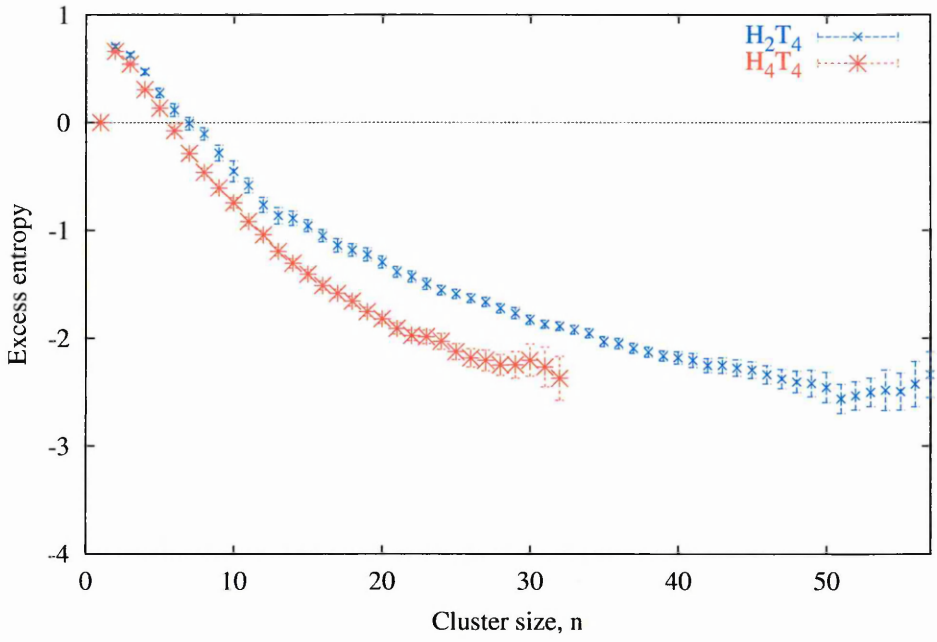

Figure 4.8: Excess entropy per monomer, $(S_n/n - S_1)/k$

have approximately the same excess enthalpies. This latter result arises because $\bar{t}^n$ is essentially the same for both species whilst $\bar{h}^n$ and $\bar{r}^n$ are, to first order, linear in n. Hence, the head-solvent interactions and the right angle bonds do not contribute strongly to the *excess* enthalpy per molecule; the small contributions they do make, are approximately the same for both species and also cancel in the excess enthalpy. The equality of $\bar{t}^n$ for the two amphiphilic species suggests that the micelles have similar compact cores of tails for any given value of n and, hence, the difference in packing entropy between H_2T_4 and H_4T_4 chains must be attributed to the different packing constraints experienced by heads of different lengths. The larger entropic loss for the amphiphiles with longer heads probably arises because of the greater conformational hindrance experienced by the longer head groups. This greater effective head-head repulsion for the H_4T_4 would be expected to lead to smaller, more

curved micelles, as is observed.

4.4 Mechanisms of micellisation

It is possible, now, to explore the mechanisms of micellisation within this model. From figures (4.6,4.3) it can be seen that the maximum in X_n does not occur at the minimum of the excess chemical potential. Indeed, in this model the excess chemical potential is a monotonically decreasing function of n; this is also seen by other workers [38, 69]. The turning points in the cluster size distribution are determined by the zeroes in the first differential of X_n (equation(4.1)) which correspond to solutions of the equation:

$$\ln(X_1) = d(n) = \frac{1}{kT}\left(\frac{\bar{\mu}^n}{n} - \bar{\mu}^1\right) + n\frac{1}{kT}\frac{d\mu_n^0}{dn} - \frac{1}{n} \tag{4.14}$$

where the activity coefficients have been set to unity to simplify the argument; this assumption will not qualitatively affect the conclusions.

The function d(n) is plotted on figure (4.9) from the numerical differentiation of $\frac{1}{kT}\left(\frac{\bar{\mu}^n}{n} - \bar{\mu}^1\right)$ for the H_2T_4 species.

Above some critical value of X_1, shown on figure (4.9), the equation $d(n) - \ln(X_1) = 0$ has two solutions and the cluster size distribution shows both a maximum and a minimum. The critical value of X_1 is clearly related to the *cmc*. For values of X_1 just above the critical value, the majority of the amphiphiles are in micellar clusters. The presence of micellar behaviour is dependent upon there being a turning

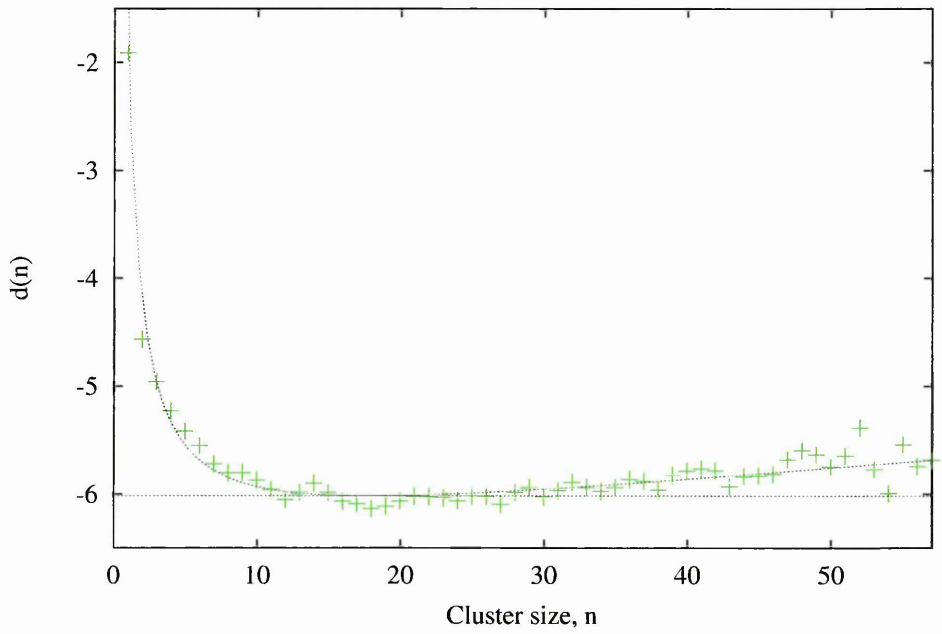

Figure 4.9: The function $d(n)$ defined in equation(4.14) for the H_2T_4 species. The dotted curve and line are included as a guide to the eye; the dotted line is the critical value of $\ln(X_1)$.

point in the function $d(n)$. However it can be shown directly from the data that the enthalpic contribution to the free energy does not, on its own, give such a turning point. Indeed, it is the competition between the excess enthalpy and the excess packing entropy which leads to a turning point in $d(n)$ and hence the formation of micelles in the model.

4.5 Conclusions

Results have been presented from simulations of a lattice model of an amphiphile and solvent mixture in which free self assembly is allowed. The results for the amphiphile types H_2T_4 and H_4T_4 both show clear *cmc*s with well defined maxima and minima in

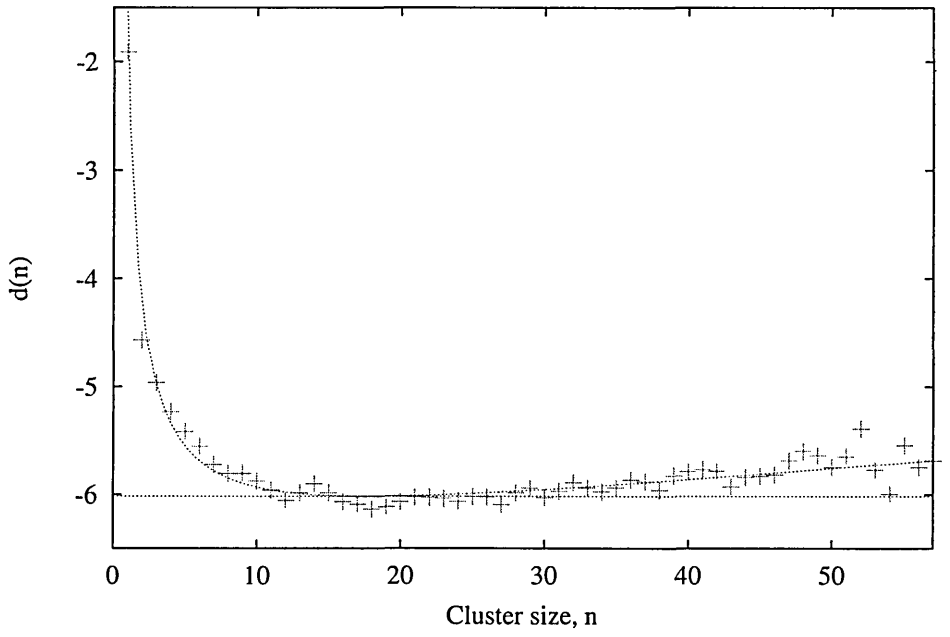

Figure 4.9: The function $d(n)$ defined in equation(4.14) for the H_2T_4 species. The dotted curve and line are included as a guide to the eye; the dotted line is the critical value of $\ln(X_1)$.

point in the function $d(n)$. However it can be shown directly from the data that the enthalpic contribution to the free energy does not, on its own, give such a turning point. Indeed, it is the competition between the excess enthalpy and the excess packing entropy which leads to a turning point in $d(n)$ and hence the formation of micelles in the model.

4.5 Conclusions

Results have been presented from simulations of a lattice model of an amphiphile and solvent mixture in which free self assembly is allowed. The results for the amphiphile types H_2T_4 and H_4T_4 both show clear *cmc*s with well defined maxima and minima in

the cluster size distribution. The data were then analysed to separate the enthalpic and entropic contributions to the excess free energy. For clusters greater than a few monomers, the entropy per monomer was found to decrease with increasing cluster size. The competition between the decreasing internal energy per monomer and entropy per monomer was found to be the source of the micellar behaviour.

The results obtained establish that the entropy of chain packing plays a central role in the formation of micelles in the class of model used in this work. It seems possible that similar arguments should apply to micellisation in non-ionic surfactants although electrostatic effects are likely to be important in ionic systems. In Chapter 5 the results presented here are confirmed using an independent algorithm which grows amphiphilic clusters.

Chapter 5

A novel scheme for the enumeration of amphiphilic chain clusters

The work in this chapter is motivated by a requirement to test the applicability of the analysis in Chapter 4 by establishing a method to enumerate directly the cluster partition function of amphiphile clusters. It also develops a method which may have wider applicability. The cluster enumeration method described here is based on an extension of a scheme first proposed by Rosenbluth [12] for enumerating self avoiding polymer chains, see section 5.1. The new scheme is itself an extension of a "degenerate" Rosenbluth scheme developed by Care [13] for lattice animal enumeration and this is summarised in section 5.3. The work by Care [13] identified that the central problem in developing a Rosenbluth algorithm for cluster counting is the problem of

determining a *degeneracy* associated with the cluster growth. This *degeneracy* is the number of different ways a cluster of the same size and shape can be constructed. In the method presented in this chapter, the degeneracies become trivial to calculate as the clusters are grown and data can be collected for all cluster sizes. However, the penalty for the simplicity of calculating the degeneracy is the need to control the way in which a cluster can grow. An alternative method of correcting for the degeneracy has been proposed by Pratt [84]. In this latter scheme, the correcting weight is more complicated to calculate and must be recalculated at each stage of the cluster growth; however the Pratt scheme does not require any restriction on the growth of the cluster.

Results are obtained for the enthalpic and entropic contributions to the process of micellisation and are compared with those obtained in the previous chapter. As for the previous chapter two surfactant systems are studied, H_2T_4 and H_4T_4.

5.1 Rosenbluth single chain growth

The original Rosenbluth scheme [12] was developed to calculate the statistical properties of self avoiding polymer chains using a Monte Carlo growth process. An ensemble of M chains is grown and during the growth a weight is calculated which can be used to construct weighted averages whose expectation values give, for example, the number of independent chains c_N of length N or the root mean square chain extension.

Each chain in the ensemble is grown by placing an initial segment on a 2- or 3-dimensional simple cubic lattice. Successive segments are then added to the end of the chain thus growing the chain in a linear sequence. Considering a chain which already has i segments, the $(i+1)^{th}$ segment is added to the end of the chain using the following algorithm:

1. assigning a normalised probability p_i^{ω} for the addition of the $(i+1)^{th}$ segment to one of the ω sites adjacent to the end segment of the chain (assigning any site that is occupied with a probability of 0 so that the chain does not grow into itself);

2. selecting one of these sites, ω_i, by simple Monte Carlo sampling, with probability $p_i^{\omega_i}$;

3. repeating steps 1 and 2 until the chain has grown to the required length N;

4. associating a weight, W_α, associated with the construction of each member, α, of the ensemble. Rosenbluth and Rosenbluth chose:

$$W_\alpha = \frac{1}{P_\alpha} = \frac{1}{\prod_{i=2}^{N} p_i^{\omega_i}} \tag{5.1}$$

   If it is impossible to complete the growth of the chain, because all directions are blocked, the weight for the chain is set to zero. The chain must be included in the counting associated with the weighted average defined below.

Provided that $\sum_\omega p_i^{\omega} = 1$, there is no necessity for all of the p_i^{ω} to be equal, but this is usually the case in the construction of athermal chains. It is important that

the choice of the p_i^ω allows the growth of all possible chains (*ie* is ergodic) and it should be noted that this choice affects the way in which the method converges to the required averages. A weighted average over the ensemble may be defined for any property, O, of the chains as follows:

$$\langle O \rangle_W = \frac{1}{N_E} \sum_{\alpha=1}^{N_E} W_\alpha O_\alpha$$

where N_E is number of chains grown in the ensemble. The expectation value of weighted averages gives [13]:

$$E[\langle O \rangle_W] = \sum_{\nu=1}^{c_N} O_\nu.$$

where the summation is over all possible distinguishable chain configurations, ν, and hence, for example:

$$E[\langle 1 \rangle_W] = c_N \tag{5.2}$$

$$E[\langle R_\nu^2 \rangle_W] = \sum_{\nu=1}^{c_N} R_{N\nu}^2 = c_N \overline{R_N^2} \tag{5.3}$$

It is possible to calculate averages in the canonical ensemble if the $p_i^{\omega_i}$ are chosen to be:

$$p_i^\omega = \frac{\exp^{-\beta(U_i^\omega - U_{i-1})}}{\sum_\omega \exp^{-\beta(U_i^\omega - U_{i-1})}}$$

and W_α is set to:

$$W_\alpha = \prod_{i=1}^{N} \left(\sum_\omega \exp^{-\beta(U_i^\omega - U_{i-1})} \right)$$

where U_i is the energy of a chain of length i and U_i^ω is the energy of the chain if the i^{th} segment is placed in position ω. Using this it is possible, for example, to calculate an estimate of the canonical partition function using:

$$E[\langle 1 \rangle_W] = \sum_{\nu=1}^{c_N} \exp^{-\beta U_\nu}$$

This is the technique used in algorithms such as the Configurational Bias Monte Carlo scheme [67].

5.2 Rosenbluth cluster growth

As previously stated, Care [13] developed a Rosenbluth technique for growing lattice animals (clusters of single sites). The technique allows the enumeration of the number of independent clusters of n single lattice sites. The method constructs each cluster by repeatedly adding sites to the surface of a connected cluster and calculating an associated weight as in the standard Rosenbluth scheme. The principal problem to be overcome is that the growth process introduces a "degeneracy" which arises from the many different ways in which the same cluster can be constructed. Thus, if each addition to the cluster is indexed sequentially as the cluster grows, there are many different labellings which may be given to the final cluster shape; this problem does not arise in chain growth because the segments are added to the chain in a linear sequence. Unfortunately, the calculation of the degeneracy is non-trivial as its value depends upon the details of the growth algorithm and the connectivity of any given cluster.

The method developed [13] for correcting for this degeneracy involves restricting the cluster growth sequence in such a way that each possible cluster labelling can be grown in only one way. This reduces the degeneracy to the number of different labellings, *ie* the degeneracy is $n!$. In the scheme [13], the clusters are constructed

using a set of labelled "bricks" and the method is based on the observation that for any connected cluster of labelled objects, a unique growth sequence can be devised in which, at each stage of the cluster growth, the next object to be added to the surface of the cluster is that which carries the lowest label. An arbitrary cluster of seven labelled bricks is shown in figure (5.1(a)) and the associated growth sequence is shown in figure (5.1(b1-b7)). In [13] the following algorithm is shown to enforce the above growth sequence during the growth of a labelled cluster.

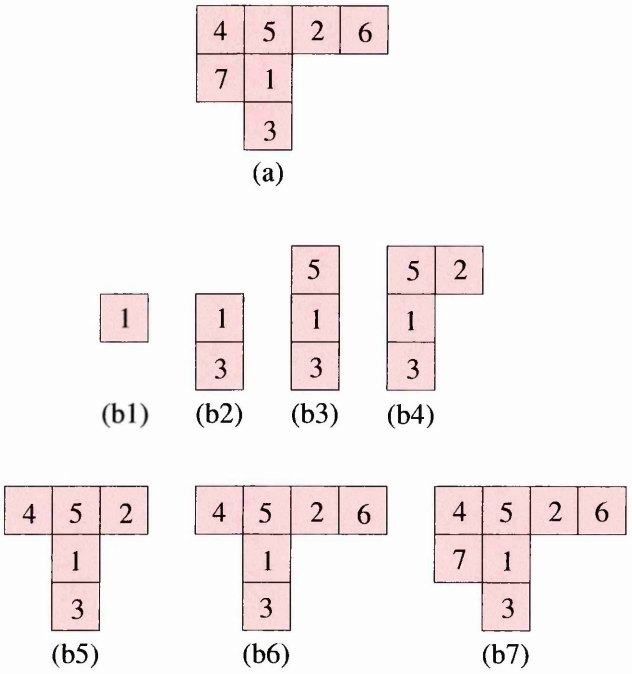

Figure 5.1: Example of growth sequence for a cluster of 7 labelled bricks. (a) Final cluster with arbitrary labelling. (b1) - (b7) Unique growth sequence to achieve labelled cluster.

5.3 Single site cluster algorithm

An ensemble of clusters of size n is constructed and for each cluster a weight is calculated which can subsequently be used to calculate weighted averages of cluster properties. Each cluster is constructed in a connected growth sequence from a set of labelled "bricks"; the label on each brick is denoted by κ, an integer in the range $1 \ldots n$ inclusive. As bricks are added to the cluster a record is maintained of the set of "surface" sites (ω in number) which are adjacent to the cluster *ie* vacant and connected to the cluster. For each such surface site a quantity κ_m is recorded which denotes the minimum κ value allowed at that site. The value of κ_m for any given surface site changes, in a manner described in detail below, as the cluster is grown.

Each cluster growth is begun by placing the brick with $\kappa = 1$ on the lattice and repeating the following steps until the cluster is fully grown:

1. Select one of the surface sites as the site which is next to be occupied and delete the site from the list of available surface sites.

2. Select one of the remaining bricks with a κ value greater or equal to the κ_m for that surface site.

3. Add the brick to the cluster and remove it from the set of available bricks.

4. Adjust the record of surface sites and their associated κ_m values.

5. Accumulate the data necessary to calculate the weight to be associated with the cluster.

Each of these steps are now commented upon in more detail:

1. The surface site to be used for the attachment of a brick is chosen from the set of ω available surface sites by simple Monte Carlo sampling with a normalised probability p_i^ω. The value of p_i^ω associated with the selected surface site is recorded for the subsequent evaluation of the weight W_α to be associated with cluster α.

2. A brick is selected from the subset of remaining bricks which have $\kappa \geq \kappa_m$ where κ_m is the minimum allowed κ value for that surface site. The brick is chosen with a normalised probability p_i^κ. The value of p_i^κ for the chosen brick is recorded to calculate W_α. In the following it is assumed that the selected brick has $\kappa = \kappa_s$;

   It was found in [13] to be preferable if the p_i^κ are chosen such that $p_i^\kappa \propto \lambda^\kappa$ where $1 \geq \lambda \geq 0$ and the parameter λ is chosen empirically, for given n, to minimise the skewness of the probability distribution of the weights, $P(W)$. λ was typically set to be 0.9.

3. The brick is added to the record of the current cluster and removed from the list of available bricks.

4. For each *old* surface site in the *current* table of surface sites, set:

$$\kappa_m|_{new} = \max(\kappa_m|_{old}, \kappa_s + 1) \tag{5.4}$$

   If none of the remaining bricks has a κ value greater than, or equal to, $\kappa_m|_{new}$,

the site is removed from the list of surface sites since no bricks could subsequently be placed at that site.

New surface sites associated with the brick placed at step 2 are identified; in order to qualify as a new surface site, the site must not appear in the current table of surface sites. The new surface sites are added to the list of adjacent sites and for each new surface site, κ_m is set to the lowest κ value of the remaining bricks since there is no restriction on the bricks which may be placed on *new* surface sites.

The adjustment of the surface sites and their associated κ_m is the key process in enforcing the unique cluster growth sequence.

5. A weight $W_\alpha = 1/(d_M \prod_{i=2}^{M} p_i^{\omega_i} p_i^{\kappa_i})$ is associated with each cluster of size $1 \leq M \leq n$ where the degeneracy $d_M = (M(n-1)!/(n-M)!$. If it is impossible to complete the growth of the cluster, because there are no available surface sites, the weight for the cluster is set to zero. Thus data can be collected for all cluster sizes up to size n simultaneously.

Once an ensemble of clusters has been generated, weighted averages can be calculated. More details of the method are given in [13] where it is shown that the method successfully enumerates lattice animals up to size 30 on both 2- and 3-dimensional simple cubic lattices.

5.4 Chain cluster growth

It is now shown how the single site cluster algorithm may be extended to enable the growth of Boltzmann weighted clusters of amphiphilic chains. An ensemble of clusters of labelled chains is grown in an analogous manner to that described in the previous section with adjacent "surface" sites labelled with κ_m values. The weights accumulated during the cluster growth may be used for the direct enumeration of the partition function, defined in Chapter 4, as well as other Boltzmann weighted cluster averages.

Each chain in the cluster is itself grown using a modified Rosenbluth method. This modification enables all possible cluster configurations to be observed by allowing the chain to be grown from any position along its length and not in a linear sequence. As chains are being grown, and not single sites, a new "degeneracy" is introduced which is associated with the number of contact points the chain makes with the cluster.

The addition of a chain to an established cluster of chains is now described in more detail.

1. A Monte Carlo choice is made to determine if the first segment of the chain to be placed should be a head or a tail. This choice is made with a probability $p_1^{seg} = 1 - \phi$ for a tail and $p_1^{seg} = \phi$ for a head. In order to correct for the bias introduced by this choice, the weight associated with the cluster is multiplied by $1/p_1^{seg}$. It is necessary to introduce the quantity ϕ because the use of

unbiased Boltzmann weights results in the first segment nearly always being selected as a head segment and this leads to poor sampling of the partition function. The value of ϕ is adjusted empirically to minimise the variance and to maximise the rate of convergence of the averages. The value of this parameter depends greatly on the ratio of head to tail segments present in an amphiphilic chain, for a chain of length 6 (H_2T_4) it was set at 0.25.

2. Once the type of segment has been selected, a Boltzmann weighted Monte Carlo choice is made of the surface site at which the segment is to be placed. Thus the probability of the segment being placed at a given surface site is made proportional to $B_1^\omega = \exp(-\beta \Delta U_s^\omega)$ where ΔU_s^ω is the change in energy associated with placing the segment at that site. The weight for the cluster is multiplied by $Z_1 = \sum_\omega B_1^\omega$ in order to achieve Boltzmann weighted averages.

3. The growth of the chain is continued by adding segments at either end of the chain. For each segment, a choice is first made of the type of segment to be placed and then a Boltzmann weighted decision is made as to the position of the segment. Once a segment from each type (head and tail) has been placed, the probability, ρ_μ^{seg}, for the addition of segment μ must be modified to ensure that the final chain has the correct structure. Thus only tails may be grown onto the tail segment and heads onto the head segment.

4. At each stage in the growth, the weight is multiplied by the appropriate factors to generate the Rosenbluth weight. If at any point during the addition of the M^{th} chain the growth becomes blocked, the weights for the clusters from M to

n inclusive are set to zero. Note that it is essential that these zero weight terms be included in the calculation of any weighted averages. After the addition of the i^{th} chain, the weight associated with the cluster growth is multiplied by a factor:

$$w_i = \prod_{\mu=1}^{s} \frac{Z_\mu}{p_{seg}^{\mu}}$$

5. As the chain is growing, a note is kept of the *maximum* κ_m value for any surface site that becomes occupied by the chain growth. When the chain is complete, a κ label is selected for it from the set of remaining κ labels which are greater or equal to this value of κ_m with probability $p_i^\kappa \propto \lambda^\kappa$ as for the single sites. Once again the parameter λ is selected empirically to minimise the variance of the final weighted averages. For a chain of length 6 (H_2T_4) it was set at 0.95;

6. After the label for the added chain has been selected, all the old and new adjacent sites have their κ_m values set as for the single site cluster algorithm;

7. A degeneracy, d_c, is associated with the growth of the individual chain. This degeneracy arises because the final chain could have started growing from any of its contact points with the original clusters and is given by:

$$d_c = \sum_{\{c\}} \begin{pmatrix} s-1 \\ c-1 \end{pmatrix} \tag{5.5}$$

where the summation $\{c\}$ is over the set of segments which make contact with the cluster onto which the chain has just been grown; future contact points of the chain are not included in this degeneracy. In equation (5.5) the numerical

value of c is determined by indexing the segments of the chain sequentially from $c = 1$ to $c = s$. If the chain makes contact at every segment $d_c = 2^{s-1}$, as would be expected.

8. The weight associated with each cluster of size $1 \leq M \leq n$ is:

$$W_\alpha = \frac{1}{d_M} \prod_{i=1}^{M} \frac{w_i}{d_{ci} p_i^{\kappa_i}}$$

where the degeneracy $d_M = (M(n-1)!/(n-M)!$. Hence data is collected for all cluster sizes up to size n simultaneously.

It should be noted that the parameters ϕ and λ do not affect the expectation value of the weighted averages since the bias they introduce is cancelled through the Rosenbluth weights. Thus the weighted averages yield essentially exact values for the measured quantities since the Rosenbluth weights are chosen to correct for any bias introduced in the sampling process. A schematic outline of the structure of the code used to implement this algorithm is given in the appendix at the end of the chapter.

5.4.1 Validation of chain cluster growth algorithm

Before running lengthy simulations and to ensure the code was correct, the following validation tests were undertaken:

1. Lattice animals up to size 30 were grown by connecting chains of length 1 and the results compared with exact results and also estimates obtained in Care's

n	New Estimate	Care Estimate	Exact Value	Lam Estimate
2	3.000×10^{0}	3.000×10^{0}	3.000×10^{0}	
3	1.500×10^{1}	1.500×10^{1}	1.500×10^{1}	
4	8.600×10^{1}	8.597×10^{1}	8.600×10^{1}	8.594×10^{1}
5	5.340×10^{2}	5.339×10^{2}	5.340×10^{2}	5.321×10^{2}
6	3.481×10^{3}	3.485×10^{3}	3.481×10^{3}	3.475×10^{3}
7	2.350×10^{0}	2.352×10^{0}	2.350×10^{4}	2.353×10^{4}
8	1.629×10^{5}	1.629×10^{5}	1.629×10^{5}	1.631×10^{5}
9	1.153×10^{6}	1.154×10^{6}	1.153×10^{6}	1.155×10^{6}
10	8.295×10^{6}	8.296×10^{6}	8.295×10^{6}	8.291×10^{6}
11	6.050×10^{7}	6.050×10^{7}	6.049×10^{7}	6.042×10^{7}
12	4.462×10^{8}	4.461×10^{8}	4.462×10^{8}	4.442×10^{8}
13	3.323×10^{9}	3.321×10^{9}	3.323×10^{9}	3.291×10^{9}
14	2.495×10^{10}	2.493×10^{10}		2.461×10^{10}
15	1.886×10^{11}	1.884×10^{11}		1.862×10^{11}
16	1.435×10^{12}	1.434×10^{12}		1.416×10^{12}
17	1.098×10^{13}	1.095×10^{13}		1.082×10^{13}
18	8.440×10^{13}	8.412×10^{13}		8.329×10^{13}
19	6.516×10^{14}	6.507×10^{14}		6.446×10^{14}
20	5.049×10^{15}	5.036×10^{15}		5.002×10^{15}
21	3.927×10^{16}	3.917×10^{16}		3.897×10^{16}
22	3.064×10^{17}	3.059×10^{17}		3.052×10^{17}
23	2.397×10^{18}	2.388×10^{18}		2.391×10^{18}
24	1.883×10^{19}	1.872×10^{19}		1.877×10^{19}
25	1.483×10^{20}	1.461×10^{20}		1.480×10^{20}
26	1.165×10^{21}	1.165×10^{21}		1.168×10^{21}
27	9.156×10^{21}	9.321×10^{21}		9.209×10^{21}
28	7.281×10^{22}	7.251×10^{22}		7.290×10^{22}
29	5.804×10^{23}	5.555×10^{23}		5.786×10^{23}
30	4.608×10^{24}	4.359×10^{24}		4.610×10^{24}

Table 5.1: Estimates of the number of lattice animals of size n on a 3- dimensional simple cubic lattice. Comparison of (i) the chain cluster algorithm using 1×10^{9} sample clusters (ii) the original single site algorithm [13] using 1.8×10^{7} sample clusters (iii) exact values and (iv) Lam's estimate [16].

original paper [13] and a separate paper used in [13] by Lam [16]. The results are given in table (5.1) and it can be seen that the new algorithm is in good agreement with the previous results.

2. A direct enumeration method was used to count the number of independent athermal arrangements of a single chain. The results from the new chain cluster algorithm are compared with these results for chains up to length 6 in table (5.2).

Chain Length	Brute Force	Rosenbluth Chain Cluster
2	6	6
3	30	30
4	150	150
5	726	726.07
6	3534	3533.36

Table 5.2: Number of distinguishable clusters of two chains. Comparison of results from the new Rosenbluth algorithm using 1×10^6 sample chains and values obtained by direct enumeration of the possible athermal configurations of a single chain.

3. Independent code was written to grow athermal clusters of two chains using a simple extension of the standard Rosenbluth scheme [12]. This scheme grew non-polar chains from any point along the chain. The new chain cluster scheme replicates these results by setting the number of tails to zero and also setting β very low ($\beta = 1 \times 10^{-9}$). The number of independent chains of length n are enumerated for both simulations and are compared on table (5.3).

Chain length	Modified Rosenbluth	Comparison Rosenbluth
3	1.105×10^4	1.105×10^4
4	3.882×10^5	3.880×10^5
5	1.180×10^7	1.179×10^7
6	3.469×10^8	3.464×10^8

Table 5.3: Comparison of the number of independent clusters calculated from the new Rosenbluth scheme and an independent code both using 1×10^6 sample clusters.

5.5 The Cluster partition function and the excess packing entropy.

The Rosenbluth scheme described above has been used directly to evaluate the cluster partition function:

$$Q_n^c(V,T) = \sum_{\{i\}} \exp(-U_i^{cn}/kT)$$

where the summation $\{i\}$ is over all distinguishable connected n-clusters, assuming that the amphiphile chains are indistinguishable. The superscript c indicates that the summation does not include any translation of the cluster. It is also possible to evaluate the canonical averages $\bar{t}^n$, $\bar{h}^n$ and $\bar{r}^n$ of the number of tail-solvent interactions, head-solvent interactions and right angle bonds for clusters of size n defined, for example, by relations of the form:

$$\bar{t}^n = \{t_n\}_W = \sum_{\{i\}} p_i^{cn} t_i^n$$

where $\{\}_W$ is the Rosenbluth Boltzmann weighted average and:

$$p_i^{cn} = \frac{\exp(-U_i^{cn}/kT))}{Q_n^c}$$

where p_i^{cn} is the canonical ensemble probability of a particular n-cluster. The average internal energy per n-cluster, $\bar{U}^{cn}$ is defined by:

$$\frac{1}{kT}\bar{U}^{cn} = \beta(\bar{t}^n + \gamma\bar{h}^n + \epsilon\bar{r}^n) = \sum_{\{i\}} p_i^{cn} U_i^{cn}$$

Using the relation:

$$-\ln(Q_n^c) = \frac{\bar{U}^{cn}}{kT} - \frac{S^{cn}}{k} = \frac{\bar{U}^{cn}}{kT} + \sum_{\{i\}} p_i^{cn} \ln p_i^{cn}$$

With the excess packing entropy per monomer defined by:

$$\frac{1}{k}\left(\frac{S^{cn}}{n} - S^{c1}\right) = -\frac{1}{n}\sum_{\{i\}} p_i^{cn} \ln p_i^{cn} + \sum_{\{i\}} p_i^{c1} \ln p_i^{c1} \tag{5.6}$$

5.6 Rosenbluth simulations

The Rosenbluth scheme was used to evaluate the cluster excess entropy and excess enthalpy, $(1/kT)(\bar{U}^n/n - \bar{U}^1)$, for clusters up to size 6 for H_4T_4 and up to size 8 for H_2T_4 by growing 10^9 clusters and calculating appropriate weighted averages. The values of the parameters ϕ and λ were established empirically to minimise the variance of $P(W)$, the probability distribution of the cluster weights. The effect of varying these parameters is illustrated in figure (5.2) where it can be seen that this distribution is approximately log-normal.

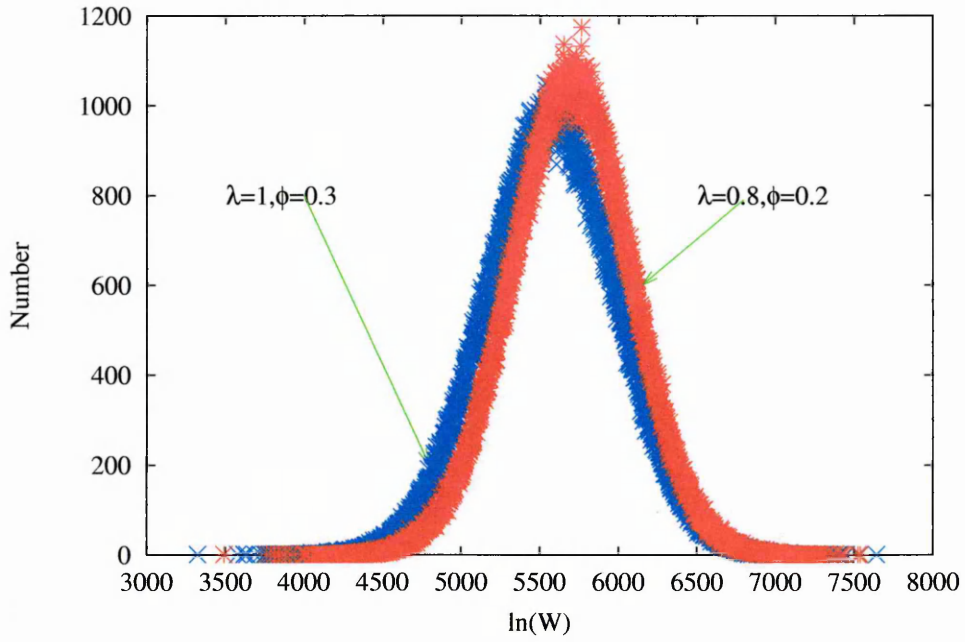

Figure 5.2: Probability distribution, $P(\ln(W))$, of the weights W for different values of the parameters λ and ϕ.

5.7 Comparison with Metropolis simulations

As a first comparison, the monomer partition function Q_1^c was calculated exactly and was found to agree with the Rosenbluth estimate to within 0.003% for H_2T_4. The quantities $\bar{t}^1$, $\bar{h}^1$ and $\bar{r}^1$ were also calculated from Q_1^c and for H_2T_4 found to agree with the Rosenbluth values to within 10^{-5} and with the Metropolis data to within 0.6%.

From Chapter 4 it is possible to obtain estimates of the excess enthalpy and entropy as a function of cluster size. This data combined with data from the Rosenbluth scheme are shown in figures (5.3 & 5.4). It can be seen that the two methods are in good agreement up to clusters of size 8 for H_2T_4 and 6 for H_4T_4. Above these

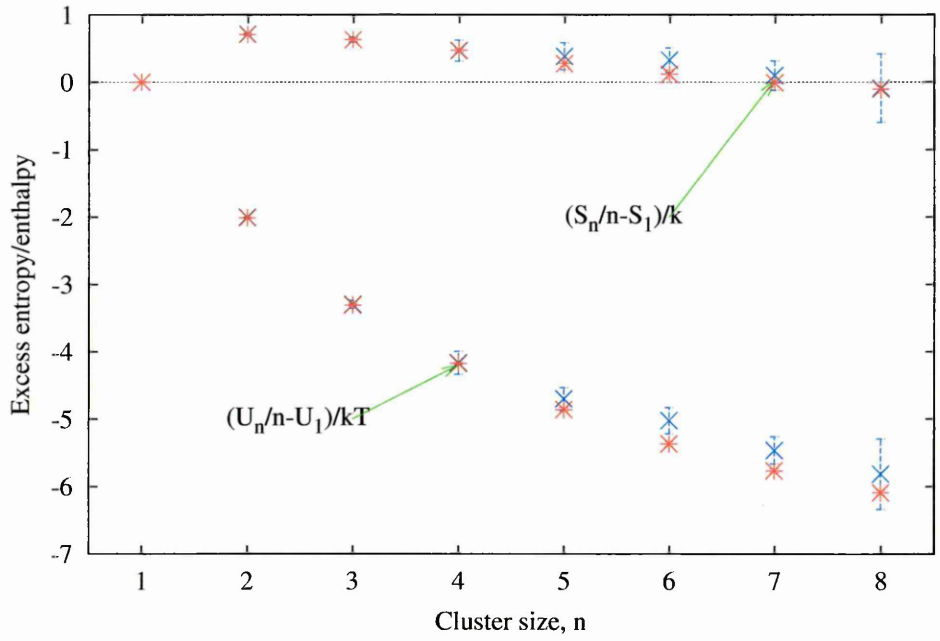

Figure 5.3: Comparison of excess entropy per molecule and excess enthalpy per molecule for the H_2T_4. Blue: Rosenbluth cluster growth; Red: Metropolis Monte Carlo.

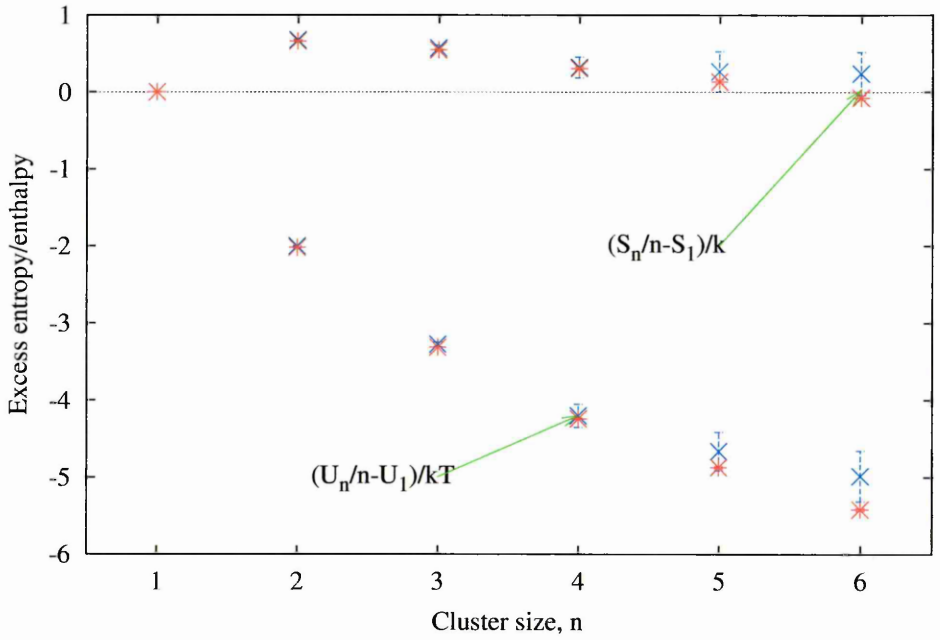

Figure 5.4: Comparison of excess entropy per molecule and excess enthalpy per molecule for the H_4T_4. Blue: Rosenbluth cluster growth; Red: Metropolis Monte Carlo.

cluster sizes, the Rosenbluth scheme becomes unusable because the sampling distribution of the weights becomes highly skew and the averages obtained have very high variance. This problem was recognised by Batoulis and Kramers in reference [85] in their study of polymer chain growth using Rosenbluth methods. However, these authors concluded that acceptable sampling of polymer chains up to length $n = 240$ was possible using Rosenbluth methods. Although a linear chain is not directly comparable with a cluster of individual chains it still seems possible that improvements to the algorithm described here may yield accurate information on significantly larger clusters than have been possible here. It seems likely that the problem arises here because the algorithm is not efficiently sampling the important clusters for large n. This is probably due to the amphiphile clusters being constructed sequentially which does not efficiently sample the lowest energy structures for large n. However, it may be possible to improve the cluster growth algorithm to more efficiently sample these low energy structures.

The logarithm of the cluster partition function is estimated to have an error of less than 1% for the data presented here. This error estimate is obtained from appropriate block averaging of the results. However the sampling distributions are highly skew and it is therefore possible that these values are underestimates of the true errors. The excess enthalpy is very sensitive to the nature of the clusters which are sampled and the measured uncertainties are correspondingly higher. Larger uncertainties are, therefore, observed in the estimates of the excess entropy which is calculated from equation (5.6).

The Rosenbluth results provide an independent check of the validity of the approximation in Chapter 4 (4.10) for small n and therefore supports the use of this result over the wider range of n in the analysis of the Monte Carlo data presented in Chapter 4.

5.8 Conclusion

It has been shown that the modified Rosenbluth scheme can successfully calculate the partition function for clusters up to size 8 for H_2T_4 and up to size 6 for H_4T_4. The results obtained are in good agreement with data extracted from Metropolis NVT simulations and allow us unambiguously to identify the entropy of packing within a micelle. They also confirm that the approximation made of a dilute solution is a correct one. This validation of the analysis of the Metropolis data supports the use of the Metropolis method to extract the excess entropy and enthalpy to higher cluster sizes than is possible with the Rosenbluth scheme. Analysis of the data obtained in this way yields an insight into the relative importance of the enthalpy and packing entropy in micellisation and these results are studied further in Chapter 6.

The Rosenbluth method samples from distributions that become highly skew as the cluster size increases and this limits the applicability of the current method to relatively small clusters. However it may be possible to improve the method of cluster growth within the spirit of the current algorithm and obtain data for larger cluster sizes.

5.9 Appendix

Cluster surface algorithm

The partition function of a cluster of chains involves a summation over a very large number of possible configurations, approximately 1.5×10^{50} for a cluster of size 10 (H_2T_4). In order to obtain a reasonable estimate of the partition function, it is necessary to sample a sufficiently large and representative set of these clusters. If this is to be carried out in an acceptable amount of time, the code used to implement it must be very efficient. The slowest part of the cluster growth code is the part that keeps track of the cluster surface and it is therefore this part which needs the most optimisation. The following algorithm is the result of this optimisation and describes the addition of a single chain to a pre-existing cluster:

1. Grow an amphiphilic chain on to a three dimensional lattice as described in section 5.4. As the chain is grown, store all of the 6 nearest neighbours of each placed chain segment in a temporary "surface" list (*templist*) as an integer value $index = x_{pos}l^2 + y_{pos}l + z_{pos}$, where x_{pos}, y_{pos} and z_{pos} correspond to the position on the three dimensional lattice of the surface site and l is the lattice box length.

2. Merge *templist* with a permanent surface list, *permlist*, from which the start of the next chain will be selected. As the lists are merged undertake the following:

(a) Check each surface site stored in *templist* before it is added to *permlist* to determine if it is occupied. This is done by examining the corresponding lattice site in the array *lattice* using the stored *index* number. This site is not added to *permlist* if it is occupied.

(b) Check each surface site stored in *templist* to determine if it is already present on *permlist*. This is done using the list $\kappa_m list$ which provides the κ_m value of the surface site. If the lattice site has not been examined before (*ie* it is not on *permlist*) then it will have a κ_m value of 0. If the surface site has been visited before then it is not added to *permlist*, however the environment of the surface site has changed and therefore this has to be updated, see 2c & 2d.

(c) Calculate Boltzmann weights associated with placing either a head or tail at a surface site to be added to the *permlist*. These values are stored in a list *boltzlist* which is related to the *permlist* using another list *sortlist*.

(d) Calculate the change in head-solvent, tail-solvent interactions and increase in right angle bonds associated with placing either a head or tail at a surface site to be added to *permlist*. These values are stored in *intlist* which is related to the *permlist* using *sortlist*.

3. Remove all surface sites stored in *permlist* that have now become occupied due to the chain just grown.

4. Update the κ_m values of all the surface sites in *permlist*.

(a) Surface sites are given a κ_m value as explained in section 5.4.

(b) Surface sites that are no longer available due to them having a κ_m value greater than that of the largest remaining κ label, are given Boltzmann weights of zero (so that they are never selected or grown into).

5. Update weights and start the growth of the next chain.

To summarise, a total of three lattice lists and four sequential lists are used for this algorithm, and they are:

- *lattice* - This is a lattice list which records whether a site is occupied by using a number greater than 0 which also identifies the amphiphile present at that site.

- *sortlist* - This lattice list gives the appropriate position on the Boltzmann and interaction list for a specific surface site, expressed as an index number (*index*).

- κ_m*list* - This lattice list stores the κ_m values of each surface site. For speed old surface sites that are now occupied by chain segments are not reset to zero; only new or changed sites are modified.

- *templist* - This sequential list stores all the surface sites of the new chain grown onto the cluster.

- *permlist* - This sequential list stores all the surface sites of the cluster, expressed as an index number, available to place the first segment of the next chain.

- *boltzlist* - This sequential list stores the Boltzmann weight associated with placing either a head or a tail at a certain lattice site, found using *sortlist*. This is used to calculate the weights and also the probability of placing a segment at that position.

- *intlist* - This sequential list stores the change in head-solvent and tail-solvent interactions associated with placing a head or a tail at a certain lattice site. This is used to calculate the enthalpy.

It should be noted that as the chain is grown, surface sites added to *templist* may be repeated or even grown into. Every surface site could be pre-checked before being added to the list but this is computationally expensive so the checking is done as *templist* is merged with *permlist*.

Chapter 6

The effect of amphiphilic properties on micellar behaviour

In Chapters 3 and 4, Metropolis Monte Carlo simulations of two micellar surfactant systems were used to calculate the entropic and enthalpic parts of the excess chemical potential. It was demonstrated that it was the competition between these two constituent parts that leads to not only the formation of micelles and their coexistence with monomers but also the position of the *cmc* and the overall phase behaviour of the surfactant. These new results were confirmed using a technique developed in Chapter 5 which directly enumerated clusters of amphiphilic chains. There has also been extensive work in the literature (*eg* [19–33]) on the organisation of amphiphiles into aggregates and how different types of amphiphile alter the shape and size distribution of micelles.

Chapters 4 and 5 used two different amphiphiles for the simulations. These had the same tail length (T_4), chain stiffness (ϵ) and head-solvent interaction energy (γ) but had differing head lengths (H_2 & H_4). It was found that the larger head resulted in smaller more compact micelles with a higher *cmc*. In this Chapter, a much wider range of amphiphiles are studied not only by changing the head length but also by making the head more soluble (increasing γ) and the amphiphilic chain less flexible (increasing ϵ). As a result of this analysis, functional forms are proposed for the excess enthalpy, the excess entropy and the excess chemical potential. All of this combined enables a prediction to be made for the behaviour of a certain type of amphiphile in solution, within the limitations of the model.

6.1 The Simulations

To analyse the excess entropy and enthalpy in more detail, it was necessary to run extensive simulations at a variety of different concentrations and with numerous chain types. Table (6.1) shows the different chain types analysed, using Metropolis Monte Carlo techniques, at the following concentrations; 0.125%, 0.25%, 0.5%, 1%, 2%, 3%, 4%, & 5%.

Each chain was cooled, as for Chapter 4, from $T^* = 1.50$ to $T^* = 1.18$ which was found to be a suitable temperature for studying micellar behaviour for chains with a tail length of 4 (T_4). The tail length was left at 4 as this effectively fixed β, leaving the molecular properties dependent on ϵ and γ. Small systems, containing only 512

Head No.	Tail No.	ϵ	γ	β^{-1}
1	4	0.0	-2.0	1.18
1	4	1.0	-2.0	1.18
1	4	2.0	-2.0	1.18
1	4	1.0	-4.0	1.18
2	4	1.0	-1.0	1.18
2	4	0.0	-2.0	1.18
2	4	1.0	-2.0	1.18
2	4	2.0	-2.0	1.18
2	4	1.0	-3.0	1.18
3	4	1.0	-2.0	1.18
4	4	1.0	-1.0	1.18
4	4	0.0	-2.0	1.18
4	4	1.0	-2.0	1.18
4	4	2.0	-2.0	1.18

Table 6.1: Chain parameters for simulations

amphiphiles, were used for the cooling to save time. The main results were obtained using larger systems replicated from these smaller systems. The amphiphiles were randomly grown onto the lattice using a self avoiding random walk. One hundred thousand steps were allowed per temperature step (2×10^4 to achieve equilibrium), and at the end of each step the temperature was lowered by $\delta T^* = 0.02$ and the process repeated.

The last lattice snapshot from the $T^* = 1.18$ step was replicated either 8 or 4 times depending on the system concentration (because of computer memory limitations). This provided a thermalised starting lattice for the larger simulations which were then run for 2×10^6 Monte Carlo steps (2×10^4 to achieve equilibrium). Data for the cluster size distribution *etc* were collected every 4^4 steps. In terms of real world time, each concentration for each amphiphilic chain type took approximately half a week to run on a Silicon Graphics R5000 giving, altogether, 56 weeks of simulations.

6.2 Results

All of the data from the simulations were analysed as for Chapter 4 with the average cluster size distribution and *cmc* calculated. Figures (6.1 & 6.2) show the effect that head length has on the average cluster size distribution and position of the *cmc*. Figures (6.3 & 6.4) show the effect of changing γ and figures (6.5 & 6.6) the effect of changing ϵ. All data shown are from systems with a total amphiphile concentration of 3%.

As observed in Chapter 4, a short head group gives large micelles with a broader distribution than a larger head group. For a head group size of 1 this reaches limiting behaviour with clusters of sizes 40-100 present combined with a low monomer concentration. The results from this head group type are not used for the analysis in this chapter as the amphiphile is too weakly hydrophilic to exhibit similar micellar behaviour to previous simulations, and may have begun to phase separate. This is also observed for the H_2T_4, $\gamma = -1$ amphiphile which forms clusters of size 30-90. Table (6.2) shows the final set of chain parameters used for the excess entropy and enthalpy analysis. Although there are not as many parameter sets as before, there is still enough information to make inferences on amphiphilic behaviour. Using the average cluster size distributions and the *cmc* from the final set of simulations, the excess chemical potential is calculated from equation (2.7) (see Chapter 3 & 4), and its constituent parts, the excess enthalpy and the excess entropy from equation (4.11). Figures (6.7-6.15) shows these data.

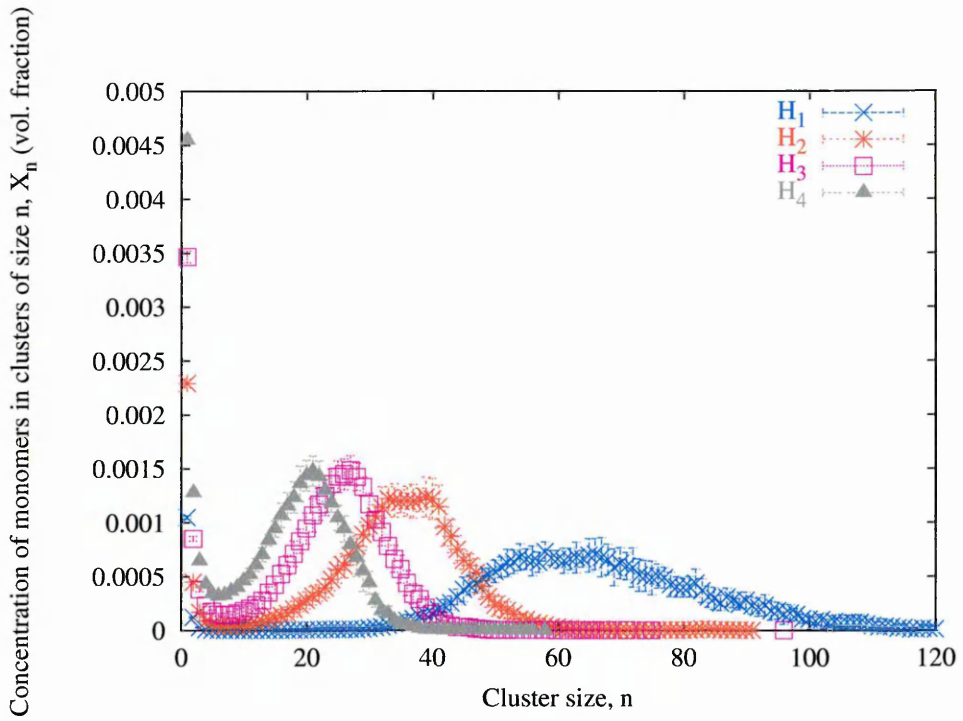

Figure 6.1: Variation in the average cluster size distribution as a result of increasing the amphiphilic head length, ($\gamma = -2$, $\epsilon = 1$, $\beta^{-1} = 1.18$, T_4, 3% vol.)

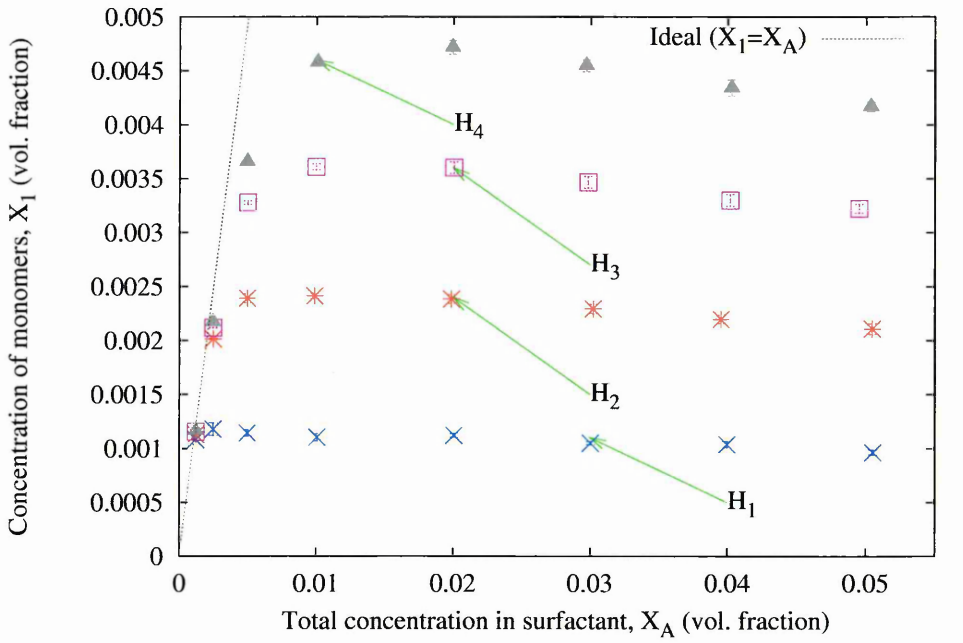

Figure 6.2: Variation in the *cmc* as a result of increasing the amphiphilic head length. ($\gamma = -2$, $\epsilon = 1$, $\beta^{-1} = 1.18$, T_4, 3% vol.)

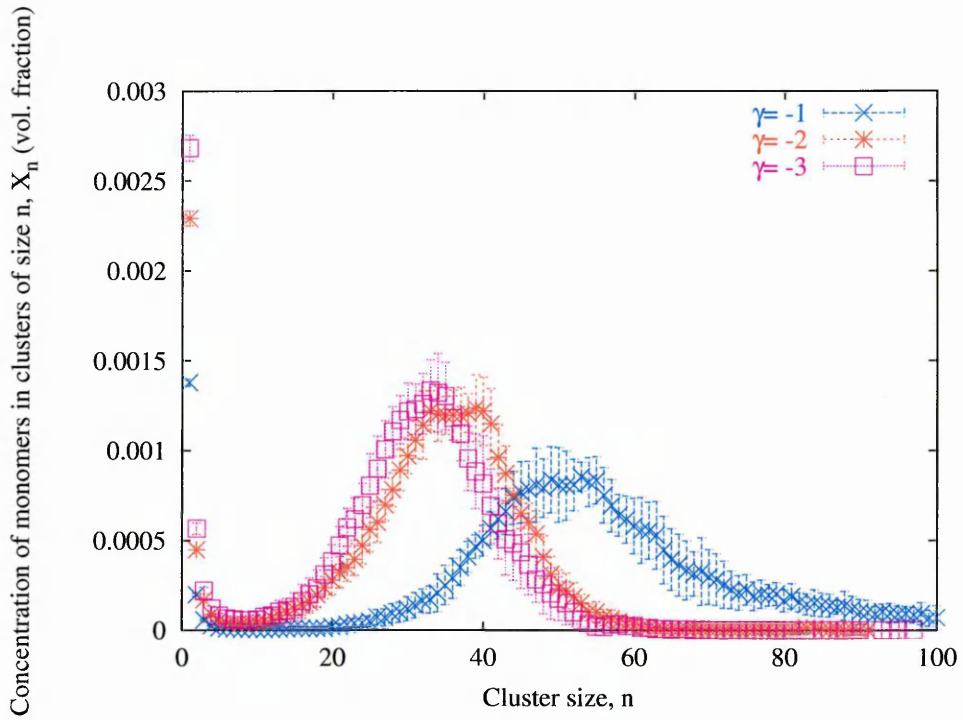

Figure 6.3: Variation in the average cluster size distribution as a result of increasing the amphiphilic head-solvent interaction energy ($\epsilon = 1$, $\beta^{-1} = 1.18$, H_2T_4, 3% vol.)

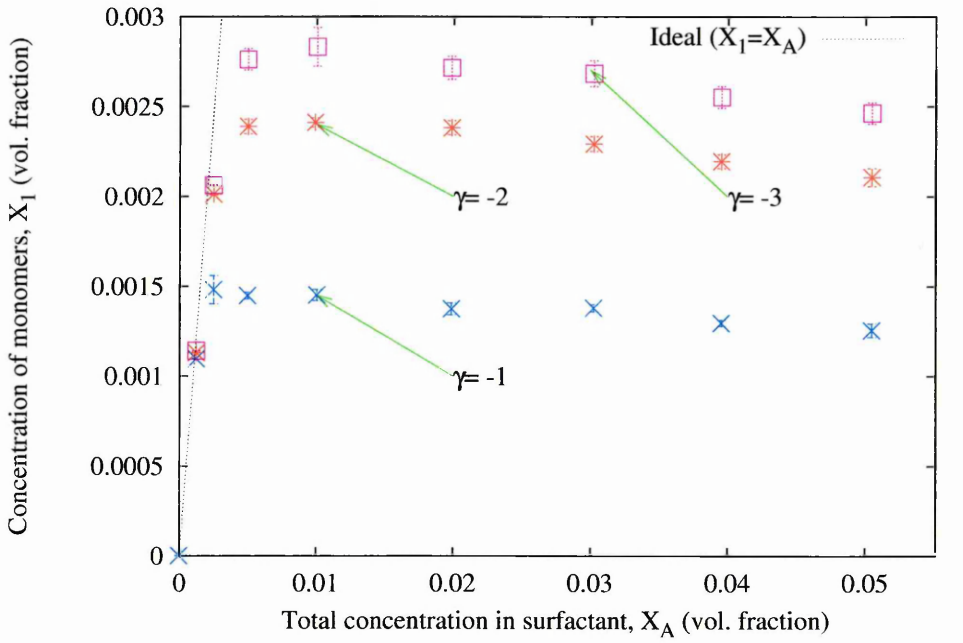

Figure 6.4: Variation in the *cmc* as a result of increasing the amphiphilic head-solvent interaction energy. ($\epsilon = 1$, $\beta^{-1} = 1.18$, H_2T_4, 3% vol.)

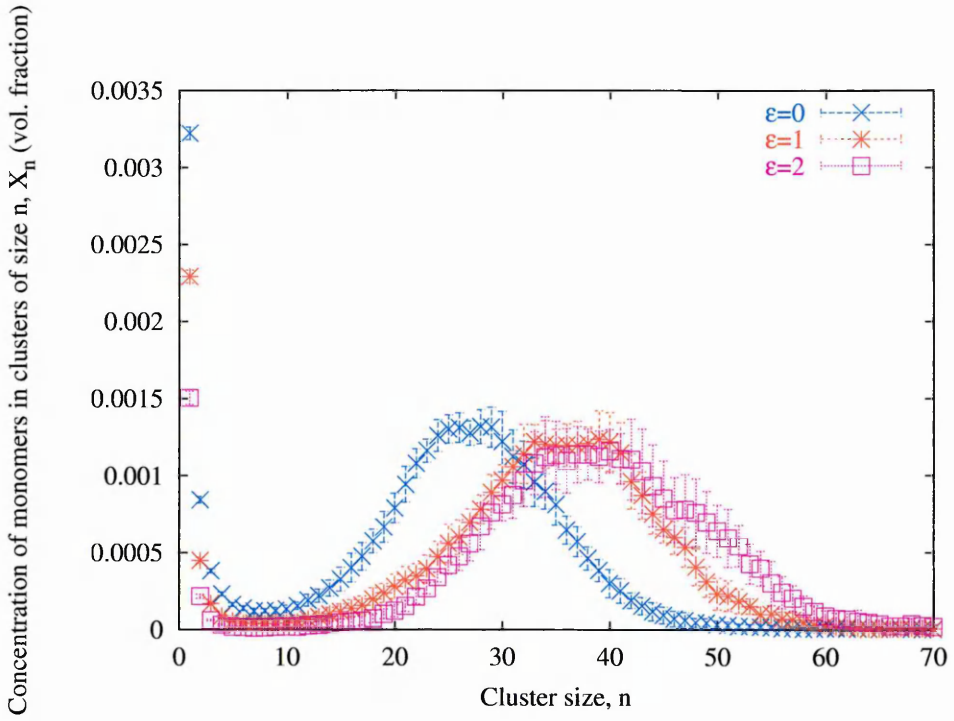

Figure 6.5: Variation in the average cluster size distribution as a result of increasing the amphiphilic chain stiffness, ($\gamma = -2$, $\beta^{-1} = 1.18$, H_2T_4, 3% vol.)

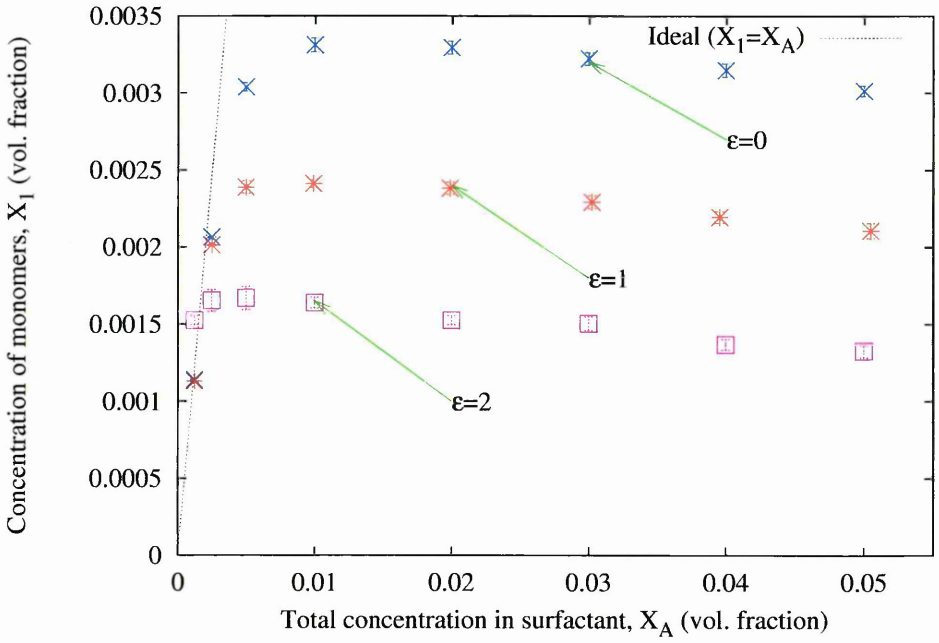

Figure 6.6: Variation in the *cmc* as a result of increasing the amphiphilic chain stiffness. ($\gamma = -2$, $\beta^{-1} = 1.18$, H_2T_4, 3% vol.)

Head No.	Tail No.	ϵ	γ	β^{-1}
2	4	0.0	-2.0	1.18
2	4	1.0	-2.0	1.18
2	4	2.0	-2.0	1.18
2	4	1.0	-3.0	1.18
3	4	1.0	-2.0	1.18
4	4	1.0	-1.0	1.18
4	4	0.0	-2.0	1.18
4	4	1.0	-2.0	1.18
4	4	2.0	-2.0	1.18

Table 6.2: Chain parameters used for excess entropy and enthalpy analysis

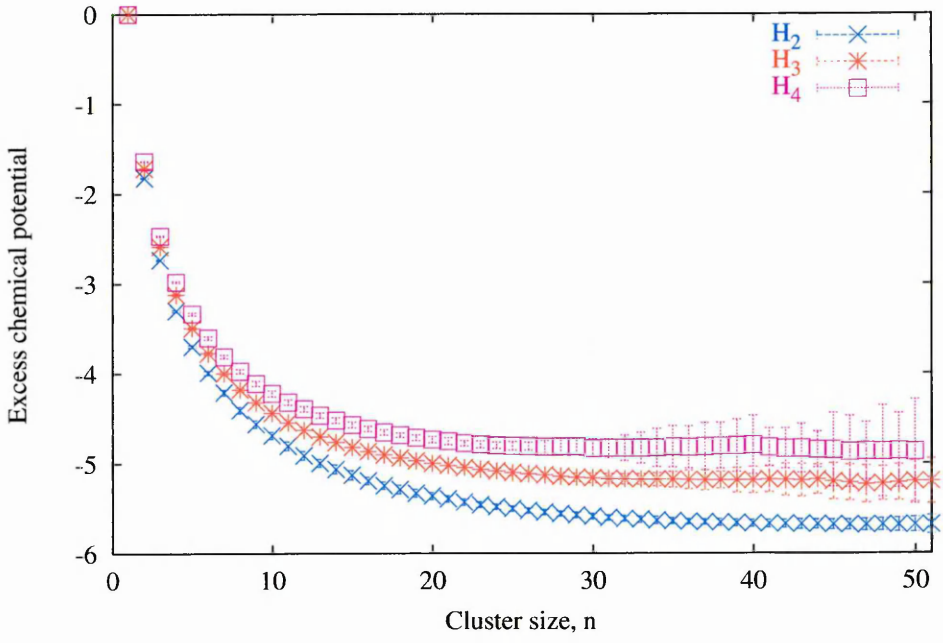

Figure 6.7: Variation in the excess chemical potential as a result of increasing the amphiphilic head length. ($\gamma = -2$, $\epsilon = 1$, $\beta^{-1} = 1.18$, T_4, 3% vol.)

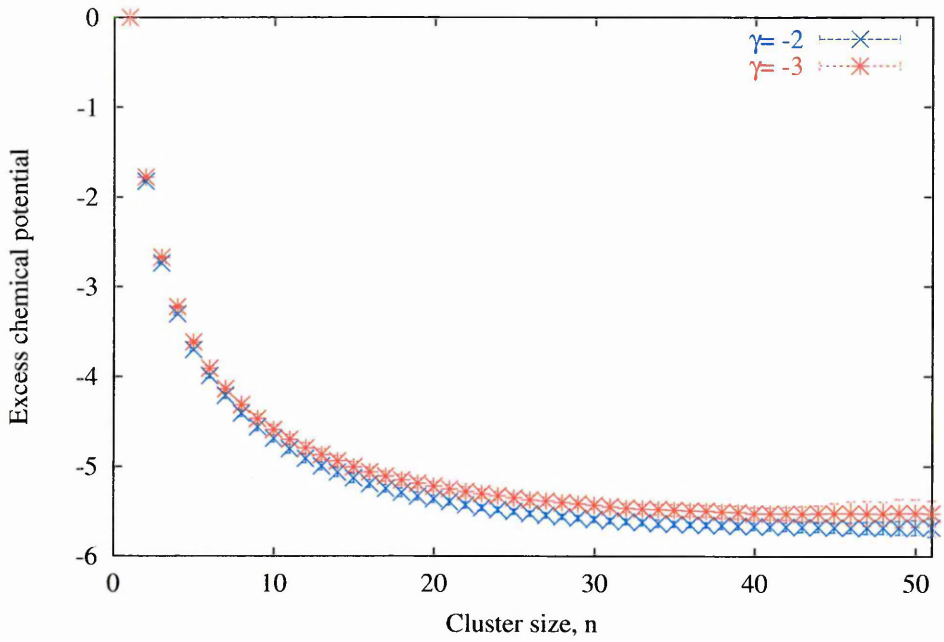

Figure 6.8: Variation in the excess chemical potential as a result of increasing the amphiphilic head-solvent interaction energy. ($\epsilon = 1$, $\beta^{-1} = 1.18$, H_2T_4, 3% vol.)

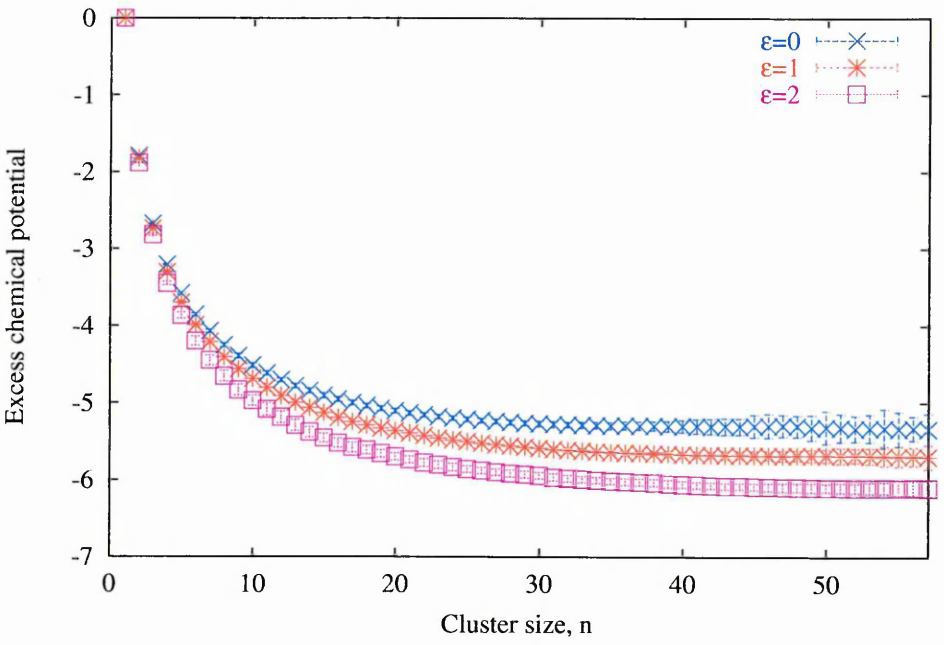

Figure 6.9: Variation in the excess chemical potential as a result of increasing the amphiphilic chain stiffness. ($\gamma = -2$, $\beta^{-1} = 1.18$, H_2T_4, 3% vol.)

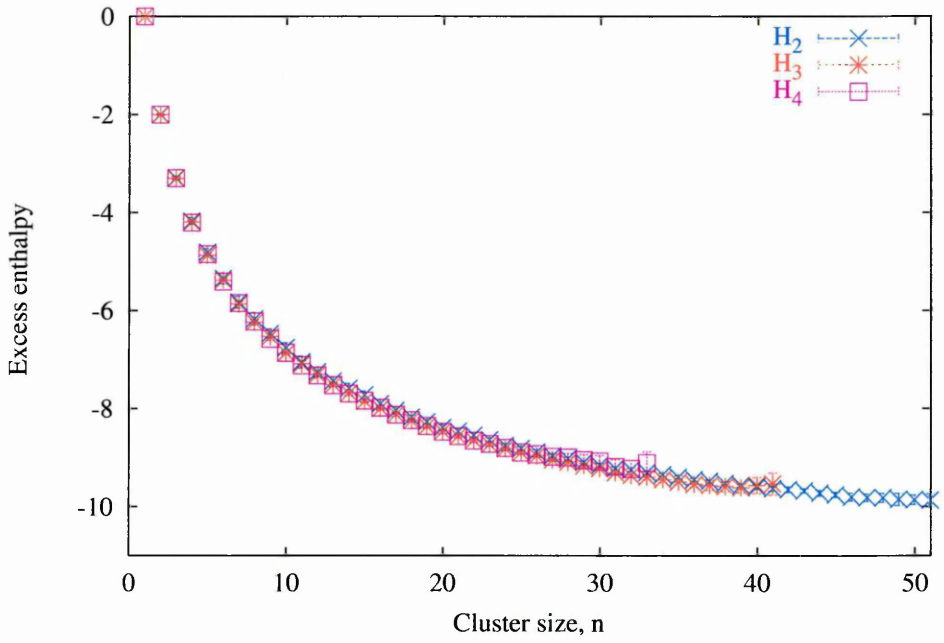

Figure 6.10: Variation in the excess enthalpy as a result of increasing the amphiphilic head length. ($\gamma = -2$, $\epsilon = 1$, $\beta^{-1} = 1.18$, T_4, 3% vol.)

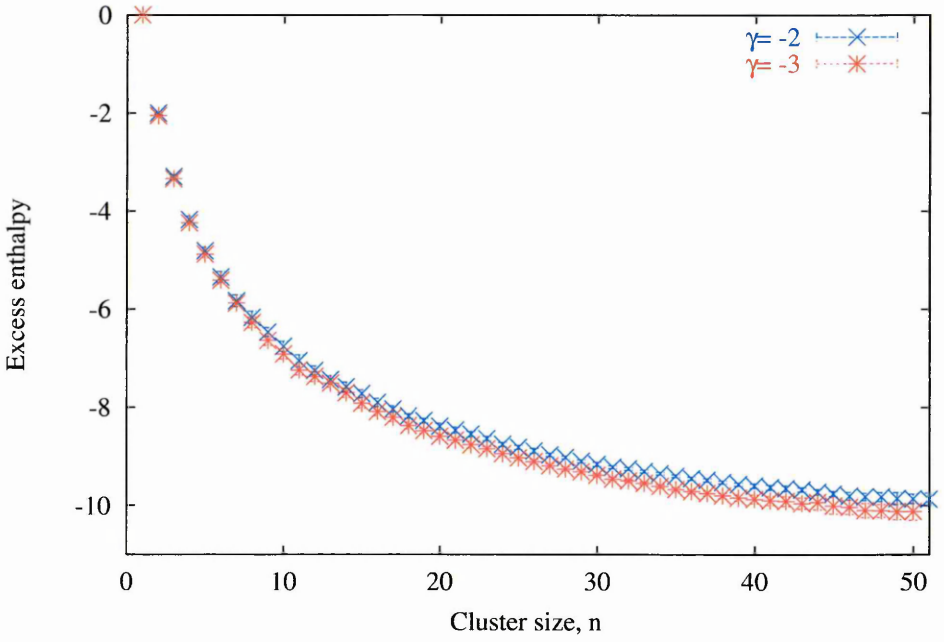

Figure 6.11: Variation in the excess enthalpy as a result of increasing the amphiphilic head-solvent interaction energy. ($\epsilon = 1$, $\beta^{-1} = 1.18$, H_2T_4, 3% vol.)

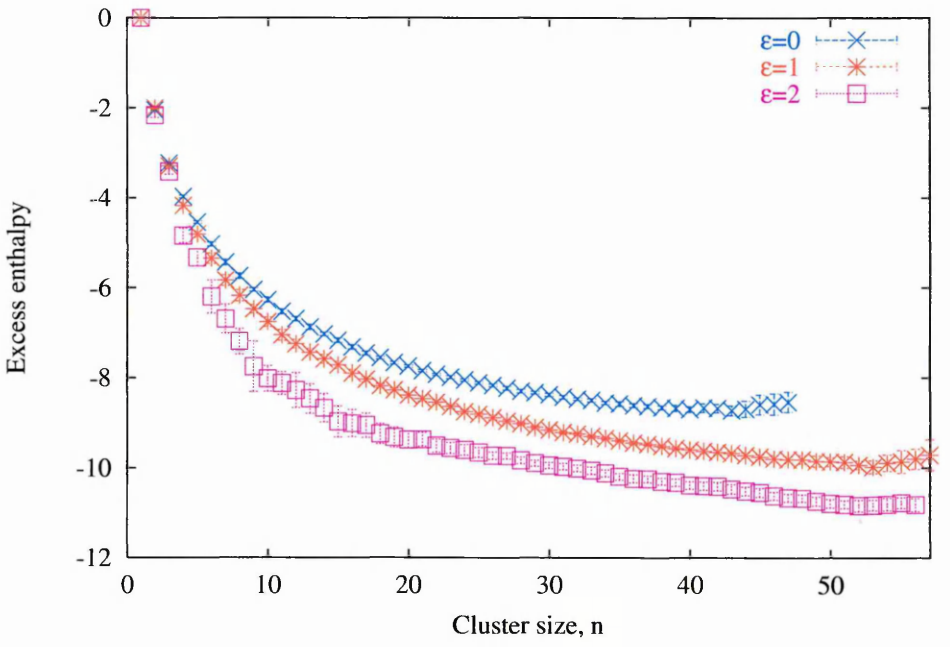

Figure 6.12: Variation in the excess enthalpy as a result of increasing the amphiphilic chain stiffness. ($\gamma = -2$, $\beta^{-1} = 1.18$, H_2T_4, 3% vol.)

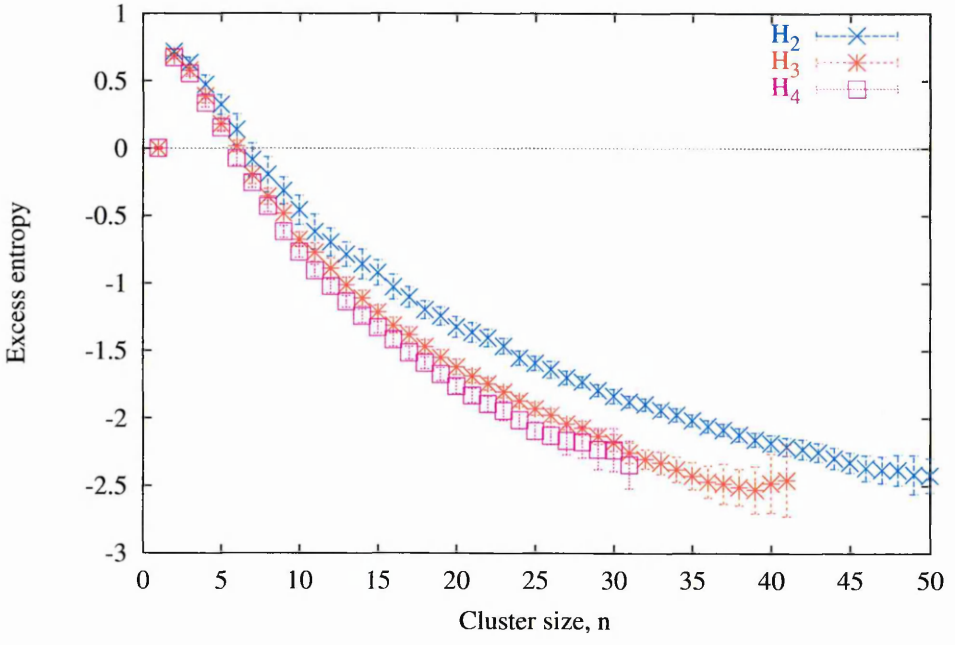

Figure 6.13: Variation in the excess entropy as a result of increasing the amphiphilic head length. ($\gamma = -2$, $\epsilon = 1$, $\beta^{-1} = 1.18$, T_4, 3% vol.)

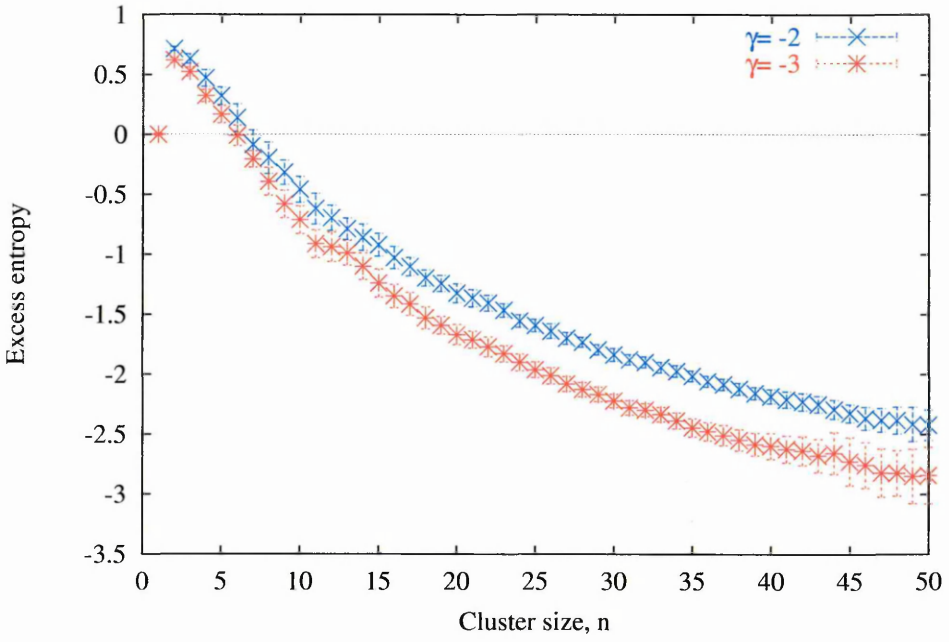

Figure 6.14: Variation in the excess entropy as a result of increasing the amphiphilic head-solvent interaction energy. ($\epsilon = 1$, $\beta^{-1} = 1.18$, H_2T_4, 3% vol.)

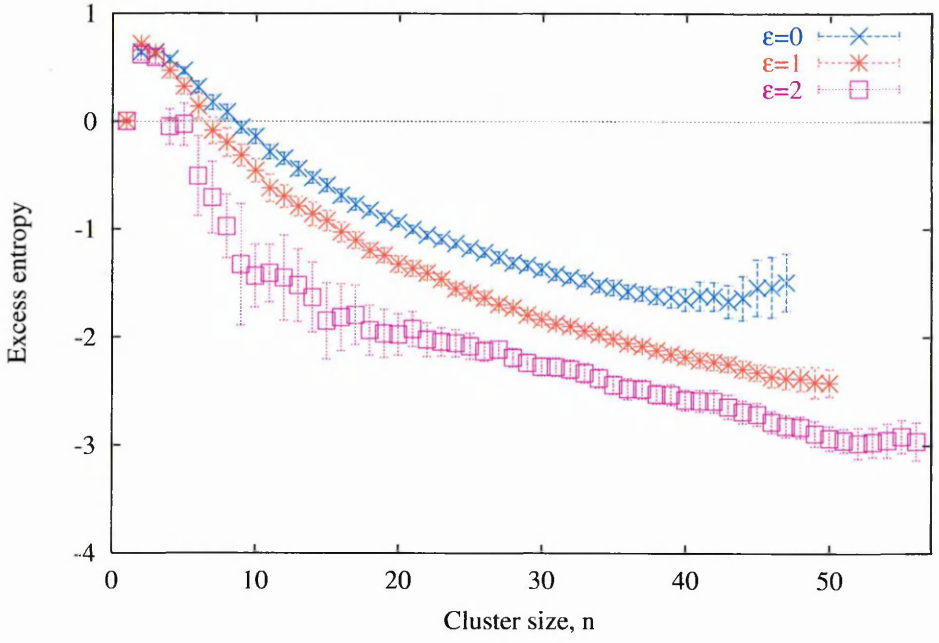

Figure 6.15: Variation in the excess entropy as a result of increasing the amphiphilic chain stiffness. ($\gamma = -2$, $\beta^{-1} = 1.18$, H_2T_4, 3% vol.)

6.3 Modelling the excess enthalpy

The excess enthalpy of an amphiphilic system is calculated using equation (4.12). This shows us that the excess enthalpy is constructed from three components:

1. The excess head-solvent interactions: $\left(\frac{\bar{h}^n}{n} - \bar{h}^1\right)$
2. The excess right angle bonds: $\left(\frac{\bar{r}^n}{n} - \bar{r}^1\right)$
3. The excess tail-solvent interactions $\left(\frac{\bar{t}^n}{n} - \bar{t}^1\right)$

Figure (6.16) shows $\bar{h}^n$, $\bar{r}^n$ & $\bar{t}^n$ for the H_2T_4, $\gamma = -2$, $\epsilon = 1$ amphiphile. It is important to understand how each of these chain variables alters $\bar{h}^n$, $\bar{r}^n$ & $\bar{t}^n$ if a suitable model for the excess enthalpy is to be formed.

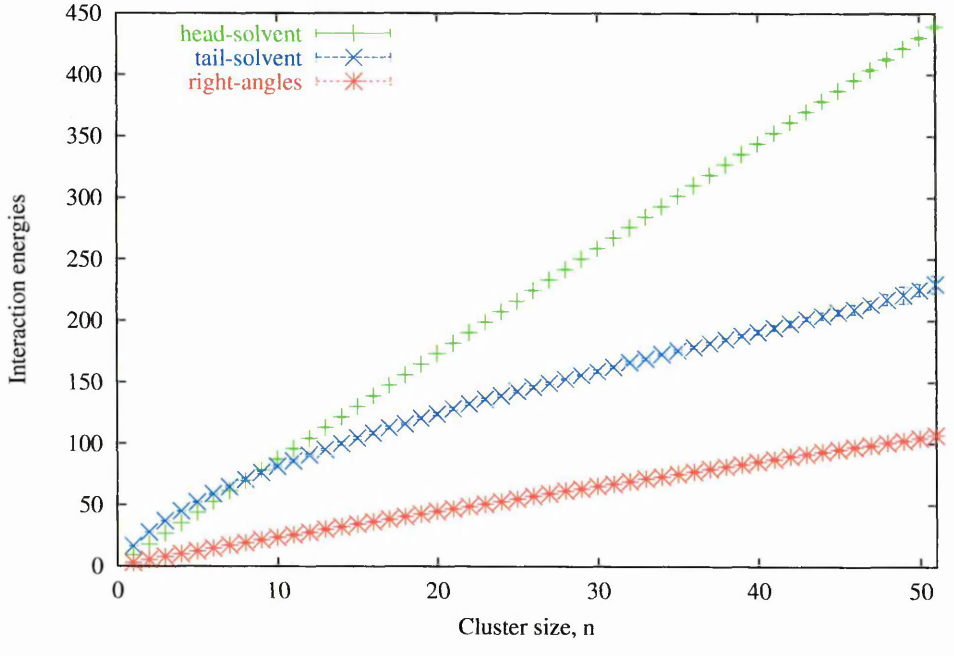

Figure 6.16: Graph of the average number of head-solvent, tail-solvent and right angle bonds for a cluster of size n. ($\gamma = -2$, $\epsilon = 1$, $\beta = 1.18$, T_4, H_2, 3%)

6.3.1 The average head-solvent interactions, $\bar{h}^n$

An initial analysis of the data in figure (6.16) suggests that $\bar{h}^n$ is approximately linearly dependent on n. To substantiate this, the head group environment (head-solvent interactions) of both a monomer in solution and a monomer in a cluster of size, n, is calculated, and the difference found $\frac{\bar{h}^n}{n} - \bar{h}^1$. Figure (6.17) shows the excess head-solvent interactions of a monomer in a cluster of size n for the amphiphile chain type H_2T_4, $\gamma = -2$, $\epsilon = 1$. From this graph it is apparent that, apart from a slight decrease as n increases, the head group environment for all sizes of cluster is approximately the same. Fitting this curve for each amphiphile chain type using the functional form $\bar{h}^1(\frac{n^{\alpha_h}}{n} - 1)$ shows the extent of this decrease and the effect of varying the head group parameters. Table (6.3) shows the results of these fits.

Table (6.3) shows that the decrease in head-solvent interactions $\bar{h}^1$ is approximately 2% of the maximum and that $\bar{h}^n$ increases approximately linearly as $\bar{h}^1 n$. There are changes in $\bar{h}^1$ and α_h associated with the different amphiphilic chains and these are summarised below:

- Increasing head length: for every extra head segment added there is an approximate increase in $\bar{h}^1$ of 4. This is due to 4 new head-solvent interactions being created. There is also a slight increase in α_h for the larger head group.
- Increasing hydrophilic strength (γ): slight increase in both $\bar{h}^1$ & α_h due to increased solubility.
- Increasing chain stiffness (ϵ): slight increase in $\bar{h}^1$ due to increase in chain

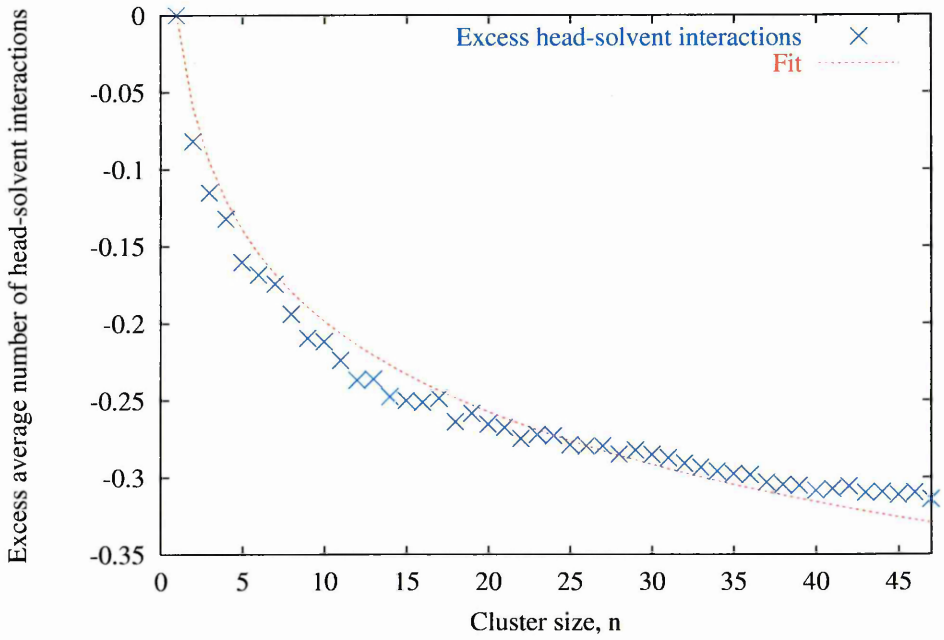

Figure 6.17: Graph of the excess average number of head-solvent interactions, $\frac{\bar{h}^n}{n} - \bar{h}^1$, for a cluster of size, n, from the H_2T_4, $\gamma = -2$, $\epsilon = -1$ system with fit added for comparison.

HeadNo.	*TailNo.*	ϵ	γ	β^{-1}	$\bar{h}^1$	α_h
2	4	0.0	-2.0	1.18	8.853	0.988
2	4	1.0	-2.0	1.18	8.910	0.990
2	4	2.0	-2.0	1.18	8.960	0.992
2	4	1.0	-3.0	1.18	8.962	0.997
3	4	1.0	-2.0	1.18	12.879	0.994
4	4	1.0	-1.0	1.18	16.620	0.982
4	4	0.0	-2.0	1.18	16.787	0.996
4	4	1.0	-2.0	1.18	16.874	0.996
4	4	2.0	-2.0	1.18	16.945	0.996

Table 6.3: $\bar{h}^1$ from the simulations & α_h from the $\bar{h}^1(\frac{n^{\alpha_h}}{n} - 1)$ fit.

stiffness. Approximately no change in α_h.

6.3.2 The average number of right-angle bonds, $\bar{r}^n$

Examining the average number of right-angle bonds on figure (6.16) it is also observed that $\bar{r}^n$ rises approximately linearly. Again calculating $\frac{\bar{r}^n}{n} - \bar{r}^1$, figure (6.18), shows that monomers in clusters of all sizes have approximately the same number of right angle bonds, with an approximate change in $\bar{r}_1$ of 20% from the maximum number of right angle bonds in a chain of length n. Fitting these curves as for the head-solvents with $\bar{r}^1(\frac{n^{\alpha_r}}{n} - 1)$ gives the results shown on Table (6.4).

The correction this time is greater than for the head-solvent interactions, however for a first approximation it is ignored as for the heads. With this approximation, the average number of right-angle bonds also increases as $\bar{r}^1 n$. The effect on $\bar{r}^1$ & α_r of the changes to the amphiphilic chains are summarised below:

- Increasing head length: significant increase in $\bar{r}^1$ and slight increase in α_r due to larger overall chain length making it possible for more right angle bonds to exist.

- Increasing hydrophilic strength (γ): slight decrease in both $\bar{r}^1$ and α_r due to increased solubility of head causing it to straighten.

- Increasing chain stiffness (ϵ): decrease in both $\bar{r}^1$ and α_r as chain becomes stiffer.

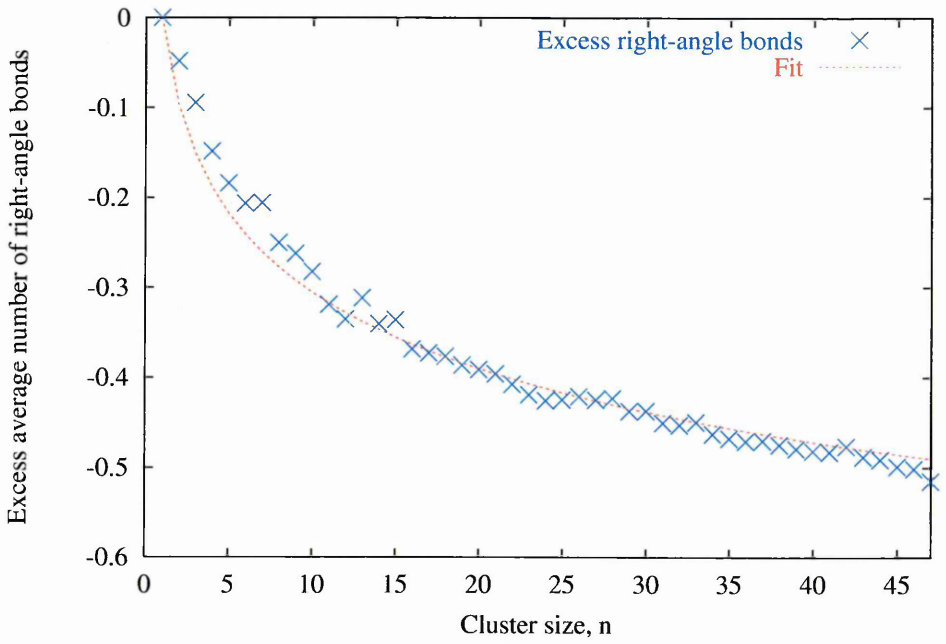

Figure 6.18: Graph of the excess average number of right-angle bonds, $\frac{\bar{r}^n}{n} - \bar{r}^1$, for a cluster of size, n, from the H_2T_4, $\gamma = -2$, $\epsilon = -1$ system with fit added for comparison.

HeadNo.	*TailNo.*	ϵ	γ	β^{-1}	$\bar{r}^1$	α_r
2	4	0.0	-2.0	1.18	3.242	0.969
2	4	1.0	-2.0	1.18	2.612	0.946
2	4	2.0	-2.0	1.18	1.796	0.903
2	4	1.0	-3.0	1.18	2.573	0.943
3	4	1.0	-2.0	1.18	3.191	0.949
4	4	1.0	-1.0	1.18	3.868	0.957
4	4	0.0	-2.0	1.18	4.697	0.976
4	4	1.0	-2.0	1.18	3.736	0.954
4	4	2.0	-2.0	1.18	2.551	0.917

Table 6.4: $\bar{r}^1$ from the simulations & α_r from the $\bar{r}^1(\frac{n^{\alpha_r}}{n} - 1)$ fit.

6.3.3 The average number of tail-solvent interactions, $\bar{t}_n$

From figure (6.16) it is clearly shown that the behaviour of $\bar{t}^n$ is not linear. Plotting $\frac{\bar{t}^n}{n} - \bar{t}^1$, figure (6.19), shows a similar monotonically decreasing function in n as for h^n and r^n although t^n has much stronger n dependence. Table (6.5) shows the variable α_t from the fit to the functional form $\bar{t}^1(\frac{n^{\alpha_t}}{n} - 1)$, as for $\bar{h}$ and $\bar{r}$.

From the power law fit it is apparent that the excess tail-solvent interactions grow as $n^{\frac{2}{3}}$. This is of course only approximate as both α_t and $\bar{t}^1$ change with the type of amphiphile studied. These changes are summarised below:

- Increasing head length: approximately no change in $\bar{t}^1$ and α_t as the head length does not dramatically altering the solvent contact with the hydrophobic core.
- Increasing hydrophilic strength (γ): approximately no change in $\bar{t}^1$ and α_t again due to all micelles in this study having similar core interactions.
- Increasing chain stiffness (ϵ): increase in $\bar{t}^1$ as increase in chain stiffness causes more tails to be in contact with the solvent, decrease in α_t.

6.3.4 Examining the micellar core.

As described in Chapter 2, a micelle consists of a hydrophobic core surrounded by a hydrophilic outer shell. What has been shown from this analysis is that the excess enthalpy of a micellar system is dominated by the contribution from the tail-

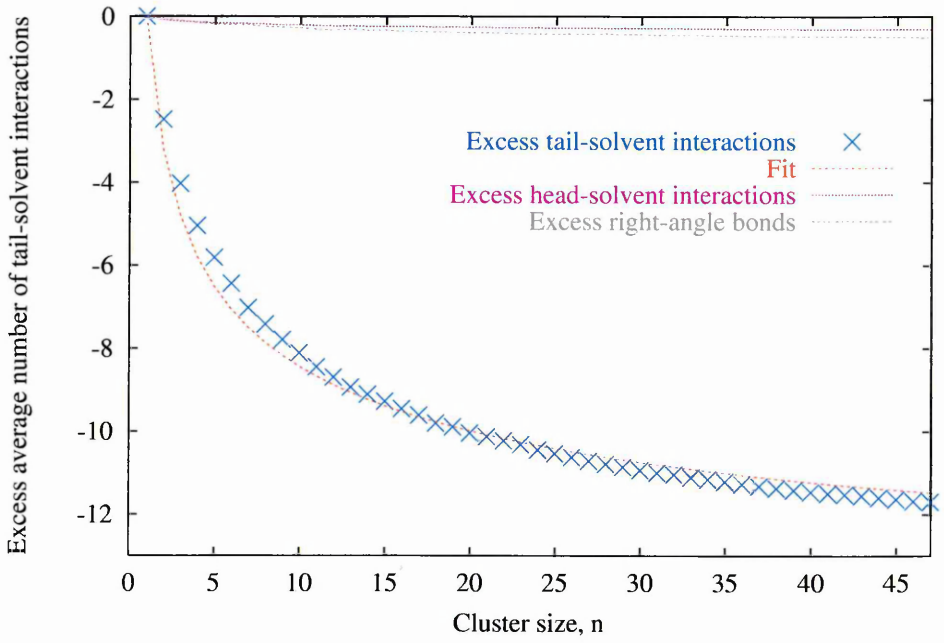

Figure 6.19: Graph of the average number of tail-solvent interactions, $\frac{\bar{t}^n}{n} - \bar{t}^1$, for a cluster of size, n, with fit, $\frac{\bar{h}^n}{n} - \bar{h}^1$ and $\frac{\bar{r}^n}{n} - \bar{r}^1$ added for comparison.

HeadNo.	*TailNo.*	ϵ	γ	β^{-1}	$\bar{t}^1$	α_t
2	4	0.0	-2.0	1.18	15.927	0.689
2	4	1.0	-2.0	1.18	16.235	0.681
2	4	2.0	-2.0	1.18	16.587	0.670
2	4	1.0	-3.0	1.18	16.295	0.684
3	4	1.0	-2.0	1.18	16.199	0.686
4	4	1.0	-1.0	1.18	15.973	0.675
4	4	0.0	-2.0	1.18	15.870	0.702
4	4	1.0	-2.0	1.18	16.200	0.691
4	4	2.0	-2.0	1.18	16.577	0.677

Table 6.5: $\bar{t}^1$ from the simulations & α_t from the $\bar{t}^1(\frac{n^{\alpha_t}}{n} - 1)$ fit.

solvent interaction energy and hence the structure of the hydrophobic core. The core is also affected by altering the chain conformation directly, by varying ϵ, but not by altering the hydrophilic strength, increasing γ or the head length. As the clusters grow the environment of a tail segment changes consistent with the growth of spherical micelles, however the environment of a hydrophilic head group does not change and there is no significant straightening or bending of the amphiphilic chains. The average number of head-solvent interactions per cluster of size n, $\bar{h}_n$, and the average number of right-angle bonds per cluster of size n, $\bar{r}_n$, are both approximately linear. The average number of tail-solvent interactions per cluster of size n grows as $n^{\frac{2}{3}}$ and with all these facts in mind the following can be written from equation (4.12):

$$\frac{\bar{h}_n}{n} - \bar{h}_1 \simeq 0 \quad , \quad \frac{\bar{r}_n}{n} - \bar{r}_1 \simeq 0 \quad \text{so} \quad \frac{1}{kT}\left(\frac{\bar{U}^n}{n} - \bar{U}^1\right) \simeq \beta\left(\frac{\bar{t}_n}{n} - \bar{t}_1\right)$$

To understand this better an ideal micellar core is considered. This is constructed using amphiphilic tail segments which can be visualised as simple cubes of side a. A perfect sphere grown using amphiphilic tails with a length, T_s, would have a volume of:

$$\text{Volume} = T_s a^3 n = \frac{4}{3}\pi r^3 \quad \text{with} \quad r = \left(\frac{3T_s a^3 n}{4\pi}\right)^{\frac{1}{3}}$$

As the interest here is in the number of tail-solvent interactions present in a micelle, which all reside on the surface of the core, the surface area of a sphere is:

$$Area = 4\pi r^2 = 4\pi\left(\frac{3T_s a^3 n}{4\pi}\right)^{\frac{2}{3}} = 4\pi\left(\frac{3}{4\pi}\right)^{\frac{2}{3}} T_s^{\frac{2}{3}} n^{\frac{2}{3}} = A T_s^{\frac{2}{3}} n^{\frac{2}{3}}$$

where $A = 4\pi\left(\frac{3}{4\pi}\right)^{\frac{2}{3}}$. This area would translate to tail-solvent interactions if it

where not for the attachment of head segments to every tail segment. This will reduce the number of tail-solvent interactions by at least a factor of n. This gives:

$$t_n^{ideal} = AT_s^{\frac{2}{3}} n^{\frac{2}{3}} - n \tag{6.1}$$

where t_n^{ideal} is the number of tail-solvent interactions for a perfect micellar core. The micelles observed from simulations are self-assembled onto cubic lattices and as a result will never form perfect spheres. A certain degree of solvent penetration also has to be accounted for. All of this results in a higher average number of tail-solvent interactions. This can be expressed as a fraction, $R_n = \frac{\bar{t}_n}{t_n^{ideal}}$, for a cluster of size n. A plot of this surface roughness R_n for the amphiphile type H_2T_4, $\epsilon = 1$, $\gamma = -2$ is shown on figure (6.20).

From table (6.6) it can be seen that the micelles formed in the simulations have significant surface roughness approximately 50% more tail-solvent interactions than an ideal micelle. This can be examined in more detail by proposing a fit showing the n-dependence of the curves. For simplicity the fit $R_1 n^{\alpha_R}$ was used with R_1 taken directly from table (6.6). The value α_R was found to average at approximately 0.083 with the fit for the H_2T_4, $\epsilon = 0$, $\gamma = -2$ system shown on figure (6.20). This empirical fit suggests that the surface roughness is only affected by the rigidity of the amphiphilic chain, negligible changes being associated with increasing the head length and head group hydophilicity. This is in agreement with figures (6.10-6.12) and can be used to write a final equation for $\bar{t}_n$.

$$\bar{t}_n \simeq R_1 n^{0.083} \left(AT_s^{\frac{2}{3}} n^{\frac{2}{3}} - n \right)$$

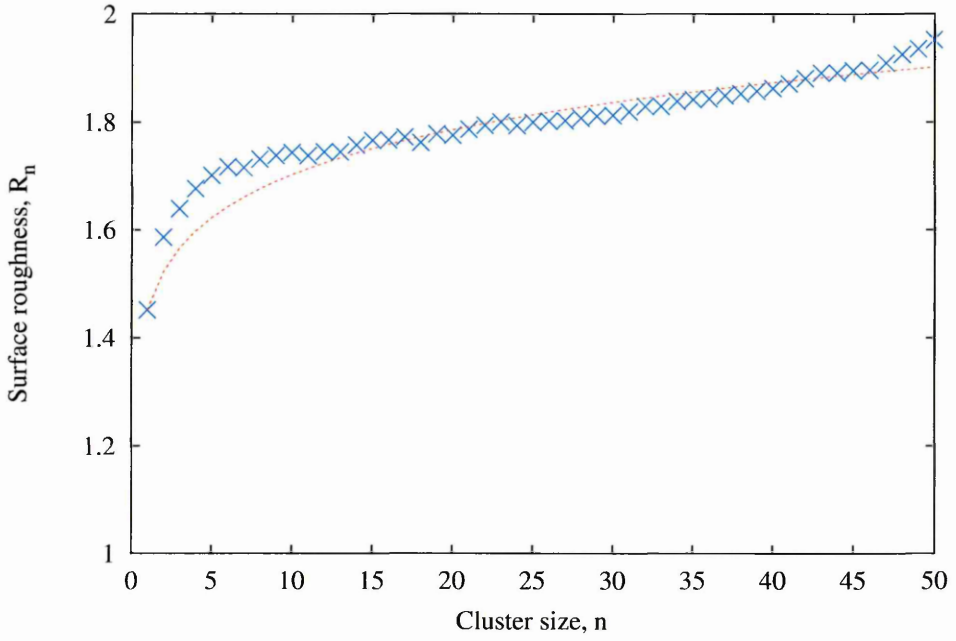

Figure 6.20: The surface roughness fraction, R_n, for the amphiphile type H_2T_4 ($\gamma = -2$, $\epsilon = 1$, $\beta^{-1} = 1.18$, 3% vol.) with fit shown.

Head No.	**Tail No.**	ϵ	γ	β^{-1}	R_1
2	4	0.0	-2.0	1.18	1.424
2	4	1.0	-2.0	1.18	1.451
2	4	2.0	-2.0	1.18	1.483
2	4	1.0	-3.0	1.18	1.457
3	4	1.0	-2.0	1.18	1.448
4	4	1.0	-1.0	1.18	1.428
4	4	0.0	-2.0	1.18	1.419
4	4	1.0	-2.0	1.18	1.448
4	4	2.0	-2.0	1.18	1.482

Table 6.6: The fraction $R_1 = \frac{\bar{t}_1}{t_1^{ideal}}$.

A first approximation for the excess enthalpy in which the contribution from the heads and right-angles (only individually as right-angles are still included in the R_n parameter) are set to zero can now be defined as:

$$\frac{1}{kT}\left(\frac{\bar{U}^n}{n} - \bar{U}^1\right) \simeq \beta R_1 \left[AT_s^{\frac{2}{3}}\left(\frac{n^{0.83}}{n^{\frac{1}{3}}} - 1\right) - n^{0.083} + 1\right] \tag{6.2}$$

6.4 The excess entropy of packing

The results from the previous section have shown that the excess enthalpy is only slightly affected by the change in head length and head hydophilicity (γ). This does not account for the significant shifts in the excess chemical potential curves seen on figures (6.7 & 6.8). Examining figures (6.13 & 6.14) shows that the entropy is altered by the head group and also by the chain stiffness. The following is a description of the changes in the excess entropy observed due to the different amphiphilic types:

- Increasing head length: increasing the head length causes the excess entropy curve to decay faster following the initial rise.
- Increasing hydrophilic strength (γ): making the head more soluble causes the excess entropy curve to decay more rapidly.
- Increasing chain stiffness (ϵ): making the amphiphile more stiff causes the excess entropy curve to decay more rapidly up to a point ($\epsilon = 2$) where there is so little data for small clusters that it is not reliable.

Summarising the above points, it can be shown that the increasing the solubility of the amphiphiles (increasing either head length or hydrophilic strength γ) will cause the excess entropy curve to converge to a minimum more quickly.

6.4.1 Modelling the excess entropy of packing

As figures (6.13-6.15) show, the excess entropy is a complicated function. It seems to represent the competition between the increase in entropy of a cluster compared to a monomer due to the larger number of amphiphiles and the decrease in entropy caused by the restrictions imposed on the clusters by the hydrophobic effect. Using the algorithm shown in Chapter 5 for growing clusters of amphiphilic chains it is possible to construct clusters of athermal chains giving a value for the excess entropy which is not affected by the hydrophobic effect. Figure (6.21) shows this curve and it is seen that it rises steeply and begins to flatten off.

Any functional form proposed for the excess entropy curve must therefore include a strong initial rise followed by a decay which becomes dominant at large n (greater than 8). Many different functions were tried with the following showing the closest fit (it must be noted that this functional form has no physical significance):

$$\frac{S_n}{n} - S_1 = \underbrace{S_A\left(\frac{1}{n^{\alpha_d}} - 1\right)}_{decay} \underbrace{-S_B\left(\frac{1}{n^{\alpha_r}} - 1\right)}_{rise}$$

where $S_A(\frac{1}{n^{\alpha_d}} - 1)$ is the decay of the entropy due to the hydrophobic effect and $-S_B(\frac{1}{n^{\alpha_r}} - 1)$ is the rise of the entropy due to the increase in configurations possible. Fitting this function to the systems under study gives values of α_d and α_r of

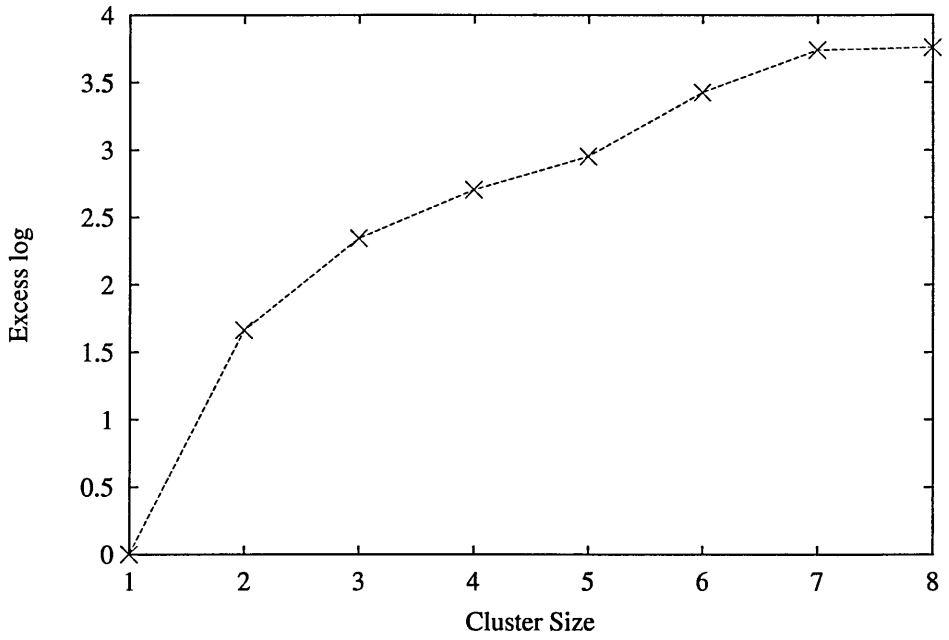

Figure 6.21: Plot of excess entropy excluding the hydrophobic effect for the H_2T_4 system.

approximately $\frac{1}{3}$ and $\frac{2}{3}$ respectively. S_A and S_B vary widely with systems; Table (6.7) shows the parameters for each case studied. Figure (6.22) shows the fit for the H_2T_4, $\gamma = -2$, $\epsilon = 1$ case with $S_A = 19.84$ and $S_B = 12.97$.

Some of the fit variables presented in the table are not reliable due to the poor quality of the original data (*eg* H_2T_4, $\epsilon = 2$, $\gamma = -2$, $\beta = 1.18$). Ignoring these bad data, the changes in the fit parameters shown on table (6.7) can be summarised as follows:

- Increasing head length: both S_A and S_B increasing resulting in a faster initial rise and a quicker fall off.

- Increasing hydrophilic strength (γ): as for the head length, increasing S_A and

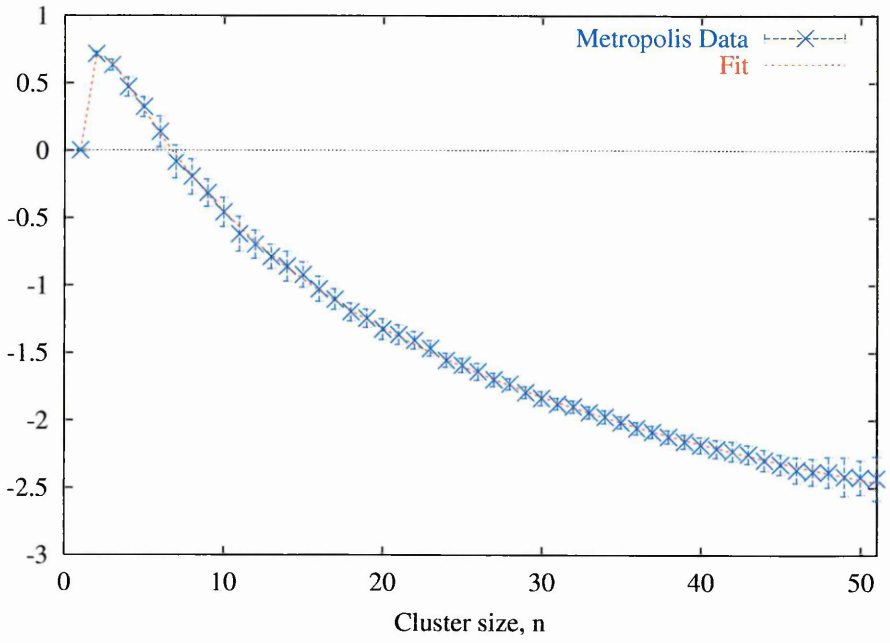

Figure 6.22: Graph of the excess entropy for the amphiphile type H_2T_4 ($\gamma = -2$, $\epsilon = 1$, $\beta^{-1} = 1.18$, 3% vol.) with the fit added.

Head No.	**Tail No.**	ϵ	γ	β^{-1}	S_A	S_B
2	4	0.0	-2.0	1.18	16.68	11.14
2	4	1.0	-2.0	1.18	19.84	12.97
2	4	2.0	-2.0	1.18	16.40	9.80
2	4	1.0	-3.0	1.18	21.33	13.68
3	4	1.0	-2.0	1.18	21.59	13.91
4	4	1.0	-1.0	1.18	19.30	12.79
4	4	0.0	-2.0	1.18	19.98	13.01
4	4	1.0	-2.0	1.18	21.32	13.60
4	4	2.0	-2.0	1.18	19.80	11.80

Table 6.7: S_A and S_B for each of the amphiphilic types studied.

S_B resulting in a faster initial rise and a quicker fall off.

- Increasing chain stiffness (ϵ): again an increase in both S_A and S_B, resulting in faster initial rise and a quicker fall off.

The fit that has been proposed, although empirical, emphasises that the increasing solubility of the amphiphile causes the decay in the entropy curve to be more rapid, and as a result, makes smaller micelles with a tighter size distribution more entropically favourable. Now, with this clearer understanding of the entropy, the enthalpy and entropy can be combined to form the excess chemical potential.

6.5 The excess chemical potential

The excess chemical potential is given by a combination of the excess enthalpy and the excess entropy, see equation (4.10). From the previous two sections it is clear that the solubility of the amphiphile (in terms of its head segment only) causes a shift in the excess entropy but little or no change in the excess enthalpy and as a result this change in the entropy is mirrored in the chemical potential. However, if the core of the clusters is altered, by changing the chain stiffness, then a significant change is seen in both curves leading to an interesting change in the excess chemical potential. These changes can be summarised as follows:

- Increasing head length: little change in the form of the enthalpy so change in the chemical potential is due to the shift in the entropy. Increasing the head

length increases the loss of packing entropy in going from a monomer to a cluster. This is due to the greater conformational hindrance experienced by the longer head groups resulting in an increased effective head-head repulsion. This increased repulsion decreases the effectiveness of the head group to shield the hydrophobic core from the solvent, causing the formation of smaller micelles, and also leads to an increased *cmc* due to the amphiphilic monomers being less inclined to form clusters.

- Increasing hydrophilic strength: little change in the form of the enthalpy so change in the excess chemical potential is again due to the shift in the entropy. Increasing the solubility of the head group has much the same effect as lengthening the head group.

- Increasing chain stiffness (ϵ): significant change in both curves as the amphiphiles become stiffer. As the chains become more rigid there is a change in the excess entropy similar to that for the previous two cases. This should mean that smaller micelles are formed, however a stiffer chain results in a larger enthalpy (more negative), see figure (6.12). This increase in enthalpy is largely due to an increase in the number of tail-solvent interactions, resulting from an increase in water penetration into the micellar core due to the stiffness of the tails. As an attempt to counteract this effect, the micelles become larger. Also, as the monomers in solution have a higher number of tail-solvent interactions due to the straightening of the chains, the incentive to form clusters becomes much greater resulting in a lower *cmc*.

It is now of interest to propose a functional form for the excess chemical potential.

6.5.1 Modelling the excess chemical potential

A number of workers ([10], [82] & [34]) have proposed a functional form for the excess chemical potential. This chapter has shown that this functional form is complicated and is composed of two parts the enthalpy and the entropy. Combining the two fits found previously the following functional form for the excess chemical potential is proposed, from equation (4.10), to be:

$$\beta R_1 \left[A T_s^{\frac{2}{3}} \left(\frac{n^{0.83}}{n^{1/3}} - 1 \right) - n^{0.83} + 1 \right] - S_A \left(\frac{1}{n^{1/3}} - 1 \right) + S_B \left(\frac{1}{n^{2/3}} - 1 \right) + \ln(s) \left(1 - \frac{1}{n} \right)$$

where s is the overall chain length.

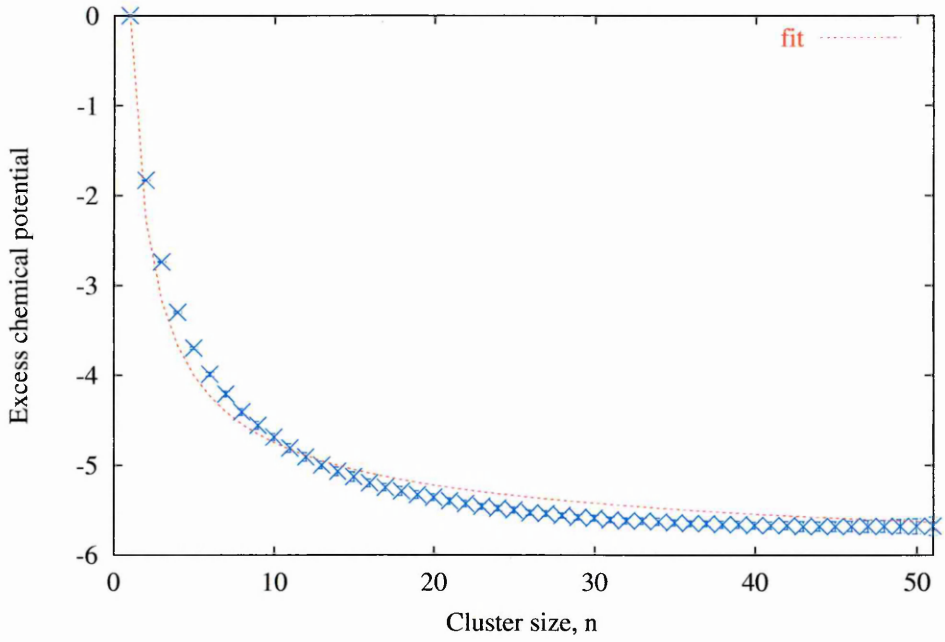

Figure 6.23: Graph of the excess chemical potential for amphiphile type H_2T_4 ($\gamma = -2$, $\epsilon = 1$, $\beta^{-1} = 1.18$, 3% vol.) with the fit added.

Figure (6.23) shows this fit for the H_2T_4, $\epsilon = 1$, $\gamma = -2$ case. Although this fit gives an estimate of the from of the chemical potential it is of too poor quality to predict either the shape of the cluster size distribution or the position of the *cmc*. This is due to the fact that the chemical potential is raised to such a large power in equation 4.1, and therefore needs to be very accurate. Each element of this final fit gives a reasonable estimate, but when combined gives a poor overall representation. All of this highlights the problems with writing the chemical potential from empirical arguments as shown by Goldstein [82].

6.6 Conclusion

From the results presented in this chapter it can be seen that changes in the head group lead to changes in the excess chemical potential due to changes in excess entropy of packing. However, if the core of the micelle is altered, by changing the chain stiffness, the enthalpy plays an equally if not more important role in determining this change. A study of the n-dependence of the constituent terms in the chemical potential gives a physical insight into the mechanisms controlling micellisation. However the exact form of the cluster size distribution function and the position of the *cmc* are very poorly predicted by such models of the excess chemical potential.

Chapter 7

Conclusion

In this thesis, results have been presented from simulations of a lattice model of an amphiphile and solvent mixture in which free self assembly is allowed. The results confirm the presence of micelles giving a clear *cmc* with a well defined cluster size distribution. As a first test, the model previous defined by Care [1] was adapted to incorporate mixtures of amphiphiles and the mixture study that is shown in chapter 3 showed both the solubilisation of a weakly hydrophilic amphiphile and the formation of mixed micelles. This demonstrated that the amphiphilic model used throughout this thesis was flexible enough to show the self assembly of surfactant mixtures.

A detailed study of micellar clusters in chapter 4 provided results showing that both the number of head-solvent interactions and right-angle bonds per monomer were, to first order, independent of the cluster size and also that the tail solvent in-

teractions per monomer decrease as $n^{-1/3}$, suggesting that the clusters were approximately spherical in shape. Further analysis of these data, separating the enthalpic and entropic contributions to the excess free energy, suggest that the competition between the decreasing internal energy per monomer and entropy per monomer is the source of micellar behaviour. Thus, in order for the micellar phase, to occur the internal energy per monomer has to fall more rapidly than the entropy per monomer as the cluster size increases. These results establish that the entropy of chain packing plays a central role in the formation of micelles in the class of model used in this work. This is a somewhat new idea with only a few other researchers proposing a similar mechanism [69, 81, 82]. An independent confirmation was therefore sought, resulting in the development of a modified Rosenbluth scheme which was used to calculate the cluster partition function of micellar clusters. This gave results which were in good agreement with data extracted from chapter 4, thus supporting the use of the Metropolis method to extract the excess entropy and enthalpy to higher cluster sizes than was possible with the Rosenbluth scheme.

The final chapter in this thesis expanded upon the simulations run in chapter 4 simulating a much wider range of amphiphiles. The effects of changing the head-length, hydrophilicty and chains stiffness were studied. The head-length and hydrophilicty gave similar results to before with the importance of the entropy of packing highlighted. However changing the chain stiffness resulted in a change in the micellar core which affected micellar behaviour.

The work in this thesis has demonstrated that it is possible to obtain essentially

exact results for the thermodynamics of micellisation in a model system which is amenable to both numerical and theoretical study. Models of this type are able to give detailed insight into the process of self-assembly in micellar systems, insights which cannot be obtained using detailed inter-atomic potentials.

7.1 Future Work

There is still much work that can be done with the model developed in this thesis, especially further work with mixtures which were only briefly examined. The following should be studied in more detail.

- Mixtures: Further simulations including, among other things, the effect of differing tail-solvent interaction energies and the implementation of tail-tail repulsion (to mimic hydrocarbon to fluorocarbon substitutions) which was taken out of the model as a simplification
- The simulation of amphiphiles near surfaces/walls which are either hydrophobic or hydrophilic.
- The simulation of amphiphiles using the Grand Canonical Ensemble, evaluating the current model and comparing results against simulations already completed by other workers [86].

References

[1] C. M. Care, J. Phys. Chem. : Solid State Phys. **20**, 689 (1987).

[2] C. M. Care, J. Chem. Soc. Faraday Trans. **83**, 2905 (1987).

[3] C. M. Care, J. Phys. : Condens. Matter **1**, 8583 (1989).

[4] C. M. Care, J. C. Desplat, and D. Brindle, Tenside Surf. Det. **30**, 281 (1993).

[5] C. M. Care, T. Dalby, and J. C. Desplat, Progr. Colloid Polym. Sci. **103**, 130 (1997).

[6] C. M. Care and T. Dalby, Eurpphys. Lett. **45**, 38 (1999).

[7] D. Brindle and C. M. Care, Molecular Simulation **5**, 345 (1990).

[8] D. Brindle and C. M. Care, J. Chem. Soc. Faraday Trans. **88**, 2163 (1992).

[9] D. Brindle, PhD Thesis, Sheffield City Polytechnic (1991).

[10] J. C. Desplat and C. M. Care, Molecular Physics **87**, 441 (1996).

[11] J. C. Desplat, PhD Thesis, Sheffield Hallam University (1996).

[12] M. N. Rosenbluth and A. W. Rosenbluth, J. Chem. Phys. **22**, 356 (1955).

[13] C. M. Care, Phys. Rev. E **56**, 1181 (1997).

[14] T. Dalby, Phys. Rev. E **59**, 6152 (1999).

[15] D. J. Shaw, *Introduction to Colloid and Surface Chemistry, 3rd Edition* (Butterworths, 1980).

[16] P. M. Lam, Phys. Rev. A **34**, 2339 (1986).

[17] C. Tanford, *The Hydrophobic Effect: Formation of Micelles and Biological Membranes, 2nd Edition* (Wiley, 1980).

[18] M. Paulaitis, S. Garde, and H. Ashbaugh, Current Opinion in Colloid and Interface Science **376**, (1996).

[19] K. A. Dill, Surfactants in Solution, Plenum Publisihing Corporation **1**, (1984).

[20] K. A. Dill and P. J. Flory, roc. Natl. Acad. Sci. USA **78**, 676 (1981).

[21] K. A. Dill, D. E. Koppel, R. S. Cantor, J. D. Dill, D. Bendedouch, and S. H. Chen, Nature **309**, 42 (1984).

[22] P. J. Flory, *Statistical Mechanics of Chain Molecules* (Hanser Publishers, 1989).

[23] H. Wennerstrom and B. Lindman, Phyics Reports **52**, 1 (1979).

[24] H. Wennerstrom, Current Opinion in Collloid and Interface Science **1**, 370 (1996).

[25] A. Ben-Shaul, I. Szleifer, and W. M. Gelbar, Physics of Amphiphiles: Micelles, Vesicles and Micro emulsions, XC Corso 404 (1985).

[26] A. Ben-Shaul, I. Szleifer, and W. M. Gelbart, J. Chem. Phys. **83**, 3597 (1985).

[27] A. Ben-Shaul, I. Szleifer, and W. M. Gelbart, Procedures of the Natational Acadamy of Science USA **81**, 4601 (1984).

[28] A. Ben-Shaul and W. M. Gelbart, J. Phys. Chem. **86**, 316 (1982).

[29] A. Ben-Shaul and W. M. Gelbart, Ann. Rev. Phys. Chem. **36**, 179 (1985).

[30] A. Ben-Shaul and P. J. Flory, Procedures of the Natational Acadamy of Science USA **78**, 676 (1981).

[31] K. L. Mittal, *Micellization, Solubilization and Microemulsions, Volumes 1 and 2* (Plenum Press, 1977).

[32] F. M. Menger, Accounts of Chemical Research **12**, 111 (1979).

[33] P. Mukerjee, J. Phys. Chem. **76**, 565 (1972).

[34] J. N. Israelachvili, D. J. Mitchell, and B. W. Ninham, J.C.S Faraday II **72**, 1525 (1976).

[35] J. N. Israelachvili, *Intermolecular and Surface Forces, 2nd Edition* (Academic Press, 1991).

[36] P. A. Winsor, Chemical Reviews **68**, 1 (1968).

[37] P. Mukerjee and J. Mysels, U.S. Goverment Printing Office (1971).

[38] A. D. Mackie, A. Z. Panagiotopoulos, and I. Szleifer, Langmuir **13**, 5022 (1997).

[39] F. A. M. Leermakers and J. A. H. M. Scheutjens, Journal of Colloid and Interface Science **136**, (1990).

[40] R. G. Laughlin, *The Aqueous Phase Behaviour of Surfactants* (Academic Press, 1994).

[41] G. J. T. Tiddy, Physics Reports **57**, 1 (1980).

[42] G. J. T. Tiddy, Modern Trends of Colloid Science in Chemistry and Biology 148 (1985).

[43] K. Hatchman, Albright and Wilson Internal Report (1993).

[44] T. H. F. Tadros, Euro Cosmetics **17**, 17 (1995).

[45] J. F. Scamehorn, ACS Symposium **311**, 1 (1986).

[46] S. Puvvada and D. Blankschtein, Journal of Physical Chemical **96**, 5567 (1992).

[47] P. M. Holland and D. N. Rubingh, American Chemical Society, Mixed surfactant systems **72**, 1 (1992).

[48] R. G. Larson, Current Opinion in Colloid and Interface Science **2**, 361 (1997).

[49] S. Karaborni and B. Smit, Current Opinion in Colloid and Interface Science **1**, 411 (1996).

[50] B. Smit, B. A. J. Hilbers, K. Esselink, L. A. M. Rupert, N. M. van Os, and A. G. Schlijper, J. Phys. Chem. **95**, 6361 (1991).

[51] B. Smit, B. A. J. Hilbers, K. Esselink, L. A. M. Rupert, N. M. van Os, and A. G. Schlijper, Nature **348**, 624 (1990).

[52] S. Karaborni and J. P. OConnell, Current Opinion in Colloid and Interface Science **1**, 411 (1996).

[53] S. Karaborni, Tenside Surf. Det. **30**, 235 (1993).

[54] J. C. Wheeler and B. Widom, Journal of the American Chemical Society **90**, 3064 (1968).

[55] B. Widom, J. Chem. Phys. **84**, 6943 (1986).

[56] K. A. Dawson, Pure and Appl. Chem. **64**, 1589 (1992).

[57] K. A. Dawson and Z. Kurtovic, J. Chem. Phys. **92**, 5473 (1990).

[58] A. Hansen, M. Schick, and D. Stauffer, Phys. Rev. A **44**, 3683 (1991).

[59] R. G. Larson, J. Chem. Phys. **96**, 7904 (1992).

[60] R. G. Larson, J. Phys. (France) .

[61] R. G. Larson, L. E. Scriven, and H. T. Davis, J. Chem. Phys. **83**, 2411 (1985).

[62] R. G. Larson, J. Chem. Phys. **89**, 1642 (1988).

[63] R. G. Larson, J. Chem. Phys. **91**, 2479 (1989).

[64] R. G. Larson, Chemical Engineering Science **49**, 2833 (1994).

[65] A. D. Mackie, E. M. O Toole, D. A. Hammer, and A. Z. Panagiotopoulos, Fluid Phase Equilbria **82**, 251 (1993).

[66] A. D. Mackie, A. Z. Panagiotopoulos, D. Frenkel, and S. K. Kumar, Europhysics Letters **27**, 549 (1994).

[67] J. I. Siepmann and D. Frenkel, Mol. Phys. **75**, 59 (1992).

[68] A. D. Mackie, K. Onur, and A. Z. Panagiotopoulos, J. Chem. Phys. **104**, 3718 (1996).

[69] C. M. Wijmans and P. Linse, Langmuir **11**, 3748 (1995).

[70] N. Metropolis and S. Ulam, J. Am. stat. Ass. **44**, 335 (1947).

[71] K. Binder, *The Monte Carlo Method in Condensed Matter Physics* (Springer-Verlag, 1992).

[72] D. Frenkel, Computer Modelling of Fluids Polymers and Solids, Kluwer Academic Publishers 83 (1990).

[73] M. P. Allen and D. J. Tildesley, *Computer Simulation of Liquids* (Oxford University Press, 1987).

[74] A. Z. Panagiotopoulos, Fluid Phase Equilibria **116**, 257 (1996).

[75] N. Metropolis, M. N. Rosenbluth, A. W. Rosenbluth, A. H. Teller, and E. Teller, J. Chem. Phys. **21**, 1087 (1953).

[76] J. C. Owicki and H. A. Scheraga, Chemical Physics Letters **47**, 600 (1977).

[77] G. A. Smith, S. D. Christian, E. E. Tucker, and J. F. Scamehorn, Journal of Colloid and Interface Science **130**, 254 (1989).

[78] R. Nagarajan, American Chemical Society, Mixed Surfactant Systems 54 (1992).

[79] D. Hyams, Windows 95 Software Package (1997).

[80] J. F. Scamehorn, Future Perspectives 324 (1986).

[81] H. J. Woo, C. Carraro, and D. Chandler, Faraday Discussions **104**, 183 (1996).

[82] R. E. Goldstein, J. Chem. Phys. **84**, 3367 (1986).

[83] T. L. Hill, *Statistical Mechanics: Principles and Selected Applications* (Dover, 1956).

[84] L. Pratt, J. Chem. Phys. **77**, 979 (1982).

[85] J. Batoulis and K. Kremer, J. Phys. A:Math. Gen. **21**, 127 (1988).

[86] A. Z. Panagiotopoulos and V. Wong, Macromolecules **31**, 912 (1998).